University of Alberta

High Temperature Behaviors of Asphaltene Aggregates in Heavy Feed Stocks and in Mixtures with Diluents

by

Bei Zhao 

A thesis submitted to the Faculty of Graduate Studies and Research
in partial fulfillment of the requirements for the degree of

Doctor of Philosophy

in

Chemical Engineering

Department of Chemical and Materials Engineering

Edmonton, Alberta
Fall 2008

Your file Votre référence
ISBN: 978-0-494-46458-8
Our file Notre référence
ISBN: 978-0-494-46458-8

University of Alberta

Library Release Form

Name of Author: Bei Zhao

Title of Thesis: High Temperature Behaviours of Asphaltene Aggregates in Heavy Feedstocks and in Mixtures with Diluents

Degree: Doctor of Philosophy

Year this Degree Granted: 2008

Signature

University of Alberta

Faculty of Graduate Studies and Research

The undersigned certify that they have read, and recommend to the Faculty of Graduate Studies and Research for acceptance, a thesis entitled **High Temperature Behaviors of Asphaltene Aggregates in Heavy Feedstocks and in Mixture with Diluents** submitted by **Bei Zhao** in partial fulfillment of the requirements for the degree of **Doctor of Philosophy**.

(Supervisor) Dr. John M. Shaw

Dr. Murray R. Gray

Dr. Sieghard E. Wanke

Dr. William C. McCaffrey

Dr. Carlos F. Lange

Dr. Harvey W. Yarranton

Date_____

Abstract

The propensity of asphaltenes to aggregate can cause severe coke deposition problems during catalytic hydroprocessing of heavy oils. Numerous studies on this subject have been performed. However, asphaltene aggregate size is an uncontrolled and unexplored and potentially important variable.

Athabasca bitumen and Maya crude were filtered through commercial nano ceramic membranes to separate asphaltene aggregates by size in their native media without dilution. Two distinct nanostructures, one enriched in pentane asphaltenes and one enriched in mineral matter, were identified. The asphaltene-rich nanostructures are polydispersed with a broad size distribution extending from less than 5 nm to more than 100 nm. Their composition is independent of size and they do not associate preferentially at 473 K with other constituents, such as mineral matter or resins in native feeds, as prevalent notions suggest.

Coke deposition experiments were conducted in a 15 mL batch reactor on a commercial hydroprocessing catalyst NiMo/γ-Al_2O_3 at 653 K for 2 h at a 30:1 feed to catalyst ratio (weight basis). Two sets of experiments were performed: one with feedstock, permeates, and retentates of Athabasca bitumen and Maya crude oil focused on the impact of asphaltene aggregate size on coke deposition; the other with Athabasca bitumen diluted with n-dodecane, n-decane or 1-methylnaphthalene to investigate the interplay among thermophysical properties in mixtures at diverse length scales in hydroprocessing environment.

Coke deposition outcome is shown to be a combination of mixture properties at the macroscopic scale (the number, nature, and composition of phases present), the nano scale (asphaltene nanoaggregation within phases) and the molecular scale (hydrogen solubility by phase). Asphaltene-rich nanoaggregate size and maltene composition are shown to play secondary roles in coke deposition. Elemental analyses of sectioned catalyst pellets showed that coke deposition within pellets was diffusion limited, while vanadium deposition, arising primarily from the maltene fraction, was not diffusion limited. The findings suggest that prevalent asphaltene-rich nanostructure models and their chemistry be re-evaluated and underscore the need for the explicit incorporation of physical phenomena in the development of coke deposition models.

Acknowledgements

I am much obliged to my supervisor, Dr. John M. Shaw, for his guidance, discussion, and teaching during my Ph.D. study. I thank previous colleagues, Drs Xiaohui Zhang and Richard McFarlane, for discussion and great help for my experiment. I appreciate Dr. Denis Rioux and his team (National Centre for Upgrading Technology, Devon, Alberta), Dr. Sergei Matveev (Electron Microprobe Lab, University of Alberta), and Dr. Long Wu (Chemical and Materials Engineering Department, University of Alberta) for their analytical work. I would like to thank Drs. Murray Gray, Jacob Masliyah and William McCaffrey (Chemical and Materials Engineering Department, University of Alberta) for advice and support. I also thank Carlos Lira-Galeana at Mexican Petroleum Institute for providing a Maya crude sample.

Great appreciation goes to all the sponsors for my thesis research: Alberta Energy Research Institute, Albian Sands Energy Inc., Computer Modeling Group Ltd., ConocoPhillips Inc., Imperial Oil Resources, Kellog Brown and Root, NEXEN Inc., Natural Resources Canada, the Petroleum Society of CIMM, Oilphase, Oilphase DBR-a Schlumberger Company, Schlumberger, Syncrude Canada Ltd., Shell Canada, and the Natural Science and Engineering Research Council (NSERC).

I would like to show my heartfelt appreciation to my husband, Mr. Moran Lu, who gave up his successful work in China and joined me to face all the challenges here; and to our sweet son, Jerry, who suffered one-year-apart from parents and then had to adapt himself to a new environment. I sincerely appreciate the support from my family: my dear brother, Dr. Yun Zhao, who keeps encouraging me like a mentor; my dear parents (Mr. Ruhai Zhao and Mrs. Shuang Zhao) and parents-in-law (Mr. Changpeng Lu and Ms. Xiaoxin Xie), who consistently gave me spiritual and emotional support in the past five years. Without their great love, generosity, patience, encouragement, and support, I would not complete my thesis.

Table of Contents

List of Figures

List of Tables

Nomenclature

Notations:

A	pore surface area of fresh catalyst
A'	pore surface area of catalyst after reaction
C_A	asphaltene weight percent in the feed
C_{Bulk}	bulk carbon weight percent in a catalyst after reaction
C_C	carbon weight percent in the catalyst following reaction
C_{Core}	carbon weight percent at the core area of a catalyst pellet cross-section
f	normalized pore size distribution functions of catalyst pre-reaction
f'	normalized pore size distribution functions of catalyst post-reaction
L	unit length of pore column in catalyst
r	pore radius of catalyst
$\bar{r}$	mean pore radius of the fresh catalyst
S	vanadium selectivity, defined as the mass ratio of vanadium to carbon in the deposit to the mass ratio of vanadium to carbon in the feed
S_m^0	vanadium selectivity for maltenes
$S_{Asph.}^0$	vanadium selectivity for asphaltenes
T	reaction temperature
T_C	critical temperature
t	reaction time
V	pore volume of fresh catalyst
V'	pore volume of catalyst after reaction

X_{V-m} the mass of vanadium present in the maltenes divided by the total mass of vanadium in a sample

σ^2 variance of pore radii in fresh catalyst

Abbreviations

AB	Athabasca bitumen
$AB_{Asph.}$	Asphaltenes separated from Athabasca bitumen
AB_{Oil}	Asphaltene-free Athabasca bitumen
ABVB	Athabasca vacuum residue
ABP10	Athabasca bitumen 10 nm permeate
ABP20	Athabasca bitumen 20 nm permeate
ABP50	Athabasca bitumen 50 nm permeate
ABP100	Athabasca bitumen 100 nm permeate
ABP200	Athabasca bitumen 200 nm permeate
ABR10	Athabasca bitumen 10 nm retentate
ABR20	Athabasca bitumen 20 nm retentate
ABR50	Athabasca bitumen 50 nm retentate
ABR100	Athabasca bitumen 100 nm retentate
ABR200	Athabasca bitumen 200 nm retentate
C10	*n*-decane
C12	*n*-dodecane
CMC	critical micellar concentration

CNAC critical nanoaggregation concentration

FIB focused-ion-beam technique

Heated AB (20) heated Athabasca bitumen collected from the reservoir after 30 days at 473 K

Heated Maya (10) heated Maya crude collected from the reservoir after 30 days at 473 K

$Maya_{Asph}$ Asphaltenes separated from Maya crude oil

$Maya_{Oil}$ Asphaltene-free Maya crude oil

1-MN 1-methylnaphthalene

MP5 Maya crude 5 nm permeate

MP10 Maya crude 10 nm permeate

MP20 Maya crude 20 nm permeate

MP50 Maya crude 50 nm permeate

MP100 Maya crude 100 nm permeate

MP200 Maya crude 200 nm permeate

MR5 Maya crude 5 nm retentate

MR10 Maya crude 10 nm retentate

MR20 Maya crude 20 nm retentate

MR50 Maya crude 50 nm retentate

MR100 Maya crude 100 nm retentate

MR200 Maya crude 200 nm retentate

Oxygen free AB heated Athabasca bitumen collected from the reservoir after filtration of AB. Nitrogen first bubbled through bitumen for 5 days

and then followed the same filtration procedure

Oxygen free ABP20 Athabasca bitumen 20 nm permeate collected from bubbled Athabasca bitumen

Oxygen free ABR20 Athabasca bitumen 20 nm retentate collected from bubbled Athabasca bitumen

PV pore volume

PVL pore volume loss

SA surface area

SAL surface area loss

SANS small-angle neutron scattering

SARA saturates, aromatics, resins, and asphaltenes analysis

SAXS small-angle X-ray scattering

SC sulfided catalyst

1. Introduction

1.1 Background

1.1.1 Catalytic hydroprocessing

As the world's supply of light sweet crude oils becomes depleted, the demand for upgrading heavy hydrocarbon resources such as bitumen has increased greatly. These heavy resources often contain significant amounts of asphaltenes, sulfur, nitrogen and metal-containing organic compounds. Thus, significant refining is required to convert them into light distillates and to remove heteroatoms and metals to meet increasingly strict environmental specifications.

Many such upgrading processes have been developed. These processes can be classified roughly into two types: carbon rejection and hydrogen addition, with or without catalysts. Carbon rejection processes remove hydrocarbons with the lowest hydrogen to carbon ratio, such as asphaltenes, from heavy residual oils in the form of coke and obtain cracked distillates from the balance of feeds. Part of the sulfur and nitrogen compounds and most of the organometallic compounds of nickel and vanadium are removed concomitantly. Examples of this approach include coking, catalytic cracking of residuum, etc. Hydrogen addition processes, such as hydrocracking and hydrotreating, are extensively employed in the petroleum industry. Heavy fractions including part of the asphaltenes and part of the precursors of carbon residue are converted into light distillates by hydrocracking, metals are removed by deposition on catalysts, and heteroatoms, such as nitrogen and sulfur, are removed in the form of H_2S and NH_3.

Regardless of the technologies employed, carbon rejection or hydrogen addition, coke formation arises. In coking, coke formation is a process objective; while in catalytic upgrading coke formation is undesirable and may cause vessel, heat exchanger and furnace tube fouling, and catalyst deactivation. Catalytic hydroprocessing is one of the primary upgrading processes. The most attractive aspects of this technology are high volumetric yield of liquid product, which may exceed 100 %, and high heteroatom removal. The less attractive aspects are the high consumption of hydrogen and catalysts. For light feeds, deactivation of catalyst is minimal and processes can operate for a long time before catalyst replacement. However, in hydroprocessing heavy residuals, catalyst deactivation resulting from coke deposition can be severe and rapid.

1.1.2 Coke deposition modes

Though catalyst deactivation can occur by the mechanisms of poisoning, sintering, and fouling, the main cause of catalyst deactivation in hydroprocessing of residue fractions is coke and metals deposition. Typically the deactivation process has three stages:[1] 1) rapid initial deactivation is usually attributed to rapid coke deposition; 2) after rapid initial deactivation, pseudo steady state is reached; the intrinsic activity of catalyst decreases due to gradual accumulation of coke layers and metal deposition, which may cause the blockage of access to the remaining active sites in porous pellets; 3) later, the final catastrophic deactivation has been associated with pore mouth blockage where catalytic activity is completely lost due to diffusion limitations. Under commercial operation conditions, catalyst activity is maintained by constantly increasing temperature. The typical S-curve of temperature rise as a function of time on stream is shown in Figure 1.1.

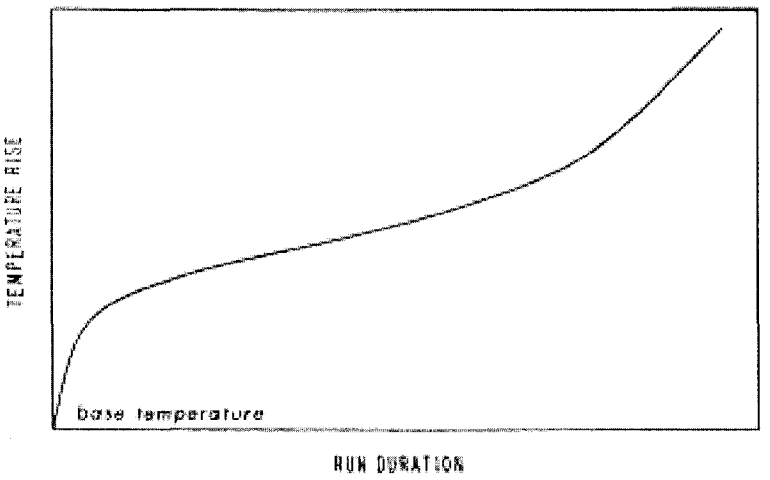

Figure 1.1 Typical S-shaped deactivation curve[1]

Coke deposition on catalyst can be simply classified into three modes: uniform surface deposition,[2] pore-mouth plugging,[3] and bulk-phase coke formation[2, 4] (Figure 1.2). The uniform deposition mode assumes that coke deposition accumulates uniformly through the catalyst structure and pore channels are expected to narrow and shift to smaller sizes. The pore-mouth plugging mode includes uniform coke deposition both on inner channels of catalysts and at network intersections where local micropores become blocked. The bulk-phase coke formation mode not only involves these two coke deposition modes, but also concerns large amounts of coke formed in the bulk liquid phase and deposited on the outer surface of catalysts and all surfaces within reactors. Detailed descriptions of these three coke deposition modes are presented in literature review (Chapter 2).

The uniform surface deposition mode and the pore-mouth plugging mode concern coke deposition within catalysts and are debated because different outcomes are predicted for coke layer thickness, impacts on catalyst activity and selectivity, and probable location of

coke deposition.[2] The bulk-phase coke formation mechanism involves the formation of mesophase either by liquid phase separation or by the flocculation of asphaltenes. This multiphase behavior makes the coke deposition mechanism more complex. All of these three modes can be supported by experimental findings. However, no unified answers have been developed to explain the phenomena observed.

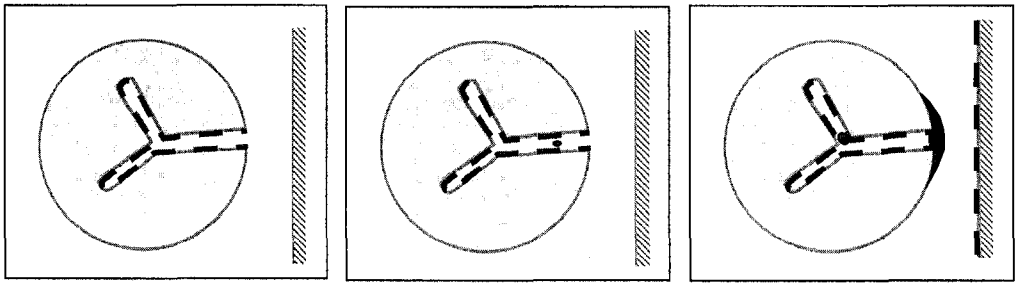

Figure 1.2 Schematic representation of coke deposition modes

1.1.3 Asphaltenes—a major source for coke deposition

Catalytic hydroprocessing must be carried out at reasonably high temperatures (375 — 420 °C) and pressures (500 — 2000 psi). Thus, it is not surprising that coke arises from either thermal coking or catalytic coking. Banarjee et al.[5] systematically investigated the thermal pyrolysis of various fractions of heavy crudes and found the tendencies of different fractions to form coke in the decreasing order: asphaltenes > resins > aromatics > saturates. The rapid deactivation of catalysts in hydroprocessing heavy oils is inevitably attributed to asphaltenes.

However, controversies about the definition of asphaltenes persist. The simplistic operational definition describes asphaltenes as an n-alkane insoluble and toluene soluble

fraction, where this petroleum fraction can be filtered from dilute mixtures with n-alkanes using filters with nominal pore sizes in the micron range, but pass through filters with the same nominal pore size when dispersed in aromatic solvents. Many standard separation methods based on this operational definition have developed, such as ASTM D2006, ASTM D2007, and ASTM D4124. The effect of temperature, contact time, solvent, solvent-to-feed ratio,[6] and washing[7] on asphaltene separation results have been studied systematically. However, the impact of filter pore sizes has been underappreciated. In practice, the selection of filters is arbitrary and the filters employed cover a broad range of pore sizes[8-13] from as small as 220 nm to as large as 20-25 μm. A recent report by Savvidis et al.[14] showed clearly that the amount of asphaltenes recovered increases sharply as pore size is decreased. This study suggests that the pore size of filters is a key variable as well as a solvent for asphaltene separation.

Meanwhile, several other independent studies[15-18] show that asphaltenes can aggregate at low concentration about 100 ~ 200 mg/L, even in toluene, or in asphaltene plus solvent or deasphalted oil mixtures.[19] These values are much lower than earlier reported critical concentrations in toluene 2-18 g/L, which have now been attributed to be the formation of larger secondary aggregates[15] and not the smaller primary aggregates. A review by Sheu[20] concludes that asphaltene molecules are of the order of 0.5-0.6 nm in radius and that elementary asphaltene aggregates possess radii of approximately 3.0 nm. At higher concentrations these elementary aggregates appear to cluster. Other pioneering studies[21-23] show that asphaltenes in crude oil comprise small aggregates with radii of gyration between 2 and 4 nm as well as large aggregates with leading dimensions in the hundreds of nanometers. Earlier ultrafiltration experiments[24, 25] carried out with membranes having

different pore size ranges confirmed that asphaltene aggregate sizes are not uniform. Significant aggregation and broad asphaltene size distributions are therefore expected for heavy feed stocks in general. Most research investigations related to asphaltenes involve the addition of hydrocarbons. Whether the nanostructures identified by chemical separation resemble those arising in the original hydrocarbon resource remains an unresolved question in the literature. Thus, the nature of asphaltene aggregates in hydrocarbon resources is poorly defined.

Regardless of their structures, it is clear that asphaltenes interact with catalyst surfaces. Thus, catalyst surface and pore structure impact coke formation modes and determine the extent of coke formation. It is well known that catalytic hydroprocessing can be influenced by restrictive diffusion in catalysts. This effect can become more severe when the size of reactant molecules or nanostructures approach pore diameters. Heavy oils, such as bitumen or vacuum residues, contain large polynuclear aromatic molecules and asphaltene aggregates. Experimental size ranges for asphaltene aggregates range from several nanometers to several hundred nanometers.[19, 21-23] The average pore size of hydroprocessing catalysts ranges from 3 and 100 nanometers. Restrictive diffusion is expected for asphaltene-rich feed penetration in typical hydrotreating catalysts. Coking outcomes, both deposition modes and amounts deposited, are likely to be sensitive to the details of asphaltene aggregate size distribution or coke precursor molar mass in a feed, and the pore size distribution of catalyst pellets employed. Accumulation of coke and metals during hydroprocessing alters pore and surface structures, pore size distribution, porosity, tortuosity, active site accessibility, and adsorption capacities over time.

Phase behavior is another important variable in coke deposition. In the phase diagram[26] of saturates, aromatics, and asphaltenes, shown in Figure 1.3, the feed composition may shift, during reaction, to a composition where asphaltenes precipitate to form sludge or sediments on external catalyst surfaces. This leads to severe coke formation. Dautzenberg and de Deken[27] suggested that this is more likely to occur at lower temperatures. In heavy oil + diluent mixtures, the phase behaviour becomes more complex and is characterized by large multiphase zones, for example, for Athabasca vacuum residue + n-alkane mixtures.[28] Coke deposition outcomes depend on which liquid phase the catalyst pellet is exposed to. The impact of phase behavior on coking outcomes was addressed explicitly for Athabasca vacuum residue + decane mixtures.[29]

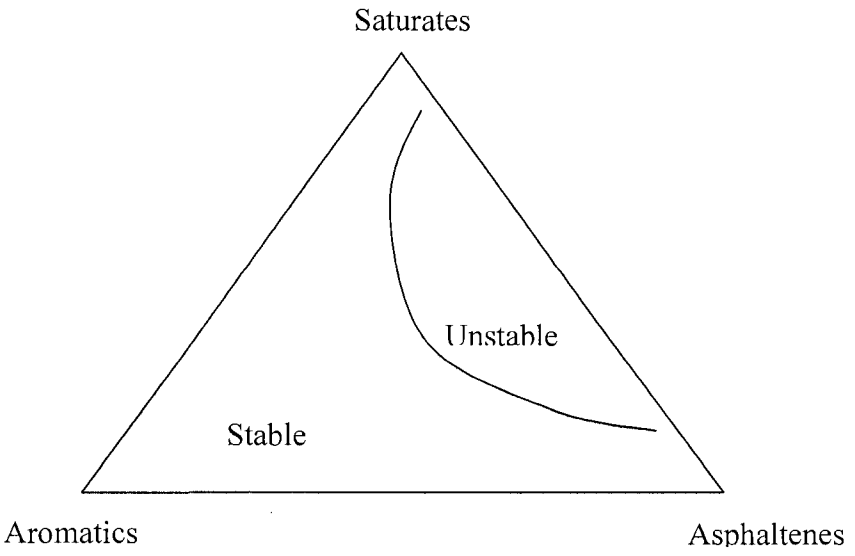

Figure 1.3 Asphaltenes/aromatics/saturates stability diagram

Variables, such as asphaltene aggregate size distribution, the phase behavior of diluent + feed stock mixtures, and molecular or abstractable hydrogen availability by phase, are unmeasured and therefore uncontrolled for experimental results reported in the literature.

These can influence coke deposition modes and outcomes. The interplay among these physical properties in heavy oil + diluent mixtures merits detailed investigation and may facilitate interpretation of observed coking phenomena during hydroprcessing.

1.2 Hypothesis

The principal hypothesis in this work is that the relationship between the size of asphaltene aggregates and the pore size distribution in hydroprocessing catalyst pellets, an uncontrolled variable in typical experimental programs, dictates the mode and amount of coke deposited within and on them. Secondary hypotheses include:

1. that asphaltene aggregates in their native hydrocarbon resource differ from those obtained through solvent based partitioning;

2. that the deposition of metal poisons such as vanadium, which is present in asphaltenes at high concentration, is linked to asphaltene deposition.

1.3 Thesis outline

Following this brief introduction, a comprehensive literature review related to this thesis is presented in Chapter 2. It includes the characteristics of heavy oils, asphaltenes, catalytic coking, and restrictive diffusion. Chapter 3 describes experimental equipment, analytical methods, materials and procedures related to nanofiltration and nanofiltered sample analysis, catalyst coking experiments and catalyst pellet analysis. Measurement accuracy and reproducibility are addressed. The experimental results and discussion are

divided into three chapters. Chapter 4 focuses on the composition and size distribution of coherent nanostructures in Athabasca bitumen and Maya crude oil. Chapter 5 focuses on the impact of asphaltene-rich aggregate nanostructure on coke deposition. The Coke deposition mode is discussed and a simple model is proposed which underscores the independence of vanadium deposition from asphaltenes and maltenes. The interplay between the physical properties of Athabasca bitumen + diluent mixtures and coke deposition is discussed in Chapter 6. Coke deposition and coke outcomes are reconciled with the mixture properties at various length scales. Chapter 7 comprises a general discussion and comes up with some suggestions for future work. Finally, conclusions are summarized in Chapter 8.

References

(1) Tamm, P. W.; Harnsberger, H. F.; Bridge, A. G., Effects of Feed Metals on Catalyst Aging in Hydroprocessing Residuum. *Industrial & Engineering Chemistry Process Design and Development* **1981,** 20, (2), 262-273.

(2) Richardson, S. M.; Nagaishi, H.; Gray, M. R., Initial Coke Deposition on a NiMo/gamma-Al_2O_3 Bitumen Hydroprocessing Catalyst. *Industrial & Engineering Chemistry Research* **1996,** 35, (11), 3940-3950.

(3) Muegge, B. D.; Massoth, F. E., Basic Studies of Deactivation of Hydrotreating Catalysts with Anthracene. *Fuel Processing Technology* **1991,** 29, (1-2), 19-30.

(4) Zhang, X. H.; Chodakowski, M.; Shaw, J. M., Impact of Multiphase Behavior on Coke Deposition in a Commercial Hydrotreating Catalyst under Sedimentation Conditions. *Energy & Fuels* **2005,** 19, (4), 1405-1411.

(5) Banerjee, D. K.; Laidler, K. J.; Nandi, B. N.; Patmore, D. J., Kinetic-Studies of Coke Formation in Hydrocarbon Fractions of Heavy Crudes. *Fuel* **1986,** 65, (4), 480-484.

(6) Speight, J. G.; Long, R. B.; Trowbridge, T. D., Factors Influencing the Separation of Asphaltenes from Heavy Petroleum Feedstocks. *Fuel* **1984,** 63, (5), 616-620.

(7) Alboudwarej, H.; Beck, J.; Svrcek, W. Y.; Yarranton, H. W.; Akbarzadeh, K., Sensitivity of Asphaltene Properties to Separation Techniques. *Energy & Fuels* **2002,** 16, (2), 462-469.

(8) Berna, A. C. S.; Moran, V. C.; Guzman, E. T. R.; Yacaman, M. J., Asphaltene Aggregation from Vacuum Residue and Its Content of Inorganic Particles. *Petroleum Science and Technology* **2006,** 24, (9), 1055-1066.

(9) Nalwaya, V.; Tangtayakom, V.; Piumsomboon, P.; Fogler, S., Studies on Asphaltenes through Analysis of Polar Fractions. *Industrial & Engineering Chemistry Research* **1999,** 38, (3), 964-972.

(10) Wang, J. X.; Buckley, J. S., Asphaltene Stability in Crude Oil and Aromatic Solvents - The Influence of Oil Composition. *Energy & Fuels* **2003,** 17, (6), 1445-1451.

(11) Tanabe, K.; Gray, M. R., Role of Fine Solids in the Coking of Vacuum Residues. *Energy & Fuels* **1997,** 11, (5), 1040-1043.

(12) Yang, X. L.; Hamza, H.; Czarnecki, J., Investigation of Subfractions of Athabasca Asphaltenes and Their Role in Emulsion Stability. *Energy & Fuels* **2004,** 18, (3), 770-777.

(13) Duong, A.; Chattopadhyaya, G.; Kwok, W. Y.; Smith, K. J., An Experimental Study of Heavy Oil Ultrafiltration Using Ceramic Membranes. *Fuel* **1997,** 76, (9), 821-828.

(14) Savvidis, T. G.; Fenistein, D.; Barre, L.; Behar, E., Aggregated Structure of Flocculated Asphaltenes. *Aiche Journal* **2001,** 47, (1), 206-211.

(15) Andreatta, G.; Bostrom, N.; Mullins, O. C., High-Q Ultrasonic Determination of the Critical Nanoaggregate Concentration of Asphaltenes and the Critical Micelle Concentration of Standard Surfactants. *Langmuir* **2005,** 21, (7), 2728-2736.

(16) Freed, D. E.; Lisitza, N. V.; Sen, P. N.; Song, Y.-Q., *Chapter 11. Molecular Composition and Dynamics of Oils from Diffusion Measurements. Asphaltenes, Heavy Oils, and Petroleomics*. Springer: New York, 2007.

(17) Sheu, E.; Long, Y.; Hamza, H., *Chapter 10. Asphaltene Self-Association and Precipitation in Solvent--AC Conductivity Measurements. Asphaltenes, Heavy Oils, and Petroleomics.* . Springer: New York, 2007.

(18) Yudin, I. K.; Anisimov, M. A., *Chapter 17: Dynamic Light Scattering Monitoring of Asphaltene Aggregation in Crude Oils and Hydrocarbon Solutions. Asphaltenes, Heavy Oils, and Petroleomics.* Springer: New York 2007.

(19) Kim, H. G.; Long, R. B., Characterization of Heavy Residuum by a Small-Angle X-Ray-Scattering Technique. *Industrial & Engineering Chemistry Fundamentals* **1979,** 18, (1), 60-63.

(20) Sheu, E. Y., Small Angle Scattering and Asphaltenes. *Journal of Physics-Condensed Matter* **2006,** 18, (36), S2485-S2498.

(21) Dwiggins, C. W., A Small Angle X-Ray Scattering Study of Colloidal Nature of Petroleum. *Journal of Physical Chemistry* **1965,** 69, (10), 3500-3506.

(22) Dwiggins, C. W., The Study of Colloidal Nature of Petroleum with an Automated Bonse-Hart X-Ray Small Angle Scattering Unit. *Journal of Applied Crystallography* **1978,** 11, (5), 615-619.

(23) Dwiggins, C. W., Absorption Correction and Normalization of X-Ray Small-Angle Scattering Data for Materials Producing Intense Scattering at Extremely Low Angles. *Journal of Applied Crystallography* **1979,** 12, (4), 401-402.

(24) Nuemann, H. J., Untersuchungen Zur Kolloidchemie des Erdols. *Erdol und Kohle Erdgas Petrochemie* **1965,** 18, 865.

(25) Briant, J.; Hotier, G., Research on the State of Asphaltenes in Hydrocarbon Mixtures—Size of Molecular Clusters. *Revue de l'Institut Francsais du Petrole* **1983,** 38, (1), 83-100.

(26) Absi-Halabi, M.; Stanislaus, A.; Trimm, D. L., Coke Formation on Catalysts During the Hydroprocessing of Heavy Oils. *Applied Catalysis* **1991,** 72, (2), 193-215.

(27) Dautzenberg, F. M.; de Deken, J. C., Modes of Operation in Hydrodemetalation. *Division of Petroleum Chemistry, ACS* **1985,** 30, (1), 8-20.

(28) Zou, X. Y.; Zhang, X. H.; Shaw, J. M., Phase Behavior of Athabasca Vacuum Bottoms plus n-Alkane Mixtures. *Spe Production & Operations* **2007,** 22, (2), 265-272.

(29) Zhang, X. H.; Shaw, J. M., Impact of Multiphase Behavior on Coke Deposition in Heavy Oils Hydroprocessing Catalysts. *Energy & Fuels* **2006,** 20, (2), 473-480.

2. Literature Review

2.1 Heavy oils/Bitumen

2.1.1 Heavy oils/Bitumen—our current energy resources

From the *International Energy Outlook* 2007 *(IEO2007)*, it is clear that fossil fuels continue to be the dominant supply of the increased world consumption of energy from all sources over 2004 to 2030 period. Petroleum-based liquid fuels remain the largest fraction of world energy consumption. It is estimated by *IEO2007* that the world use of petroleum and other liquids will grow from 83 million barrels oil equivalent per day in 2004 to 97 million barrels per day in 2015 and 118 million barrels per day in 2030. The transportation sector accounts for 68 % of the total projected increment, followed by the industrial sector which accounts for 27 % of the increment in liquid demand over the next two decades.

However, as the conventional sweet light crude oils in the world become depleted, the petroleum industry is forced to refine heavy crude oils and bitumen to meet the increasing consumption needs for transportation fuels and petrochemical feeds. As reported in *IEO2007*, the world production of unconventional liquids totaled only 2.6 million barrels per day in 2004; unconventional liquids production is expected to grow to 10.5 million barrels per day in 2030. Canada and Venezuela are the world's two largest sources of oil sands, also referred to as bitumen. Since early 80's, in Athabasca and Alberta (Canada), and more recently, in Orinoco (Venezuela), most liquid hydrocarbons are produced from bitumen. There are about 300 billion barrels of bitumen (one third of the world's known

petroleum reserves, Figure 2.1) in Alberta, which could meet Canada's energy needs for the next two centuries.

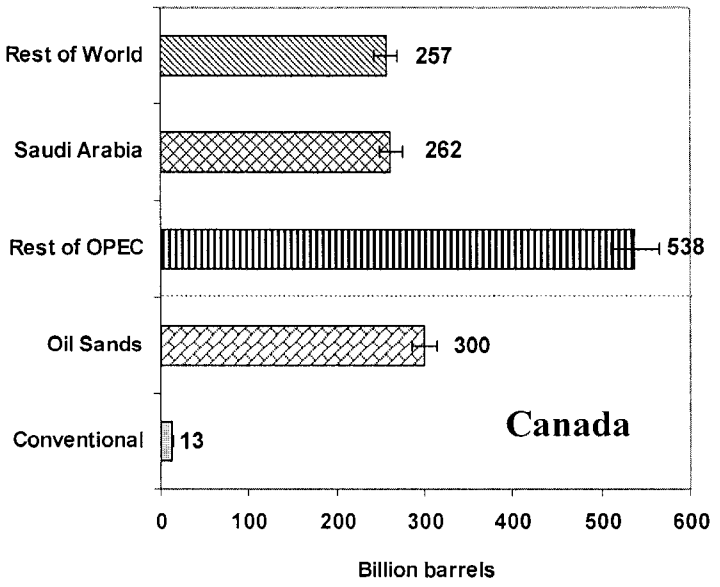

Figure 2.1 World proven oil reserves

Source: BP Statistical Review; National Energy Board (NEB). From the chart, the total OPEC crude oil reserve is 800 billion barrels and the world crude oil reserve is 1,057 billion barrels.

2.1.2 Characteristics of heavy oils/bitumen

As mentioned above, the interest in processing heavier feeds is increasing. However, these heavier feeds contain 40 % or more vacuum residue.[1] The refining of these residues and residues in conventional crudes into distillable fractions is crucial to meet the challenge of the increasing consumption in the world. Understanding of heavy oils/bitumen composition and properties is a prerequisite for the investigation of coke formation and catalyst deactivation in hydroprocessing of heavy oil mixtures, one refining option.

Heavy oils and bitumen[1] are characterized by: high density (1000 — 934 kg m^{-3}), high viscosity (100 — 10,000 mPa s), and low API gravity (10 — 20 °API). These feed stocks generally have a low hydrogen-to-carbon ratio (~ 1.5) and contain large amounts of asphaltenes (more than 10 wt %) and high concentrations of heteroatoms (such as sulfur, 2 — 7 wt %; nitrogen, 0.2 — 0.7 wt %; and oxygen, ~ 1 wt %) and metals (nickel, 20 — 200 ppm; and vanadium, 100 — 1000 ppm). Mined bitumen may also contain significant amounts of inorganic mineral matter. The inorganic mineral matter, heavy metals, and heteroatoms usually concentrate in the vacuum residue and are thought to be associated or combined with asphaltenes.

The classification of fractions in heavy oils/bitumen is on the basis of combined solubility and adsorption characteristics. Coke is defined as the fraction insoluble in tetrahydrofuran. Asphaltenes are the fraction insoluble in alkane (such as pentane and heptane) but soluble in aromatics (such as benzene or toluene). Maltenes are the fraction soluble in alkane and can be further separated into three fractions according to polarity and adsorption characteristics on chromatographic columns: resins, aromatics and saturates. Many standard methods (ASTM D2006, ASTM D2007, and ASTM D4124) have been developed to characterize heavy oil fractions. The typical fractionation of petroleum is shown in Figure 2.2.

2.2 Asphaltenes

Asphaltenes are generally thought to be the culprit for coke formation and the rapid deactivation of catalysts. Understanding asphaltene structures and chemistry can shed light on coke deposition and catalyst deactivation. Though many efforts have been made

to investigate asphaltene structures and chemistry, controversies persist. Asphaltenes comprise a broad distribution of molecular structures that vary greatly from one crude oil to another. Only average structures for asphaltenes can be discussed.

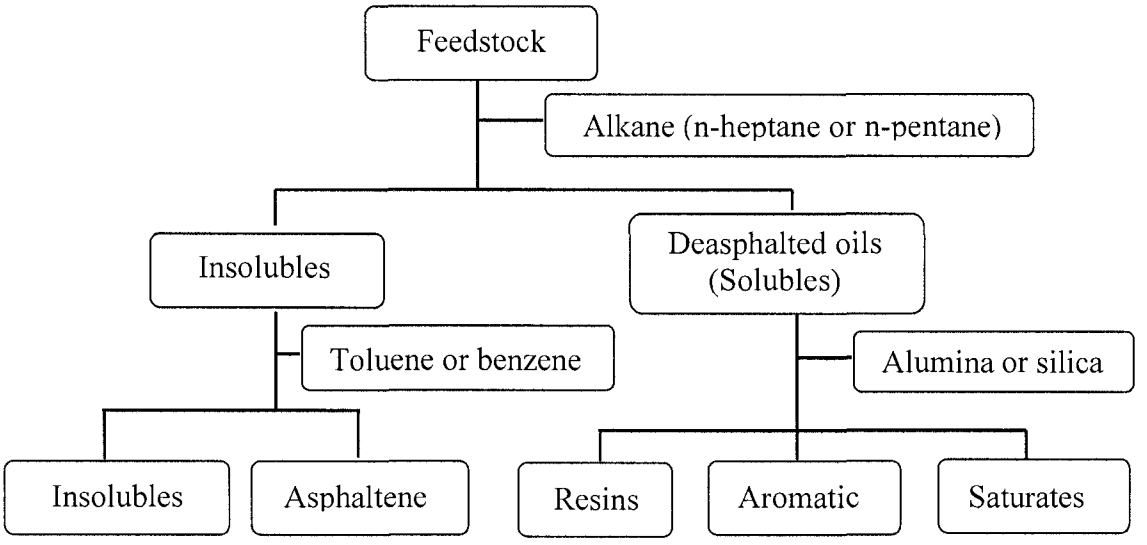

Figure 2.2 Petroleum fraction

2.2.1 Asphaltene molecular structure models

In general, asphaltenes are characterized by fused aromatic rings, small aliphatic side chains, polar heteroatom-containing functional groups, H/C ratios between 1.0 and 1.2 and N, S, and O content of a few weight percent. The unit sheet of asphaltenes is believed to contain the polynuclear aromatic cores which bear heteroatoms such as nitrogen and nickel and connect with alkyl chains and aromatic groups, with vanadium and sulfur associated either with the sheet or with the functional groups attached to the sheet.

Much research has been focused on the study of asphaltene molecular structures and various structure models have been proposed, but a consensus has yet to be achieved.

The pericondensed asphaltene molecular structure model[2-5] is characterized by one or two highly condensed aromatic core groups comprising more than 7 fused rings with all the aromatic carbons clustered within and attached to short peripheral alkyl groups. A typical pericondensed structure is shown in Figure 2.3. Fluorescence depolarization results[6] further support this model by indicating insignificant bridge links between aromatic groups and low molecular weight on the basis of spectroscopic studies. The archipelago asphaltene structure model,[7-9] by contrast, suggests that asphaltene molecules comprise small aromatic groups linked with multiple bridges, shown in Figure 2.4. This molecular structure model is supported by pyrolytic and selective oxidation studies.[10-13]

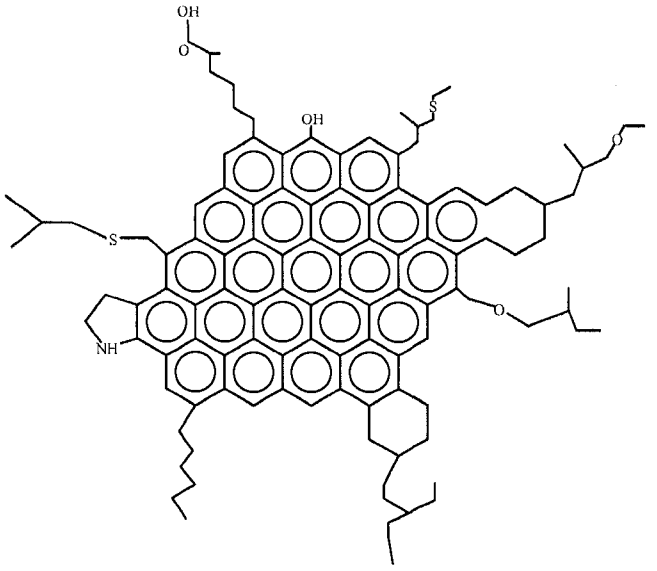

Figure 2.3 Pericondensed asphaltene molecular structure model[3]

2.2.2 Asphaltene aggregation

A macrostructure model for asphaltenes[14] proposed during the early 1960's distinguished four different entities: the elemental molecule, the particle, the micelle, and

the aggregate where pericondensed asphaltene molecules form elemental particles by stacking planar aromatic parts of the molecules (π-π association) or through hydrogen bonds.[15]

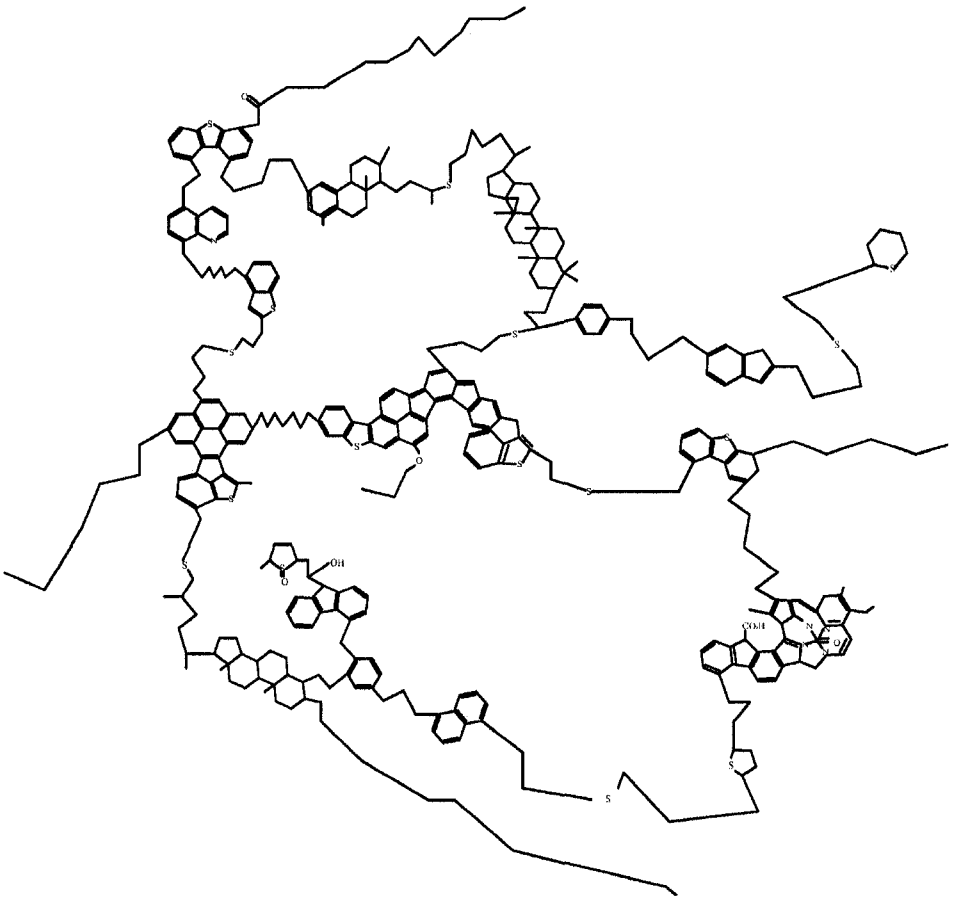

Figure 2.4 Archipelago asphaltene molecular structure model[10]

The estimated weight of such particles is 10,000 g/mol with a radius of gyration (Rg) of 20 Å.[15] These particles self-associate to form large aggregates with estimated weights of 10^4 to 10^5 g/mol and Rg = 43 Å.[16, 17] Thus, the molecular weight and sizes for these four distinct entities have a broad range of variation as shown in Figure 2.5. For archipelago asphaltene molecular structures, the aggregation formation is more complex due to the involvement of rotation of bridge chains to optimize conformation allowing π-

π association and the combination between stacking, bridged interactions, and hydrogen bonds. Regrettably, stacking has yet to be proven in solvents or in natural media.

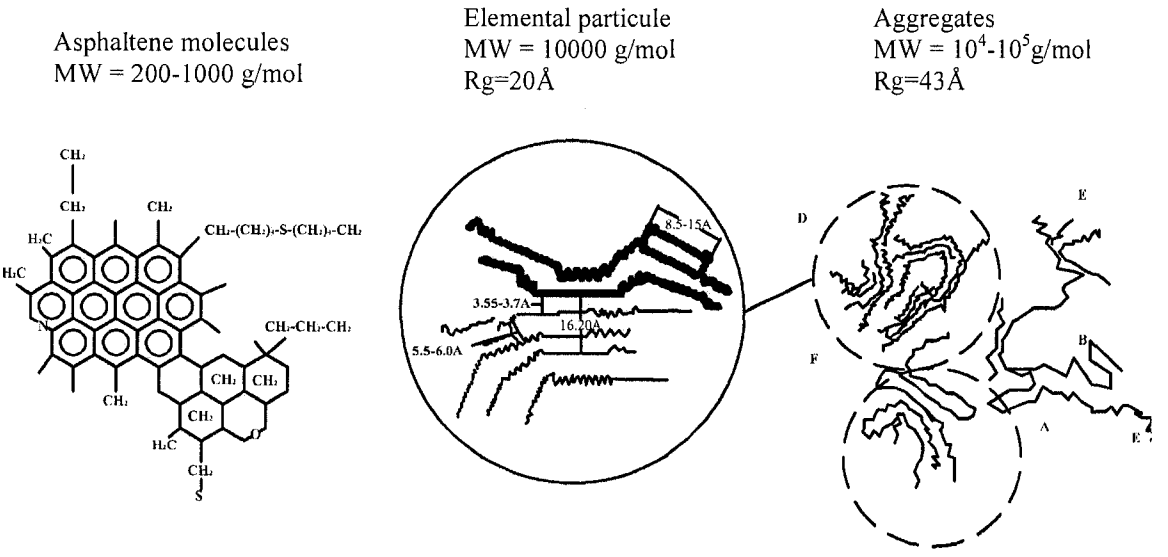

Figure 2.5 Asphaltenes according to Yen's model[14]

The peptization model[18] suggests that in natural media asphaltenes form the center of some micellar entities surrounded and stabilized by resins and then by other constituents of oil. This indicates that a nearly continuous transition exists from the most polar entities (asphaltenes) at the centre of the micelles to the less molar (aliphatic) entities. Once the shortage of resins occurs, the attraction force between micelles results in asphaltene aggregation and eventually leads to extended gel-type structure (Figure 2.6).

The self-assembled aggregates fall into the length scale 0.5 to 100.0 nm. Techniques such as small angle x-ray scattering (SAXS) and small angle neutron scattering (SANS) are readily applicable to characterize the colloidal structures of asphaltene aggregates. In Sheu's recent review,[19] he concluded that the elementary asphaltene particles are about

3.0 nm (gyration radius) and do not increase upon increasing asphaltene concentration. The conclusion that asphaltene aggregate size is an independent function of concentration leads to the structural evolution. However, these elementary particles may further aggregate. Elementary particles retain their integrity within intraparticle structures.

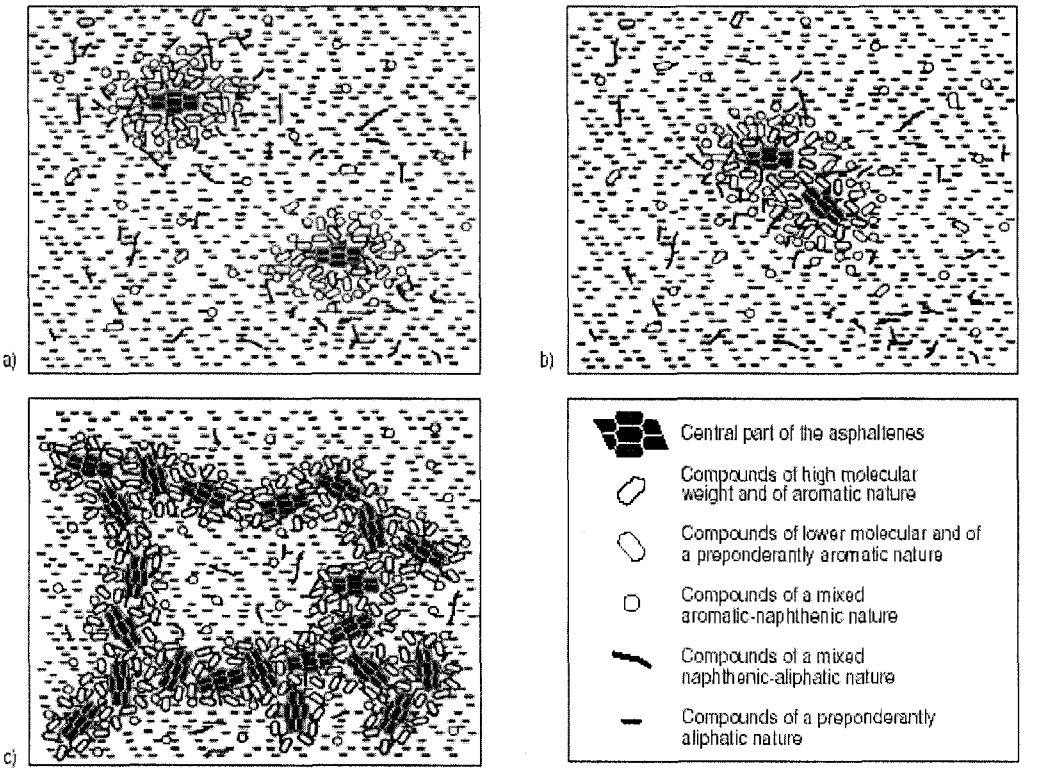

Figure 2.6 Illustration of peptization model[18] of asphaltene molecules in natural media a) peptized asphaltenes, b) asphaltene aggregates, c) gel structure due to aggregation.

Asphaltene aggregation is influenced by many factors, such as asphaltene concentration, temperature, pressure, and solvents. At lower asphaltene concentration and in a good solvent, asphaltene entities may dissociate. Castillo et al[20] strongly suggest that the colloidal approach should be used to represent solutions of asphaltenes and the

combination of low solubility and packing should be considered for the asphaltene colloidal structure and behavior. They suggest that the colloidal particles are composed of a series of layers with solubility and packing capacity decreasing from the core with the well-packed insoluble fractions A_1 impervious to the solvents to the periphery with the loosely packed fractions (low soluble fraction A_2, 1 g/L and high soluble fraction A_3, 57 g/L) in which solvents or media can penetrate and help to disperse the colloidal particles. Solubility behavior is a collective property of these three fractions. The adsorption isotherms of asphaltenes on glass and silica in toluene exhibit a step-wise adsorption. The adsorption of free asphaltene molecules and small asphaltene aggregates forms the first layer. After the first layer is saturated, the second or more layers can be formed. The analysis of the first layer suggests the aggregation of asphaltene in toluene begins at very low concentration (less than 100 mg/L). These data and results are consistent with a sequential aggregation process rather than a process of micelle formation with a sharp change above critical micellar concentration (CMC).

Though experimental data can be gathered to support the colloidal nature of asphaltenes in the solution or natural media and the colloidal and micellar models for asphaltenes have been applied to explain some phenomena, other arguments and data cast doubt on the colloidal or micellar concept for asphaltenes. Isothermal titration calorimetry has been widely used in surfactant science to determine the CMC. The concentration interval could be divided into three regions: monomer region, micellation region, and micelle region. The coincidence of the absence of the first region (monomer) in the concentration range for measuring CMC and the usually reported CMC region of asphaltenes in the literature falling in first region indicates that CMC concept is not

appropriate for asphaltene self-association. A step-wise association mechanism of asphaltenes, contrary to micelle formation mechanism, is proposed based on calorimetric measurements.[21] The driving force of association is found to be in aromatics and heteroatomic nature of asphaltenes. This is not in disagreement with the fact that the aggregates may end up having a definite size. The final size of aggregation is reached by steric hindrance from the alkyl branches of asphaltenes.

Sirota[22] argues that the concept of colloidal structure of asphaltenes in solution or natural media is overused. He argues that one of the distinguishing features of micellar aggregation is the formation of specific structure based on the geometry of molecules. Thus, there is a well defined aggregation number. For polydisperse system, the variation of number of molecules in each micelle leads to a finite mean value of the aggregate size distribution (typically larger than 20) and the aggregate size distribution should be highly bimodal. However, no such evidence is found. He believes that asphaltenes are molecules with high solubility parameter and moderately high molecular weight. The behavior of asphaltenes is similar to that of other miscible liquids in the vicinity of phase separation. Phase separation is thermodynamically liquid-liquid phase separation. The solid-like character of asphaltene enriched phase is due to the fact that the material in the heavier phase is below its glass transition temperature. At high temperature, the precipitation of asphaltenes result from the solubility difference between asphaltenes and the rest of the fluid caused by the different decreasing rate upon temperature (rather than the strong response of solubility compared to the adsorption ability of resins to temperature), which can overcome the enhanced entropy of mixing and promote the system to phase separation. The fractal like structure of precipitated asphaltenes is due to the high

viscosity, which prevents them from condensing into a low-surface-area morphology. The high viscosity of bitumen and asphaltene containing mixtures is related to their proximity to the glass transition.

2.2.3 Asphaltene property summary

Asphaltene molecular and supra-molecular structures are complex and the subject of ongoing debate. The only certainty, given their operational definition, is that the amount of asphaltenes recovered, by standard solvent separation methods, increases sharply when filter pore sizes are decreased. In this thesis, a key objective is to determine whether asphaltene aggregates can be filtered directly from their native heavy oil media without dilution. If this is possible, do the structures obtained by physical separation resemble those identified by solvent separation? Do they support or refute one or more of the aggregation models cited above? For example, if the asphaltene-rich retentates are not enriched in resins, the peptization model is refuted, at least under the conditions of the filtration measurements.

2.3 Coke deposition

2.3.1 Hydroprocessing catalysts

Hydroprocessing catalysts are quite versatile and exhibit activities for various important reactions: hydrodesulfuriztion (HDS), hydrodenitrogenation (HDN), hydrodemetallization (HDM), and aromatic hydrogenation (HYD) reactions. Usually

these catalysts consist of active Mo supported on a high surface area carrier, most commonly alumina, and promoted by nickel or cobalt. The supports usually have a high surface area, ~ 200 m^2/g, consisted of transition-alumina, or silica-alumina or zeolite for hydrocracking. The average pore size is generally in the range from 0.3 to 10.0 nm. Pore size distributions vary. For HDM catalysts, macropores may be present and the catalysts tend to possess bimodal pore structures.

These catalysts are active in the sulfided state, either presulfided or sulfided on stream. A monolayer slab or clusters of slabs of MoS_2 partially cover the alumina surface. The slab is small and roughly in a hexagonal shape. Due to the smaller size, a considerable fraction of sulfur anion will be absent at the edge of the slab to create vacancies. These coodinatively unsaturated sites, which are thought to be the active sites for catalytic reactions, have Lewis acid character and can absorb molecules with unpaired electrons, such as NO, pyridine. The presence of Co or Ni does not increase the number of vacancies appreciably, but the vacancies associated with Co or Ni are more active than those associated with Mo, leading to the promotion of the activity of the catalyst. The vacancy concentration under hydroprocessing conditions is thought to be a function of H_2 and H_2S concentration.

Hydroprocessing reactions occur on the active sites of catalysts. Any interference of a reactant access to active sites reduces catalyst activity. There is broad agreement that the rapid initial coke deposition during the first stage of catalyst deactivation in hydroprocessing is due to asphaltenes sorption on the most acidic sites of the catalyst. Both Lewis and Bronsted acid sites may take part during coking.[23] Lewis acid sites facilitate the strong interaction with basic species in the feed, whereas Bronsted acid sites

promote the formation of carbonium cations by supplying protons, which is responsible for coking.[24] Lewis and Bronsted acid sites are associated with the catalyst active phase, whereas only Lewis sites are present on alumina supports.[25] It was well established that coking increases with acidity of the surface and/or increasing basicity of the precursor.[23] Less coke is produced by replacing α-alumina supports with more acidic γ-alumina supports,[26] or by replacing alumina supports with carbon supports,[27] or by neutralizing $CoMo/Al_2O_3$ to Na_2MoO_4/Al_2O_3.[28] Preferential adsorption of Safaniya asphaltenes[28] were observed on sulphided $CoMo/Al_2O_3$ catalyst at room temperature. The enhanced nitrogen content of deposits[29, 30] indicated that the nitrogen containing groups in asphaltene molecules are primarily responsible for the preferential adsorption of asphaltenes.

Poisoning of active sites by adsorbing basic chemical compounds is irreversible and reduces the number of active sites. Sintering causes the surface area to decrease dramatically. Pore mouth plugging prevents reactants from accessing still active sites inside micropores. Pore mouth restriction does not block access completely, however the narrowed channel makes diffusion more difficult and reaction rates become diffusion limited. Coke deposition is the main reason for catalyst deactivation in hydroprocessing of heavy residues. The deactivation caused by coke deposition is reversible. Deactivated catalyst can be recovered by controlled combustion.

2.3.2 Coke formation chemistry

The link between coke formation and asphaltenes as opposed to other SARA fractions in feeds is well known.[31] Many researchers have tried to understand the mechanism of coke formation through chemical nature of carbonaceous deposits and the feed stocks.

Eberly et al.[32] using infrared spectroscopy showed that coke deposits are highly condensed carbon-rich (hydrogen-deficient) aromatics. Appleby et al.[23] systematically studied coke formation with a series of cracking experiments involving paraffinic, naphthenic, aromatic, and heterocyclic hydrocarbons on a synthetic silica-alumina zirconia or a synthetic silica-alumina catalyst. Their experiments with light hydrocarbons such as n-butane, n-butene and 1,3-butadiene showed clearly that unsaturated paraffins formed significantly more coke than saturated paraffin and that these light hydrocarbons with lower molecular weight could form higher-boiling and higher molecular weight products and coke by polymerization and dehydro-cyclization reactions. They also established a relationship between coke formation and compounds with polynuclear aromatic rings. For example, coke formation is more significant for compounds with polyaromatic rings than for compounds having bridge linked rings. Subtle structural differences among polyaromatics could cause striking differences in coke deposition. They also found that heterocyclics produced less coke than their hydrocarbon analogs. Overall, their work suggests that coke precursors form coke via polymerization or dehydrogenation reactions.

Studies of hydrogen transfer reactions assessed with tagged 1-butene with decalin and tetrolin[33, 34] show that coke forms most rapidly when a hydrogen acceptor (such as an olefin) is present to remove hydrogen from the adsorbed material. The hydrogen transfer mechanism[35] was studied with radioactively labeled mixtures of hexane and aromatics over mordenite and Y-zeolites at 100-150 psi hydrogen pressures. The authors suggested the initial coke formation reaction from paraffin-aromatic mixtures over large pore of

zeolites is via alkylation of the aromatics, they also assigned a major role to hydrogen transfer during the continuing transformation of deposits to coke.

Others[36] argue that organic bases in feedstock are the predominant cause of deactivation of cracking catalysts. The activity was found to decline exponentially with the amount of base on the catalyst, but no correlation between activity and the amount of coke on the surface was observed. Their experiments also showed that the active area of the catalyst was only a small part of the total surface area and the catalyst surface was non-uniform. This observation is in agreement with a newer concept[37] proposed a few years later that carbonaceous deposits comprised strongly chemisorbed inhibitors deactivating the catalyst and harmless carbonaceous materials not affecting catalyst activity. This concept leads to a view that there are two kinds of sites on cracking catalysts: active centers and non-active centers and that the active centers only occupy a small portion. The active centers are not only for cracking reactions but also for coke formation[38]. After coke is formed, the coke may desorb and migrate to non-active centers. Others[39] suggested that coke formed on non-active sites from the main reaction and coke formed on active centres could not desorb under reaction conditions. They conclude that there is no cause-and-effect relationship between the activity and coke deposition.

2.3.3 Coke formation mechanism

Coke formation is the major cause for the deactivation of catalysts used for hydroprocessing heavy oils. In many cases, the mechanism of coke formation is visualized as the result of polymerization of polynuclear compounds in the reaction mixture, shown in Figure 2.7. These hydrogen-deficient carbonaceous material deposits

on catalysts surface to decrease activity either by covering the active sites or by building up to the point of blocking the pore of internal volume of the catalyst, leading to the restriction of the reactants to access to active surface. This polymerization coke formation mechanism illustrates that both light and heavy hydrocarbons could form coke. Experimental support for this mechanism can be found from the coking study of small molecules like butadiene.[40] This study revealed that the formation and the growth of rings mainly involved cyclo-addition through a Diels-Alder reaction. As for heavy oils, the heavy fractions (asphaltenes and resins) present in the feed stocks are not completely evaporated under hydroprocessing conditions and consequently adsorb on catalyst surfaces. As the heat transfer between catalyst particles is poor and the heat transfer between oil and catalyst by partly evaporation or cracking the adsorbed oil is limited, the coated catalyst particles easily adhere to reactor walls to form carbonization centers, and constitute a major contributor to coking.

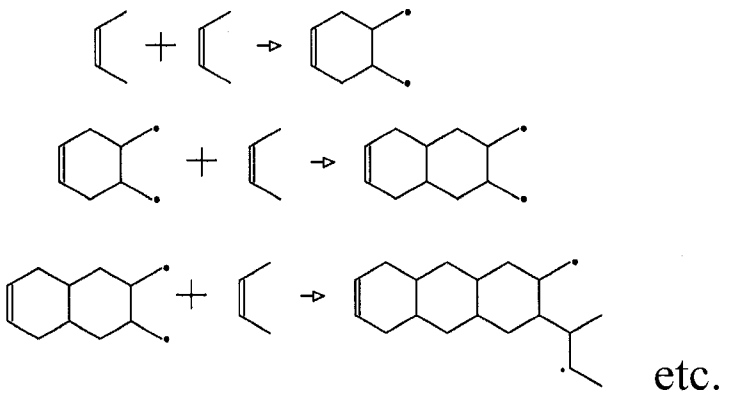

Figure 2.7 Mechanism of coke formation via polymerization-condensation[41]

Some authors[40, 42-44] proposed free radical coke formation mechanism. High temperature favors such a mechanism by enhancing the formation of free radicals. The

initiation of free radical chains usually occurs by heating hydrocarbons or by the reactions of metal ions on unsaturated hydrocarbons. Hydrogen, methyl, and ethyl radicals are the most active species. At the gas/coke interface layer, hydrogen abstraction reactions with the polyaromatics by free radicals from the gas phase can occur. Once the free radicals are formed, the propagation of free radical chains proceeds rapidly. All unsaturated molecules from the gas phase are potential coke precursors. On the coke surface, certain molecules or radicals (coke precursors) react via an addition mechanism at the free radical positions. The long aliphatic side chain of these molecules is subjected to decomposition. The remaining part of the molecule reacts to form a ring structure through dehydrogenation reactions rapidly. Thus, the aromatic structure continues to grow further and the free radical site at the coke surface is regenerated by further hydrogen abstraction. This mechanism is shown in Figure 2.8.

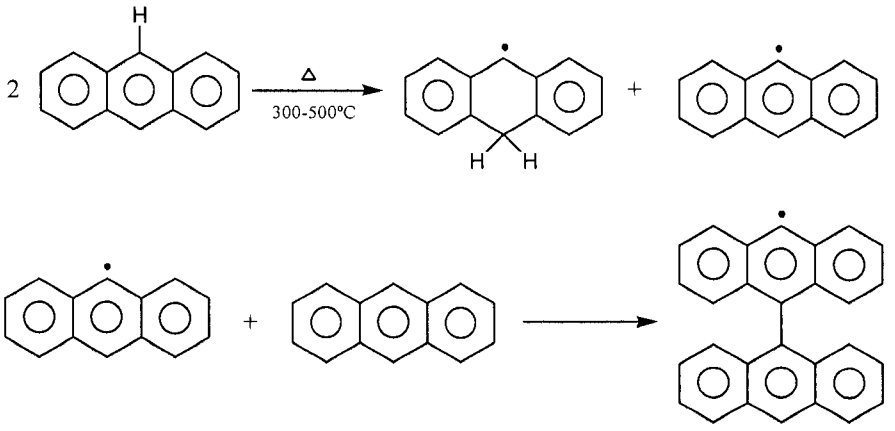

Figure 2.8 Free radical mechanism for formation of coke from anthracene[45]

Another coke formation mechanism involving carbonium ions was proposed by Gates et al.[46] for coking of anthracene. This mechanism is supported by the study of several

model compounds in the present of $CoMo/Al_2O_3$ catalyst.[47] These authors proposed that the carbonium cations were formed by electron transfer between the aromatic and hetero rings and the catalyst surface. Appleby et al.[23] discussed the coke formation in catalytic cracking process through intermediate carbonium ions. The coke forming tendency of many aromatics and their alkyl derivatives increases with their basicity or with the acidity of the surface. Carbonium ions can undergo addition, dehydrogenation and hydrogen transfer to form larger, immobile and tightly absorbed molecules that eventually become coke. Carbonium ions can also crack into small fragments which in turn participate in the coke formation as hydrogen transfer agents.

In processing heavy residues, coke formation is more severe and the mechanism is more complicated due to the presence of the asphaltene fraction where a phase separation coke formation mechanism was proposed.[48] According to this mechanism, thermally unstable bonds, connecting stable polynuclear aromatic cores with pendent chains, are broken off to form free radicals when exposed to high temperature. No coke forms as these free radicals abstract hydrogen from hydroaromatics in the resid and terminate the reaction. However, the scission of the pendent chains makes asphaltene cores less soluble to the surrounded medium. A liquid-liquid phase separation occurs eventually when the solubility limit of asphaltene cores in heptane solubles is exceeded. The asphaltene free radicals combine to form high-molecular-weight and insoluble coke because the asphaltene rich phase has little or no donor hydrogen to be abstracted.

2.3.4 Coke deposition mode

Coke accumulates within catalyst pores. As a result, pore size distributions and diffusion resistance to reactants and products are altered over time. Three principal coke deposition modes have been proposed: uniform surface deposition, pore mouth plugging and bulk-phase coke formation. Each of these modes affects catalyst activity differently.

Uniform surface deposition assumes that coke deposits and spreads uniformly on the internal surface of catalysts. Haldeman and Botty [49] "proved" uniform surface deposition based on the observation that the decreased pore volume corresponded well to the coke volume. Ternan et al.[50] investigated coke formation on a series of laboratory prepared hydrodesulphurization catalysts with various promoters and a commercial counterpart with Athabasca bitumen as feedstock. The observation that two chromium catalysts, which were calcined at different temperature, had markedly different surface areas but very similar coke contents per unit area indicated that the coke was deposited in a consistent and uniform layer. Diez et al.[51] suggested uniform coke layer formed on the hydroprocessing catalysts. They estimated approximately 0.5 nm in thickness corresponding to 3 % carbon on coked catalyst when processing light catalytic cycle oil and 1.1 nm in thickness corresponding to 11 % carbon on coked catalyst when processing coal residuum. The exposure of nickel and molybdenum sulfides measured by XPS was not much different for catalyst containing 3 % carbon and that containing 11 % carbon. They suggested that the active nickel and molybdenum sulfides have the self-cleaning ability to keep them free of coke. Their conclusion was supported by Richardson et al.,[52] who further proposed a physical coke deposition model with an annular coke-free zone around each crystallite due to active hydrogen.

Pore-mouth plugging mechanism is another widely accepted coke deposition mode. It suggests that some local pore mouths can be blocked, isolating interior regions that are presumably still active. Richardson[53] investigated the regeneration of coked catalysts under diffusion-controlled conditions. The cobalt-molybdenum catalysts were deactivated and coked using metal-free coal derived liquids. The results showed that the carbon concentration profile was non-uniform, with approximately 18 % carbon at the exterior of the particle and only about 0.9 % at the center. Lee et al.[54] studied restrictive diffusion under catalytic hydroprocessing conditions with four model compounds having various molecular sizes. Their studies showed the effective diffusivities of these four compounds were less than their corresponding bulk diffusivities and decreased with increasing ratio of molecular diameter to pore diameter. The restrictive effect increased with the buildup of coke deposits and became more significant under reaction conditions. Muegge and Massoth[55-57] studied the effect of coke produced from a model coke precursor, anthracene, on a Ni-Mo catalyst. A relatively small amount of coke located near pore mouths has a large effect on the reactant access to active sites even though its effect on the average pore radius is minimal. A wedge-like coke deposition at pore mouths was proposed to explain the continual decrease in coronene uptake with the coke content and a sharp decline in diffusivity. Johnson et al.[58] studied three different pore sizes of $CoMo/Al_2O_3$ with atmospheric resid. Though complete pore mouth blockage by metals and coke deposits did not occur, wedge-type deposit constricted pore mouths throughout the catalyst particles and had great effect on effective diffusivities in the catalyst.

Another coke deposition mode, bulk phase coke formation, involves more complicated situation. It assumes that coke not only deposits on the internal surface and

causes local pore mouth blockage, but also can form in the bulk liquid phase and deposit on the exterior surface of the catalyst and even on the surface of reactors. Usually it is attributed to the condensation, polymerization, and dehydrogenation. However, an alternative view[48] suggests that coking follows the formation of the mesophase either by liquid-phase separation or by flocculation of asphaltenes. At typical coking temperature (>400°C), asphaltenes are converted to an asphaltene core pseudo-component,[59] also referred to as mesophase embryos,[60] neophases,[61, 62] or mesogens.[63] With their concentration increasing, the incompatibility of the pseudo-components with surrounded medium becomes significant. When the concentration exceeds critical limits, these pseudo-components separate as a second liquid phase and irreversibly polymerize to form particles of mesophase. Initially mesophase particles are very small (~20 nm), but their size can increase and become more than 1μm. Storm et al.,[64] according to the data of dispersed asphaltene sizes and rheological measurements, suggested that coke formation proceeded via the flocculation of asphaltenes at around 200°C, well below the temperatures at which chemical reaction occurred. This flocculated phase is the precursor to the coke-producing phase in the reacting residue. Storm et al.[65] also suggested another explanation through the rheological observation that dispersed droplets of liquid phase formed in the reaction medium. Multiphase behavior and phase-behavior-dependent deposition phenomena have also been observed under hydroprocessing conditions and phase behavior is thought to play an important role for coke formation under these conditions. Richardson et al.[52] observed that coke formed in the liquid phase and blocked the outlet of their reactors. Zhang et al.[66] studied the influence of multiphase behavior on coke deposition on and within commercial hydrotreating catalyst pellets with the model

mixture of Athabasca vacuum residue (ABVB) + decane. The experiments were designed to expose catalyst pellets to specific phases. They concluded that the impact of phase behavior on the amount of coke deposited on and within catalyst pellets and the distribution of coke within catalyst pellets is a secondary factor even though the physical properties of the liquid phases differed significantly.

2.3.5 Coke formation kinetics

An early classic work by Voorhies[67] focused on coke formation as a function of time on stream during catalytic cracking in both fixed and fluidized beds. The proposed equation relating coking to time on stream is given by:

$$C_C = At^n \tag{2.1}$$

where C_C is the weight percent carbon on the catalyst, t is the time on stream, A and n are constants depending on feedstock, reaction condition and reactor type. One distinguishing feature of this simple correlation is that the amount of coke deposited on the catalyst surface after a given time interval appears to be independent of the hydrocarbon feed rate. This direct correlation of coke as a function of time on stream is widely used to represent not only coke but other deactivation processes as well. Another important early work[68] on the activity changes of cracking catalyst in fixed-bed reactors showed rapid deactivation of catalyst under cracking conditions and similar deactivation trends at both higher and lower temperatures. The cracking rate constant increased greatly at higher temperature. The activation energy was about 11 cal/mol after 10 s on stream and became 19 kcal/mol after 2 h. Other work[69] found a strong temperature

dependence of coke formation kinetics in an integral reactor and obtained deactivation and coke formation as a function of time as a Voorhies-type correlation. These models and corresponding proposed equations are more applicable to cracking catalysts. The trend for the effect of coke on the loss of activity is more linear than for hydroprocessing catalysts. In these cases, the catalyst particle sizes are significantly smaller and the contact time is much shorter than for hydroprocessing catalysts.

Massamune and Smith[70] assumed three types of fouling mechanism: series fouling, parallel fouling and independent fouling, which can be represented as below:

Series fouling: $A \rightarrow P \rightarrow C$

Parallel fouling: $\begin{cases} A \rightarrow P \\ A \rightarrow C \end{cases}$

Independent fouling: $S \rightarrow C$

where A, P, S, and C are the reactant, the product, the impurity, and the coke, respectively. Absi-Halabi et al.[41] derived the first order rate expressions for the corresponding fouling reactions:

Series fouling: $\frac{dq}{dt} = k_{Pf} C_P \left(1 - \frac{q}{q_0}\right)$ (2.2)

Parallel fouling: $\frac{dq}{dt} = k_{Af} C_A \left(1 - \frac{q}{q_0}\right)$ (2.3)

Independent fouling: $\frac{dq}{dt} = k_{Sf} C_S \left(1 - \frac{q}{q_0}\right)$ (2.4)

where C_A, C_P, and C_S are concentrations of A, P and S, k_{Af}, k_{Pf}, and K_{Sf} are rate constants for the series, parallel and independent fouling, respectively, q and q_0 the amount of coke at time t and that corresponds to complete deactivation, respectively.

Calculations with these models reveals that deactivation is least for series fouling when diffusion resistance is lowest for the main reaction; for parallel fouling, catalyst with some diffusion resistance are more stable for long processing time; and for independent fouling, the deactivation is least when the diffusion resistance of the main reaction is a minimum and that of the foulant is a maximum.

Richardson et al.[52] developed a model to predict coke formation during the initial stages of hydroprocessing of heavy feeds based on their proposed physical model that coke deposits uniformly with an annular coke-free zone around each crystallite due to active hydrogen. It assumed that most of coke originates from the asphaltenes in the feed and the maximum coke equals to monolayer coverage. The derived first order kinetic equation is:

$$C = C_{\max}(1 - e^{-kw}) \tag{2.5}$$

where C is the actual amount of carbon on the catalyst; $C_{\max}$ is the maximum monolayer carbon deposition; w is the cumulative feed to catalyst ratio and k is an adsorption constant. The model agrees with the experimental data very well. This model also took into consideration the physical structure change of the aged catalyst, i.e. surface area, pore size distribution, and pore volume. The effect of these structure changes on diffusion is estimated from the following equation:

$$\frac{D_{e,C}}{D_{e,f}} = \frac{\varepsilon_C}{\varepsilon_f} e^{-(\lambda_C - \lambda_f)} \tag{2.6}$$

where D_e, ε, and λ are diffusivity, pellet porosity, and the ratio of molecule size to pore size, respectively, and subscripts C and f are for coked and fresh catalysts, respectively. The predicted ratio of the diffusivity of the coked catalyst to the diffusivity of the fresh

catalyst decreases rapidly below a pore radius of approximately 8 nm, reaching 0.06 at 2 nm. This coincided with the observation that the pore size distribution for coked catalyst showed a peak at approximately at 2 nm. This suggests that the feed molecules may be excluded from pores with radius smaller than 2 nm.

A Langmuir-Hinshewood type kinetic equation was developed by de Jong[71, 72] in his investigation of coke formation during hydroprocessing of a vacuum gas oil. The equation takes into account of both thermal and catalytic sources of coke. In this case, thermal coke originates from condensation of aromatic radicals whereas catalytic coke results from dehydrogenation reactions. The equation is represented as:

$$R_C = \frac{k_C K_{ads} C_q}{1 + K_{ads} C_q} \tag{2.7}$$

where C_q is the concentration of coke precursor, K_{ads} is the equilibrium adsorption constant, and k_C is the rate constant dependent on the amount of the coke on the catalyst, which can be obtained from the following equation:

$$k_C = k_{C,0}\left(1 - \frac{D}{D_{C,\max}}\right) \tag{2.8}$$

where D is the amount of coke deposition, $D_{C,\max}$ is estimated by extrapolation of the steady-state coke time curve to zero time.

2.3.6 Coke deposition summary

Coke deposition has been investigated from a number of perspectives, from chemistry to kinetics. No reports appear to be available where asphaltene aggregate size is explored as a variable. From the survey above, coke deposition amounts and modes are expected to

relate to the relative size of asphaltene aggregates and catalyst pores. The impact of this variable will be explored in the thesis. As the minimum nanofilter pore size is 5 nm and the average pore size in the targeted hydrotreating catalyst is 3 nm, a fraction of the asphaltenes are expected to experience diffusion limited penetration within catalyst pellets and this topic is addressed explicitly in the next section.

2.4 Restrictive diffusion

2.4.1 Diffusion in catalysts

The effective diffusivity in porous catalysts is related to the bulk diffusivity by the following equation:

$$D_e = \frac{D_b \varepsilon}{\tau} \tag{2.9}$$

where D_e is the effective diffusivity, D_b is the bulk diffusivity in free solution, ε is the porosity, and τ is the tortuosity of the catalyst. When the diffusing molecule size approaches the catalyst pore size, the effective diffusivity becomes less than predicted by Equation 2.9. To account for the restrictive effect, a restrictive factor $F(\lambda)$ independent of pressure[73] is added into Equation 2.9:

$$D_e = \frac{D_b \varepsilon}{\tau} F(\lambda) \tag{2.10}$$

The restrictive factor is a function of λ, the molecule-to-pore size ratio. When diffusing molecules are not spherical, critical molecular diameter[74] and the average molecular diameter[75] are both proposed to represent the molecular size. The critical molecular diameter is found to give the best correlations for restrictive diffusion[76].

Empirical expressions for $F(\lambda)$ have been developed based on experimental data of liquid diffusion in porous materials. Satterfield et al.[77] proposed the equation as below:

$$F(\lambda) = e^{-4.6\lambda} \tag{2.11}$$

Chantong and Massoth[57] proposed a similar expression for $F(\lambda)$ based on their study with polyaromatic compounds using aluminas of various pore sizes:

$$F(\lambda) = 1.03e^{-4.5\lambda} \tag{2.12}$$

Beck and Schultz[78] proposed the following simple expression for $F(\lambda)$ in the region of $\lambda < 0.3$ within 6.3% average error:

$$F(\lambda) = (1-\lambda)^4 \tag{2.13}$$

However, these proposed expressions for $F(\lambda)$ were based on the experiments conducted under ambient condition. Lee et al.[54] studied the restrictive diffusion in three Ni-Mo/alumina catalysts under catalytic hydroprocessing conditions (at 623 K and 5.27 MPa of hydrogen partial pressure) with four nitrogen-containing heterocyclic model compounds (indole, 9-phenylacridine, nickel tetraphenyl porphyrin, and nickel tetra-4-bi-phenylyl porphyrin) dissolved in decalin. The molecule-to-pore size ratios were in a range of 0.03 to 0.35. They obtained the empirical correlation for $F(\lambda)$ expressed as below:

$$F(\lambda) = (1-\lambda)^{4.9} \tag{2.14}$$

The power 4.9 is higher than 4 in the expression proposed under ambient condition. This suggests that the restrictive effect under reaction conditions is larger than that at ambient and non-reaction conditions. The buildup of coke deposits decreases pore mouths rapidly and results in an increase in restrictive effect. Other factors, like bimodal pore size

distributions in catalysts and counter diffusion of reactants and products, may also influence the restrictive factor.

Besides λ, solvent can also play an important role in restrictive diffusion by altering the adsorption behavior of the solute in pores. For a particular λ, effective diffusivity is smaller for a strong adsorbing solute than for a nonadsorbing solute. In other words, the effective diffusivity of a solute would be higher if the solvent has strong adsorption strength. The solvent effect on restrictive diffusion has been investigated[74, 75] for a variety of solute-to-solvent systems in liquid-filled pores under nonreactive conditions at ambient temperature. The experimental results showed that effective diffusivity was also dependent on the equilibrium partition coefficient K_P, a ratio of solute concentration within the porous material to that in the bulk solution. They suggested that this coefficient should be incorporated into the correlation of restrictive factor to take into account of the adsorption strength.

Temperature can influence the restrictive diffusivity by altering bulk diffusivity and adsorption strength. The restrictive diffusivity has been found to increase at elevated temperature under nonreactive conditions.[73, 79] One explanation[79] is that the increasing temperature reduced the adsorption strength of solute, resulting in the increase in effective pore size. Another explanation is that the diffusing molecules obtain larger kinetic energy at elevated temperature and can easily overcome the energy barrier caused by hydrodynamic drag.

Lee et al.[80] continued their work and studied the temperature and solvent effect on restrictive diffusion under hydroprocessing conditions. Two solvents, decalin and mesitylene, were selected and the reaction temperatures were in the range of 573 K to

623 K. They found the power values for the correlation of restrictive factor were 5.1 at 573 K and 5.0 at 623 K for decalin, and 5.1 at 573 K and 4.4 at 623 K for mesitylene, respectively. These data fell very well into the range of 4.9 ± 0.6 obtained in their previous work.[54] This suggested that the solvents and the temperatures used in their study had little effect on restrictive diffusion under reaction condition. The relatively lower power value for mesitylene solvent at 623 K was attributed to the reaction temperature approaching to the solvent critical temperature, where the solvent behaves as a gas-like fluid with a significant reduction of viscosity. The authors suggested that employing a solvent with a relatively low critical temperature and operating the catalytic reactor at a temperature just below the solvent critical temperature should be an effective way to reduce the restrictive effect. Other researchers[81] found that the diffusion coefficient in the supercritical fluid state was about an order of magnitude larger than in the liquid state.

2.4.2 Effect of restrictive diffusion

Commercial hydroprocessing catalyst pellets foul rapidly in the presence of asphaltenes. Asphaltene aggregate sizes distribute broadly both in natural media or in any artificial mixtures diluted by various solvents and the size distribution depends on the nature of the feed.[82-84] Asphaltenes must penetrate into catalyst pores in order for metals (Ni and V) and heteroatom (S and N) to be removed during hydroprocessing. However, a significant size overlap is found between experimental size ranges for asphaltene aggregates, several nanometers to several hundreds nanometers,[82-85] and the pore size distribution of commercial hydroprocessing catalyst, ranging from 0.3 nm to over 10.0 nm.[86] The size overlap is a key factor for hindered/restrictive diffusion, which happens

during heavy oil hydroprocessing. Furthermore, with coke and metal deposition, pore structures of catalysts change greatly in surface area, pore volume, porosities, tortuosity, pore size distribution, active site accessibility, and adsorption capacities, which in turn hinder reactant penetration.

Several studies about the effect of porous materials on asphaltene diffusion have been conducted. Baltus and Anderson[87] studied the transport of asphaltenes extracted from Kuwait atmospheric residue through a microporous membrane with a narrow pore size distribution. The study showed strong dependence of diffusion rate on asphaltene size. Various constituents of asphaltene subfractions have an order of magnitude difference in their bulk phase diffusion coefficient. The transport of asphaltenes through membranes has been modeled.[88] Individual asphaltene molecules were approximated as spheroids and hindered diffusivities were calculated. Results showed that the diffusion coefficients decreased with increasing molecular weight (MW) and decreased more for constricted pores. The calculated asphaltene diffusivities were of the same order of magnitude as the experimental results.[87, 89]

Adsorptive uptake experiments[90] were investigated at 308 K with coal and petroleum asphaltenes in a $NiMo/Al_2O_3$ hydrotreating catalyst with tetrohydrofuran as a solvent. The uptake rates for individual asphaltene fractions with different molecular weights differed greatly. Sane et al.[89] summarized their work and strongly suggested that the polydisperse and dynamic nature of asphaltenes should be incorporated in asphaltene diffusion modeling for residue upgrading.

The inverse question i.e. the effect of coke deposition on pore structure and self-diffusion in deactivated industrial hydroprocessing catalysts was also investigated[91] using

pulsed-field gradient-nuclear magnetic resonance with pentane and heptane as probes. The effective diffusivity showed a strong correlation with coke content of the deactivated catalysts due to the large decrease in porosity. The reduction of effective diffusivity associated with coke deposition led to an increase in Thiele modulus up to 40 % and a decrease in effectiveness factor up to 10 %. The surprisingly high estimation of tortuosity illustrated that hindered diffusion was significant for liquid phase diffusion even when the diffusing molecules were considerably smaller than the average pore diameter.

2.4.3 Summary of restrictive diffusion

To summarize, many studies have been done to understand restrictive diffusion in hydroprocessing catalysts, such as coke content, temperature effect, molecule-to-pore size ratio, and the solvent effect. Models have been developed to calculate diffusivities under hydroprocessing conditions. In the present study, asphaltene aggregate penetration into catalyst pellet pores is addressed. From the forgoing, restrictive diffusion effects are anticipated and may dominate. This may prove to be a disadvantage from the perspective of discriminating coke deposition mechanisms, which under diffusion control appear similar, but should not affect discrimination of coke deposition modes although pore mouth plugging appears favored given the relative size of asphaltenes and pores.

2.5 Objectives

The design, construction and commissioning of a nano filtration apparatus suitable for partitioning feed stocks such as Maya crude and Athabasca bitumen at the nano length scale, without solvent addition, comprise the critical first step in the thesis work. Detailed chemical analysis of the permeates and retentates produced, using a variety of standard techniques, comprise the second step. The results should reveal the number and nature of nanostructures present, their respective size distributions, and their connection with expectations. Batch coking experiments and detailed coked catalyst pellet analysis comprise the third step and allow one to address the principal hypothesis of the study. With these results in hand one can tackle the interplay of thermophysical properties more broadly on coking outcomes.

References

(1) Gray, M. R., *Upgrading Petroleum Residues and Heavy Oils*. Dekker, New York: 1994.

(2) Zhao, S.; Kotlyar, L. S.; Woods, J. R.; Sparks, B. D.; Hardacre, K.; Chung, K. H., Molecular Transformation of Athabasca Bitumen End-Cuts during Coking and Hydrocracking. *Fuel* **2001,** 80, (8), 1155-1163.

(3) Leon, O.; Rogel, E.; Espidel, J.; Torres, G., Asphaltenes: Structural Characterization, Self-Association, and Stability Behavior. *Energy & Fuels* **2000,** 14, (1), 6-10.

(4) Carauta, A. N. M.; Seidl, P. R.; Chrisman, E.; Correia, J. C. G.; Menechini, P. D.; Silva, D. M.; Leal, K. Z.; de Menezes, S. M. C.; de Souza, W. F.; Teixeira, M. A. G., Modeling Solvent Effects on Asphaltene Dimers. *Energy & Fuels* **2005,** 19, (4), 1245-1251.

(5) Ancheyta, J.; Centeno, G.; Trejo, F.; Marroquin, G., Changes in Asphaltene Properties during Hydrotreating of Heavy Crudes. *Energy & Fuels* **2003,** 17, (5), 1233-1238.

(6) Groenzin, H.; Mullins, O. C., Molecular Size and Structure of Asphaltenes from Various Sources. *Energy & Fuels* **2000,** 14, (3), 677-684.

(7) Strausz, O. P.; Mojelsky, T. W.; Lown, E. M., The Molecular-Structure of Asphaltene - an Unfolding Story. *Fuel* **1992,** 71, (12), 1355-1363.

(8) Ali, F. A.; Ghaloum, N.; Hauser, A., Structure Representation of Asphaltene GPC Fractions Derived from Kuwaiti Residual Oils. *Energy & Fuels* **2006,** 20, (1), 231-238.

(9) Sheremata, J. M.; Gray, M. R.; Dettman, H. D.; McCaffrey, W. C., Quantitative Molecular Representation and Sequential Optimization of Athabasca Asphaltenes. *Energy & Fuels* **2004,** 18, (5), 1377-1384.

(10) Murgich, J.; Abanero, J. A.; Strausz, O. P., Molecular Recognition in Aggregates Formed by Asphaltene and Resin Molecules from the Athabasca Oil Sand. *Energy & Fuels* **1999,** 13, (2), 278-286.

(11) Gray, M. R., Consistency of Asphaltene Chemical Structures with Pyrolysis and Coking Behavior. *Energy & Fuels* **2003,** 17, (6), 1566-1569.

(12) Artok, L.; Su, Y.; Hirose, Y.; Hosokawa, M.; Murata, S.; Nomura, M., Structure and Reactivity of Petroleum-Derived Asphaltene. *Energy & Fuels* **1999,** 13, (2), 287-296.

(13) Zhao, Y. X.; Gray, M. R.; Chung, K. H., Molar Kinetics and Selectivity in Cracking of Athabasca Asphaltenes. *Energy & Fuels* **2001,** 15, (3), 751-755.

(14) Yen, T. F.; Erdman, J. G.; Pollack, S. S., Investigation of Structure of Petroleum Asphaltenes by X-Ray Diffraction. *Analytical Chemistry* **1961,** 33, (11), 1587-1594.

(15) Brandt, H. C. A.; Hendriks, E. M.; Michels, M. A. J.; Visser, F., Thermodynamic Modeling of Asphaltene Stacking. *Journal of Physical Chemistry* **1995,** 99, (26), 10430-10432.

(16) Ravey, J. C.; Ducouret, G.; Espinat, D., Asphaltene Macrostructure by Small-Angle Neutron-Scattering. *Fuel* **1988,** 67, (11), 1560-1567.

(17) Fenistein, D.; Barre, L.; Broseta, D.; Espinat, D.; Livet, A.; Roux, J. N.; Scarsella, M., Viscosimetric and Neutron Sattering Study of Asphaltene Aggregates in Mixed Toluene/Heptane Solvents. *Langmuir* **1998,** 14, (5), 1013-1020.

(18) Pfeiffer, J. P.; Saal, R. N. J., Asphaltic Bitumen as Colloid System. *Journal of Physical Chemistry* **1940,** 44, (2), 139-165.

(19) Sheu, E. Y., Small Angle Scattering and Asphaltenes. *Journal of Physics-Condensed Matter* **2006,** 18, (36), S2485-S2498.

(20) Castillo, J.; Fernandez, A.; Ranaudo, M. A.; Acevedo, S., New Techniques and Methods for the Study of Aggregation, Adsorption, and Solubility of Asphaltenes. Impact of These Properties on Colloidal Structure and Flocculation. *Petroleum Science and Technology* **2001,** 19, (1-2), 75-106.

(21) Merino-Garcia, D.; Andersen, S. I., Calorimetric Evidence about the Application of the Concept of CMC to Asphaltene Self-Association. *Journal of Dispersion Science and Technology* **2005,** 26, (2), 217-225.

(22) Sirota, E. B., Physical Structure of Asphaltenes. *Energy Fuels* **2005,** 19, (4), 1290-1296.

(23) Appleby, W. G.; Good, G. M.; Gibson, J. W., Coke Formation in Catalytic Cracking. *Industrial & Engineering Chemistry Process Design and Development* **1962,** 1, (2), 102-110.

(24) Furimsky, E., Deactivation of Molybdate Catalysts by Nitrogen Bases. *Erdol & Kohle Erdgas Petrochemie* **1982,** 35, (10), 455-459.

(25) Ho, T. C., Hydrodenitrogenation Catalysis. *Catalysis Reviews-Science and Engineering* **1988,** 30, (1), 117-160.

(26) Trimm, D. L.; Akashah, S.; Absi-Halabi, M.; Bishara, A., *Studies in Surface Science and Catalysis*. Elsevier, Amsterdam: 1990; Vol. 53, p 179.

(27) Mochida, I.; Inoue, S.; Maeda, K.; Takeshita, K., Carbonization of Aromatic-Hydrocarbons 6. Carbonization of Heterocyclic-Compounds Catalyzed by Aluminum-Chloride. *Carbon* **1977,** 15, (1), 9-16.

(28) Faus, F. M.; Grange, P.; Delmon, B., Influence of Asphaltene Deposition on Catalytic Activity of Cobalt Molybdenum on Alumina Catalysts. *Applied Catalysis* **1984,** 11, (2-3), 281-293.

(29) Furimsky, E., Chemical Origin of Coke Deposited on Catalyst Surface. *Industrial & Engineering Chemistry Product Research and Development* **1978,** 17, (4), 329-330.

(30) Thakur, D. S.; Thomas, M. G., Catalyst Deactivation during Direct Coal-Liquefaction - a Review. *Industrial & Engineering Chemistry Product Research and Development* **1984,** 23, (3), 349-360.

(31) Banerjee, D. K.; Laidler, K. J.; Nandi, B. N.; Patmore, D. J., Kinetic-Studies of Coke Formation in Hydrocarbon Fractions of Heavy Crudes. *Fuel* **1986,** 65, (4), 480-484.

(32) Eberly, P. E.; Kimberli.Cn; Miller, W. H.; Drushel, H. V., Coke Formation on Silica-Alumina Cracking Catalysts. *Industrial & Engineering Chemistry Process Design and Development* **1966,** 5, (2), 193-198.

(33) Blue, R. W.; Engle, C. J., Hydrogen Transfer over Silica-Alumina Catalysts. *Industrial and Engineering Chemistry* **1951,** 43, (2), 494-501.

(34) Holm, V. C. F.; Blue, R. W., Hydrogen-Deuterium Exchange Activity of Silica-Alumina Catalysts. *Industrial and Engineering Chemistry* **1951,** 43, (2), 501-505.

(35) Walsh, D. E.; Rollmann, L. D., Radiotracer Experiments on Carbon Formation in Zeolites. *Journal of Catalysis* **1977,** 49, (3), 369-375.

(36) Mills, G. A.; Boedeker, E. R.; Oblad, A. G., Chemical Characterization of Catalysts .1. Poisoning of Cracking Catalysts Nitrogen Compounds and Potassium Ion. *Journal of the American Chemical Society* **1950,** 72, (4), 1554-1560.

(37) Prater, C. D.; Lago, R. M., The Kinetics of the Cracking of Cumene by Silica-Alumina Catalysts. *Advances in Catalysis* **1956,** 8, 293-339.

(38) Plank, C. J.; Nace, D. M., Coke Formation and Its Relationship to Cumene Cracking. *Industrial and Engineering Chemistry* **1955,** 47, (11), 2374-2379.

(39) Heinemann, H., Dehydrogenation of Methylcyclopentane over Chromia/Alumina Catalysts. *Industrial and Engineering Chemistry* **1951,** 43, (9), 2098-2101.

(40) Nohara, D.; Sakai, T., Kinetic-Study of Model Reactions in the Gas-Phase at the Early Stage of Coke Formation. *Industrial & Engineering Chemistry Research* **1992,** 31, (1), 14-19.

(41) Absi-Halabi, M.; Stanislaus, A.; Trimm, D. L., Coke Formation on Catalysts During the Hydroprocessing of Heavy Oils. *Applied Catalysis* **1991,** 72, (2), 193-215.

(42) Kopinke, F. D.; Zimmermann, G.; Reyniers, G. C.; Froment, G. F., Relative Rates of Coke Formation from Hydrocarbons in Steam Cracking of Naphtha .2. Paraffins, Naphthenes, Monoolefins, Diolefins, and Cycloolefins, and Acetylenes. *Industrial & Engineering Chemistry Research* **1993,** 32, (1), 56-61.

(43) Kopinke, F. D.; Bach, G.; Zimmermann, G., New Results about the Mechanism of the Fouling in Steam Crackers. *Journal of Analytical and Applied Pyrolysis* **1993,** 27, (1), 45-55.

(44) Kopinke, F. D.; Zimmermann, G.; Reyniers, G. C.; Froment, G. F., Relative Rates of Coke Formation from Hydrocarbons in Steam Cracking of Naphtha .3. Aromatic-Hydrocarbons. *Industrial & Engineering Chemistry Research* **1993,** 32, (11), 2620-2625.

(45) Lewis, I. C.; Singer, L. S., Thermal Conversion of Polynuclear Aromatics to Carbon. *American Chemical Society, Division of Petroleum Chemistry (Preprints)* **1986,** 31, (3-4), 834-847.

(46) Gates, B. C.; Katzer, J. R.; Shuit, G. C. A., *Chemistry of Catalytic Processes.* McGraw Hill: New Youk, 1979.

(47) Scaroni, A. W.; Jenkins, R. G., Coking of Aromatics over an HDS Catalyst. *American Chemical Society, Division of Petroleum Chemistry (Preprints)* **1985,** 30, 544-548.

(48) Wiehe, I. A., A Phase-Separation Kinetic-Model for Coke Formation. *Industrial & Engineering Chemistry Research* **1993,** 32, (11), 2447-2454.

(49) Haldeman, R. G.; Botty, M. C., On the Nature of the Carbon Deposit of Cracking Catalysts. *Journal of Physical Chemistry* **1959,** 63, (4), 489-496.

(50) Ternan, M.; Furimsky, E.; Parsons, B. I., Coke Formation on Hydrodesulphurization Catalysts. *Fuel Processing Technology* **1979,** 2, (1), 45-55.

(51) Diez, F.; Gates, B. C.; Miller, J. T.; Sajkowski, D. J.; Kukes, S. G., Deactivation of a Ni-Mo Gamma-Al_2O_3 Catalyst - Influence of Coke on the Hydroprocessing Activity. *Industrial & Engineering Chemistry Research* **1990,** 29, (10), 1999-2004.

(52) Richardson, S. M.; Nagaishi, H.; Gray, M. R., Initial Coke Deposition on a NiMo/gamma-Al_2O_3 Bitumen Hydroprocessing Catalyst. *Industrial & Engineering Chemistry Research* **1996,** 35, (11), 3940-3950.

(53) Richardson, J. T., Experimental Determination of Catalyst Fouling Parameters - Carbon Profiles. *Industrial & Engineering Chemistry Process Design and Development* **1972,** 11, (1), 8-11.

(54) Lee, S. Y.; Seader, J. D.; Tsai, C. H.; Massoth, F. E., Restrictive Diffusion under Catalytic Hydroprocessing Conditions. *Industrial & Engineering Chemistry Research* **1991,** 30, (1), 29-38.

(55) Muegge, B. D.; Massoth, F. E., Basic Studies of Deactivation of Hydrotreating Catalysts with Anthracene. *Fuel Processing Technology* **1991,** 29, (1-2), 19-30.

(56) Chu, K. S.; Hanson, F. V.; Massoth, F. E., Effect of Bitumen-Derived Coke on Deactivation of an HDM Catalyst. *Fuel Processing Technology* **1994,** 40, (1), 79-95.

(57) Chantong, A.; Massoth, F. E., Restrictive Diffusion in Aluminas. *AIChE Journal* **1983,** 29, (5), 725-731.

(58) Johnson, B. G.; Massoth, F. E.; Bartholdy, J., Diffusion and Catalytic Activity Studies on Resid-Deactivated HDS Catalysts. *AIChE Journal* **1986,** 32, (12), 1980-1987.

(59) Storm, D. A.; Barresi, R. J.; Sheu, E. Y.; Bhattacharya, A. K.; DeRosa, T. F., Microphase Behavior of Asphaltic Micelles during Catalytic and Thermal Upgrading. *Energy & Fuels* **1998,** 12, (1), 120-128.

(60) Azami, K.; Yokono, T.; Sanada, Y.; Uemura, S., Studies on the Early Stage of Carbonization of Petroleum Pitch by Means of High-Temperature H-1-Nmr and Esr. *Carbon* **1989,** 27, (2), 177-183.

(61) Li, S. H.; Liu, C. G.; Que, G. H.; Liang, W. J.; Zhu, Y. J., Laboratory Study of Real-Time Optical Microscope Tracking of Thermal Reaction Progress of Vacuum

Residua .1. Physical Processes in Thermal Reaction Systems of Vacuum Residua. *Petroleum Science and Technology* **1997,** 15, (9-10), 959-971.

(62) Li, S. H.; Liu, C. G.; Que, G. H.; Liang, W. J.; Zhu, Y. J., Laboratory Study of Real-Time Optical Microscope Tracking of Thermal Reaction Progress of Vacuum Residua .2. Chemical Relevance of Physical Processes in Thermal Reaction Systems of Vacuum Residua. *Petroleum Science and Technology* **1997,** 15, (9-10), 973-983.

(63) Rodriguez-Reinoso, F.; Santana, P.; Palazon, E. R.; Diez, M. A.; Marsh, H., Delayed Coking: Industrial and Laboratory Aspects. *Carbon* **1998,** 36, (1-2), 105-116.

(64) Storm, D. A.; Barresi, R. J.; Sheu, E. Y., Rheological Study of Ratawi Vacuum Residue in the 298-673 K Temperature-Range. *Energy & Fuels* **1995,** 9, (1), 168-176.

(65) Storm, D. A.; Barresi, R. J.; Sheu, E. Y., Flocculation of Asphaltenes in Heavy Oil at Elevated Temperatures. *Fuel Science & Technology International* **1996,** 14, (1-2), 243-260.

(66) Zhang, X. H.; Chodakowski, M.; Shaw, J. M., Impact of Multiphase Behavior on Coke Deposition in a Commercial Hydrotreating Catalyst under Sedimentation Conditions. *Energy & Fuels* **2005,** 19, (4), 1405-1411.

(67) Voorhies, A., Carbon Formation in Catalytic Cracking. *Industrial and Engineering Chemistry* **1945,** 37, (4), 318-322.

(68) Blanding, F. H., Reaction Rates in Catalytic Cracking of Petroleum. *Industrial and Engineering Chemistry* **1953,** 45, (6), 1186-1197.

(69) Rudershausen, C. G.; Watson, C. C., Variables Affecting Activity of Molybdena-Alumina Hydroforming Catalyst in Aromatization of Cyclohexane. *Chemical Engineering Science* **1954,** 3, (3), 110-121.

(70) Masamune, S.; Smith, J. M., Performance of Fouled Catalyst Pellets. *AIChE Journal* **1966,** 12, (2), 384-394.

(71) de Jong, K. P., Effects of Vapor-Liquid-Equilibria on Coke Deposition in Trickle-Bed Reactors During Heavy Oil Processing .2. Modeling. *Industrial & Engineering Chemistry Research* **1994,** 33, (12), 3141-3145.

(72) de Jong, K. P., Effects of Vapor-Liquid-Equilibria on Coke Deposition in Trickle-Bed Reactors During Heavy Oil Processing .1. Experimental Results. *Industrial & Engineering Chemistry Research* **1994,** 33, (4), 821-824.

(73) Seo, G.; Massoth, F. E., Effect of Pressure and Temperature on Restrictive Diffusion of Solutes in Aluminas. *AIChE Journal* **1985,** 31, (3), 494-496.

(74) Satterfield.C.N.; Colton, C. K.; Pitcher, W. H., Restricted Diffusion in Liquids within Fine Pores. *AIChE Journal* **1973,** 19, (3), 628-635.

(75) Prasher, B. D.; Ma, Y. H., Liquid Diffusion in Microporous Alumina Pellets. *AIChE Journal* **1977,** 23, (3), 303-311.

(76) Tsai, C. H.; Massoth, F. E.; Lee, S. Y.; Seader, J. D., Effects of Solvent and Solute Configuration on Restrictive Diffusion in Hydrotreating Catalysts. *Industrial & Engineering Chemistry Research* **1991,** 30, (1), 22-28.

(77) Satterfield, C. N.; Colton, C. K.; Pitcher, W. H., Restricted Diffusion in Liquids within Fine Pores. *AIChE Journal* **1973,** 19, (3), 628-635.

(78) Beck, R. E.; Schultz, J. S., Hindered Diffusion in Microporous Membranes with Know Pore Geometry. *Science* **1970,** 170, (3964), 1302-&.

(79) Galiasso, R.; Morales, A., Adsorption Mechanism of Boscan Porphyrins on HDM Catalysts .3. Diffusion of Porphyrins. *Applied Catalysis* **1983,** 7, (1), 57-74.

(80) Lee, S. Y.; Seader, J. D.; Tsai, C. H.; Massoth, F. E., Solvent and Temperature Effects on Restrictive Diffusion under Reaction Conditions. *Industrial & Engineering Chemistry Research* **1991,** 30, (4), 607-613.

(81) Paulaitis, M. E.; Krukonis, V. J.; Kurnick, R. T.; Reid, R. C., Supercritical Fluid Extraction. *Reviews in Chemical Engineering* **1983,** 1, (2), 179-250.

(82) Dwiggins, C. W., A Small Angle X-Ray Scattering Study of Colloidal Nature of Petroleum. *Journal of Physical Chemistry* **1965,** 69, (10), 3500-3506.

(83) Dwiggins, C. W., The Study of Colloidal Nature of Petroleum with an Automated Bonse-Hart X-Ray Small Angle Scattering Unit. *Journal of Applied Crystallography* **1978,** 11, (5), 615-619.

(84) Dwiggins, C. W., Absorption Correction and Normalization of X-Ray Small-Angle Scattering Data for Materials Producing Intense Scattering at Extremely Low Angles. *Journal of Applied Crystallography* **1979,** 12, (4), 401-402.

(85) Kim, H. G.; Long, R. B., Characterization of Heavy Residuum by a Small-Angle X-Ray-Scattering Technique. *Industrial & Engineering Chemistry Fundamentals* **1979,** 18, (1), 60-63.

(86) Gray, M. R.; Masliyah, J. H., *Extraction and Upgrading of Oil Sands Bitumen: Intensive short course*. Edmonton, 1998.

(87) Baltus, R. E.; Anderson, J. L., Hindered Diffusion of Asphaltenes through Microporous Membranes. *Chemical Engineering Science* **1983,** 38, (12), 1959-1969.

(88) Ravi-Kumar, V. S.; Tsotsis, T. T.; Sahimi, M., Studies of Transport of Asphaltenes through Membranes Using Hindered Diffusion Theories for Spheres and Spheroids. *Industrial&Engineering Chemistry Research* **1997,** 36, (8), 3154-3162.

(89) Sane, R. C.; Tsotsis, T. T.; Webster, I. A.; Ravikumar, V. S., Studies of Asphaltene Diffusion and Structure and Their Implications for Resid Upgrading. *Chemical Engineering Science* **1992,** 47, (9-11), 2683-2688.

(90) Yang, X. F.; Guin, J. A., Diffusion-Controlled Adsorptive Uptake of Coal and Petroleum Asphaltenes in a $NiMo/Al_2O_3$ Hydrotreating Catalyst. *Chemical Engineering Communications* **1998,** 166, 57-79.

(91) Wood, J.; Gladden, L. F., Effect of Coke Deposition upon Pore Structure and Self-Diffusion in Deactivated Industrial Hydroprocessing Catalysts. *Applied Catalysis a-General* **2003,** 249, (2), 241-253.

3. Experimental

3.1 Filtration experiments

3.1.1 Materials

Three heavy oils, Athabasca vacuum residue (from Canada, abbreviated as ABVB), a 525°C+ boiling fraction comprising 32 wt % asphaltenes, supplied by CANMET; Athabasca bitumen (abbreviated as AB) comprising 18.7 wt % asphaltenes, supplied by Syncrude Canada Ltd.; and Maya crude oil (from Mexico) comprising 16 wt % asphaltenes, supplied by the Mexican Petroleum Institute, were used as received for this study. The compositions of these three feed stocks are summarized in Table 3.1.

3.1.2 Nano-filtration apparatus and procedure

Pall Membralox ceramic membranes were used for nanofiltration. The membranes are 250-mm-long and have an outer diameter of 10 mm and an inner diameter of 7 mm. Ceramic membranes with six different average pore sizes are available. The average pore sizes of the filters, filter materials, and filtration experiments conducted were summarized in Table 3.2. The cumulative pore size distributions for the 20, 50, 100, and 200 nm, courtesy of the Pall Corporation, are shown in Figure 3.1. The size distributions are relatively narrow and the reported nominal pore sizes reflect the midpoints of the pore size distribution.

Table 3.1 Composition of Athabasca vacuum bottom[1], Athabasca bitumen and Maya crude oil

	ABVB	AB	Maya
Elemental analysis, (wt %)			
C	81.7	83.2	84.5
H	9.5	9.7	11.3
N	0.7	0.4	0.3
S	6.9	5.3	3.3
O	-	1.7	1.2
SARA analysis, (wt %)			
saturates	6.8	16.1	31.6
aromatics	42.0	48.5	42.5
resins	19.0	16.8	10.2
asphaltenes	32.2	18.6	15.7
Metal analysis, (wppm)			
Al	734	492	1
Ca	65	163	29
Fe	322	762	4
Ni	137	93	56
V	344	247	263

A schematic of the nanofiltration apparatus is shown in Figure 3.2. At the beginning of an experiment, ~ 200 g of a feed was added to the reservoir. Prior to filtration, the reservoir was purged with nitrogen several times and the whole filtration process was conducted under a nitrogen atmosphere. Filtration temperature was maintained at 473 K for all experiments and the pressure drop over the membrane was kept below 7 bar. The mild temperature was employed to avoid cracking at higher temperature and to reduce viscosity low enough for reasonable filtration speed. ABVB cannot be filtered under the conditions considered here due to its high viscosity. To minimize the impact of filter cake build-up on the filtration process, filtration was halted when ~ 50 g of permeate was

collected. Sorption on the filter surface was a concern but Cheng[2] showed that sorbed layers were ~ 1 nm thick. So only at 5 nm, or possibly 10 nm, would this be an issue.

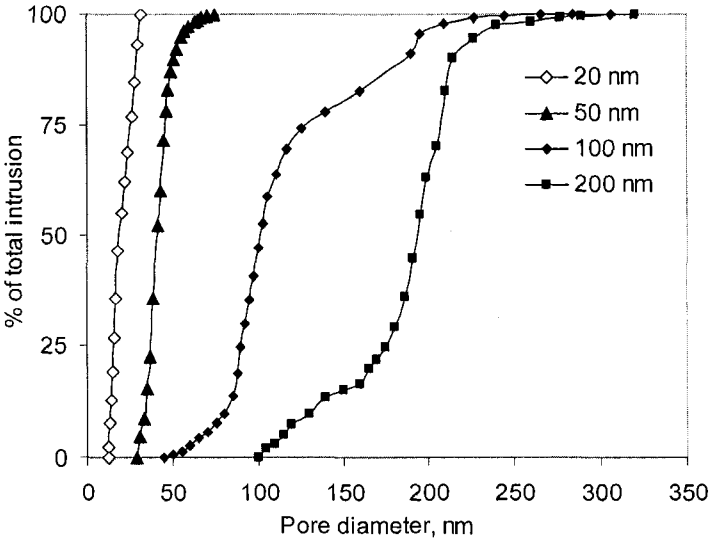

Figure 3.1 Cumulative pore size distributions for membranes

(Courtesy of Pall Corporation)

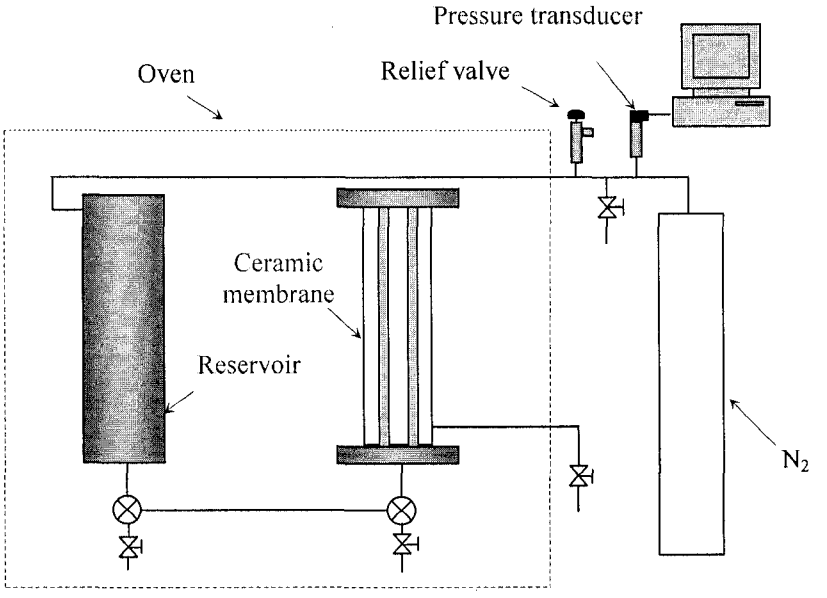

Figure 3.2 Nanofiltration apparatus

The successful filtration and duration are summarized in Table 3.2. Permeates (from the shell side), retentates (from within the membrane tube), and heated feed stocks (from the reservoir) were collected for characterization following each experiment and for later coking experiments.

Table 3.2 Nominal pore sizes, filter materials, and experiments conducted

Membrane pore size	Membrane material	Filtration	
		Heavy oils	Duration
5 nm	γ-alumina	-	-
		Maya crude	6 weeks
10 nm	γ-alumina	Athabasca bitumen	4 weeks
		Maya crude	4 weeks
20 nm	zirconia	Athabasca bitumen	4 weeks
		Maya crude	4 weeks
50 nm	zirconia	Athabasca bitumen	4 weeks
		Maya crude	4 weeks
100 nm	zirconia	Athabasca bitumen	2 weeks
		Maya crude	1 day
200 nm	γ-alumina	Athabasca bitumen	2 weeks
		Maya crude	1 day

This procedure was varied, in order to test whether trace oxygen dissolved or dispersed in Athabasca bitumen influenced the global composition arising from the filtration experiments, or affected subsequent catalyst deposition or rheological measurements. For this investigation, nitrogen was bubbled through a bitumen feed sample for 5 days at 323 K prior to filtration. The regular filtration procedure was then followed. Permeate, retentate, and heated bitumen samples collected from this experiment are designated "oxygen free" in the data tables.

Separate sets of membranes were used for Maya crude oil and Athabasca bitumen to avoid cross-contamination. Membranes were only reused for the same feeds following cleaning. Membrane cleaning comprised soaking a membrane in tetrahydrofuran until the

solution was clear. Then the filter was re-assembled and tetrahydrofuran was fed from the shell side to back-flush the membrane until the solution was clear. Nitrogen was then fed through the filter to remove residual tetrahydrofuran.

3.2 Catalytic coking experiments

3.2.1 Materials

Athabasca vacuum residue, Athabasca bitumen, Maya crude oils, and their filtered samples (permeates and retentates) are used as-is. Chemicals used in this research are listed in Table 3.3, including their suppliers and purity. The catalyst is a commercial 1 mm diameter cylindrical extrudate NiMo/γ-Al_2O_3 catalyst with 10 — 15 wt % MoO_3 and 2 — 4 wt % NiO. The catalyst has a surface area of 219 m^2/g and a pore volume of 0.59 cm^3/g. The pore size distribution and nitrogen sorption isotherm are shown in Figures 3.3 and 3.4.

Table 3.3 Chemicals used in this study and their purity and suppliers

Chemicals	Grade	Purity	Supplier
toluene	HPLC	99.9 + %	Sigma-Aldrich
carbon disulfide	HPLC	99.9 + %	Sigma-Aldrich
1-methylnaphthalene	Regeant	97.0 + %	Acros
n-dodecane	HPLC	99.0 + %	Aldrich
tetrahydrofuran	HPLC	99.9 + %	Sigma-Aldrich
hydrogen	Ultra high purity	99.999 %	Praxair
nitrogen	High purity	99.998 %	Praxair

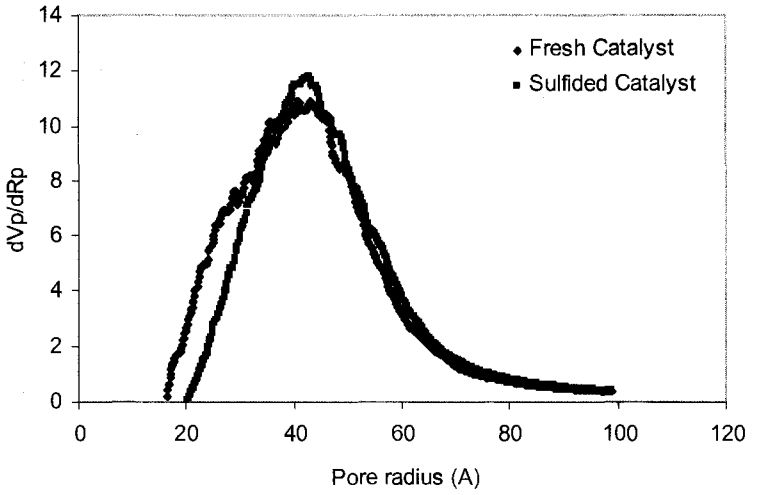

Figure 3.3 Pore size distributions of fresh and sulfided catalyst

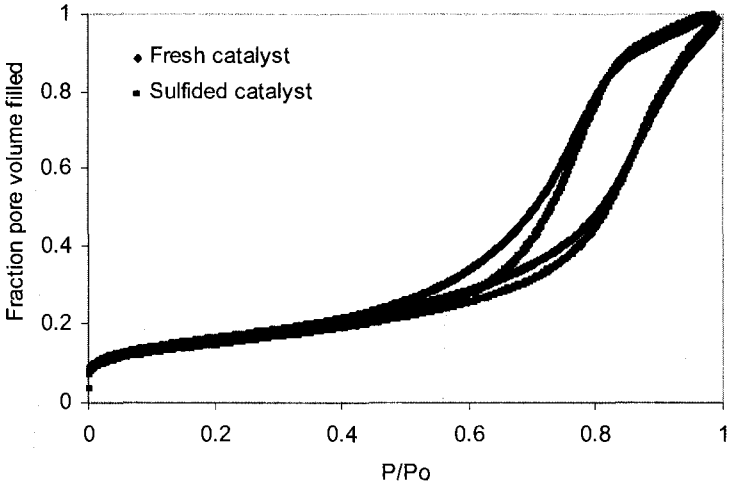

Figure 3.4 Nitrogen sorption isotherms of fresh and sulfided catalyst

3.2.2 Catalyst presulfurization

Commercial hydroprocessing catalyst samples were sulfided before coking experiments. Prior to presulfurization, 150 mg catalyst was desiccated in an oven at 473 k for 2 h. The desiccated catalyst was transferred to a 15 mL micro-batch reactor[3] made from Swagelok stainless tubing and fittings. 50 μL carbon disulfide was added into the

reactor. After purging several times with hydrogen, the sealed micro-batch reactor was pressurized with hydrogen to 81 psi (5.6 bar) at room temperature. The reactor was then put in a fluidized sand bath preheated to 623 K. After 2 h, the reactor was quenched and evacuated.

3.2.3 Catalytic coking experiments

3.2.3.1 Catalytic coking experiments without solvent dilution

The coking experiments were also carried out in the 15 mL micro-batch reactors. For each experiment, 4.5 g of feed (Athabasca bitumen or Athabasca vacuum residue alone, or their respective permeates or retentates) was combined with catalyst in a reactor. The reactor was purged with hydrogen to eliminate air before adjusting the hydrogen pressure to a desired value. The reactor was then immersed in a preheated and fluidized sand bath. The reactor vibrated up and down at approximately 1 Hz for the duration an experiment. The reaction was quenched in a water bath at room temperature. The reaction conditions were: feed to catalyst weight ratio = 30, hydrogen to feed weight ratio = 0 or 0.005, sand bath temperature of 653 K, and a reaction time of 2 h. Catalyst pellets were collected post reaction and extracted with toluene in a micro-Soxhlet extractor for 7 h and dried under vacuum at 383 K for 2 h before being subjected to analysis.

3.2.3.2 Catalytic coking experiments with solvent dilution

1-methylnaphthalene, n-dodecane, and n-decane were chosen as the solvent to dilute ABVB or Athabasca bitumen for coking experiments. Similarly, the coking experiments

were carried out in a 15 mL micro batch reactor. For each experiment, 4.5 g of feed (Athabasca bitumen and Athabasca vacuum residue alone or with a diluent) were combined with catalyst in a reactor. The reactor was purged with hydrogen to eliminate air before adjusting the hydrogen pressure to a desired value. The reactor was then immersed in a preheated and fluidized sand bath. The reactor vibrated up and down at approximately 1 Hz for the duration an experiment. The reaction was quenched in a water bath at room temperature. The reaction conditions were: feed to catalyst weight ratio = 30, hydrogen to feed weight ratio = 0 or 0.005, sand bath temperature of 653 K, and a reaction time of 2 h. Catalyst pellets were collected post reaction and extracted with toluene in a micro-Soxhlet extractor for 7 h and dried under vacuum at 383 K for 2 h before being subjected to analysis.

3.3 Analyses

3.3.1 Characterization of filtered samples

3.3.1.1 Analysis methods and equipment

All fluid samples were characterized using standard American Society for Testing and Materials (ASTM) techniques where available. The carbon, hydrogen, and nitrogen contents were determined using ASTM D5291 on a LECO CHN-1000 analyzer. Total sulfur content was determined using ASTM D1552 on a LECO SC-432 Sulfur Analyzer. Oxygen analysis was performed using a PE 2400 Series II Analyzer. There is no standard technique for this analysis.[4, 5] Here, samples were pyrolyzed in a helium/hydrogen environment at 1000 °C over platinized carbon, where the pyrolyzed oxygen products of

reaction were converted to carbon monoxide. The gases produced were then passed through a scrubber trap to remove acid gases and water. Oxygen was detected as a function of the thermal conductivity of resulting gas. Metal analyses were determined according to ASTM D5600 using an Anton Paar Multiwave-3000 Microwave Sample Preparation System coupled with a Perkin-Elmer Sciex Elan DRC-II ICP quadrupole mass spectrometer. SARA analyses were determined according to ASTM D2007 (for saturates, aromatics and resins) and according to ASTM D3279 (pentane asphaltenes). It is worth noting that the asphaltene content for many retentate samples exceeds the typical range for such measurements. All chemical analyses were performed at the National Centre for Upgrading Technology (Devon, Alberta, Canada). The applicable concentration ranges and precision of all analysis methods employed are summarized in Table 3.4.

3.3.1.2 Measurement reproducibility

Nanofiltration of Athabasca bitumen through the 10 nm membrane and the associated chemical analyses were repeated. The permeate and retentate compositions obtained for these repeated measurements are summarized in Table 4.1 (Chapter 4). The various composition measures for permeates agree within the reported repeatability of these measurements, while the composition of the retentate samples differ systematically from one another. This effect was anticipated because it is not possible to achieve a clean separation between the filter "cake" and the unfiltered feed. Further, any disturbance of the membrane material leads to sample contamination with alumina or zirconia and care must be taken in interpreting these aspects of the results.

Table 3.4 Summary and citation of method used for analysis, concentration range and precision[1]

Test	Method	Concentration range (wt %)	Repeatability	Reproducibility
C	ASTM D5291	75 ~ 87	(x + 48.48)0.0072	(x+48.48)0.018
H		9 ~ 16	$(x^{0.5})$0.1162	$(x^{0.5})$0.2314
N		0.1 ~ 2	0.1670	0.4456
S	ASTM D1552	0.0 ~ 0.5	0.04	0.13
		0.5 ~ 1.0	0.07	0.21
		1.0 ~ 2.0	0.09	0.27
		2.0 ~ 3.0	0.12	0.38
		3.0 ~ 4.0	0.13	0.44
		4.0 ~ 5.0	0.16	0.49
O	Unterzaucher method	-	±0.15%x	-
Test	Method	Concentration range (mg/kg)	Repeatability	Reproducibility
Al	ASTM D5600	15 ~ 110	$0.32*y^{-(2/3)}$	$0.92*y^{-(2/3)}$
Ba		1 ~ 65	$0.19*y^{-(2/3)}$	$0.71*y^{-(2/3)}$
Ca		10 ~ 140	7.2	20.8
Fe		40 ~ 700	$1.66*y^{-(1/2)}$	$3.77*y^{-(1/2)}$
Mg		5 ~ 50	$0.21*y^{-(2/3)}$	$0.61*y^{-(2/3)}$
Mn		1 ~ 7	0.042*(y+2.55)	0.34*(y+2.55)
Ni		3 ~ 220	$0.52*y^{-(2/3)}$	$0.96*y^{-(2/3)}$
Si		60 ~ 290	0.71*(y+4.80)	0.20*(y+4.80)
Na		30 ~ 160	$1.04*y^{-(1/2)}$	$3.52*y^{-(1/2)}$
Ti		1 ~ 7	0.75	1.16
V		2 ~ 480	$0.20*y^{-(3/4)}$	$0.35*y^{-(3/4)}$
Zn		1 ~ 20	$1.07*y^{-(1/3)}$	$2.20*y^{-(1/3)}$
saturates	ASTM D2007		2.1	4.0
aromatics			2.3	3.3
resins		< 1 wt %	0.24	0.4
		1 ~ 5 wt %	0.81	1.3
		> 5 wt %	1.2	1.8
			standard deviation	Acceptable range of two results
asphaltenes	ASTM D3279	4.0 ~ 29.0 wt %	$0.53\%x^{\blacklozenge}$	$1.51\%x^{\blacklozenge}$
		4.0 ~ 29.0 wt %	$0.93\%x^{\Delta}$	$2.78\%x^{\Delta}$

[1]x: the mean value in weight percentage; y: the mean value in mg/kg; *: multiply; ♦: single operator; Δ: multi-laboratory.

3.3.1.3 Possible impact of oxidation and thermal damage to feed samples during prolonged filtration trials

Prolonged heating at 473 K arising during a four to six-week nanofiltration experiment can cause polymerization of some components due to the activity of dissolved or dispersed oxygen in feed samples or thermolysis reactions. Chemical reactions can produce radicals which are stable enough to cause the cage effect. The radicals are caged in polycyclic aromatic hydrocarbons. This cage effect can prevent the reaction of these radicals with oxygen or other components with abstractable hydrogen and enhance the aggregation of asphaltenes.[6, 7] Simply purging feed samples at the reservoir head space with nitrogen before filtration does not eliminate dissolved or dispersed oxygen.

Athabasca bitumen and Maya crude oil feed samples heated for four weeks were collected from the reservoir [Heated AB (20), and Heated Maya (10)]. The chemical analysis results for these samples can be found in Tables 4.1 and 4.2 (Chapter 4) along with the analyses for their corresponding fresh feed samples. Composition differences for organic constituents fall well within the expected experimental error bounds. In order to examine the possible impact of oxidation on filtration outcome further, nitrogen was fed counter currently through Athabasca bitumen at 323 K for 5 days prior to filtration. These samples are labeled "oxygen-free" in Table 4.1 (Chapter 4). Again, organic constituent compositions of these samples differ within experimental error from their untreated analogues. This was expected as bitumen has a high minimum boiling point, 195°C. Stripping was not expected and oxygen analysis has significant uncertainty. Oxygen does not appear to impact permeate composition. However, potential impacts on rheological or other measurements will be addressed separately.

3.3.1.4 Systematic error introduced by nanofiltration on the nanoaggregate size distribution.

The physical retention of fine particulate material within porous media due to pore plugging and the development of filter cakes on upstream surfaces are well-understood phenomena. The potential for chemical interaction between high energy surfaces such as alumina and zirconia and surface-active organic materials such as asphaltenes is also well known. Both reduce the effective pore size. Thus, it is expected that the nanostructure size distributions, Figures 4.1 (cumulative distributions) and 4.2 (density distributions) in Chapter 4, obtained using filtration are skewed to large values. The impact on the nanostructure size results obtained is variable. At larger pore sizes, the impact is expected to be minimal as the nanostructures are significantly smaller than the nominal pore sizes and there is little retentate. At smaller pore sizes, the impact is expected to be more significant. As there are only six size levels, and the pores associated with individual membranes possess a range of sizes, it is clear that the size distribution data are coarse. The size distribution data provide the upper size limit for the nanostructures present in the fluids evaluated. However, variation of the composition of filter cakes and permeates vis-à-vis the feeds are expected to yield excellent measures of the composition of nanoaggregates present in the feeds irrespective of this effect.

3.3.2 Characterization of coked catalyst pellets

3.3.2.1 Bulk elemental analysis of coked catalyst

Bulk elemental analysis for carbon, hydrogen, nitrogen and sulfur on coked catalysts was performed on a Carlo Erba Model Strumentazione Elemental Analyzer 1108 at Micro Analytical Laboratory, University of Alberta. To ensure representative sampling, ~ 40 coked catalyst pellets were grounded to fine powders. 5 mg samples were used for elemental analysis. Due to the limited amount of samples, especially permeates and retentates, not all coking experiments were repeated. However, coking experiments with Athabasca bitumen, Athabasca vacuum residue, and Athabasca vacuum bitumen diluted with 1-methylnaphthalene were repeated. The values obtained are summarized in Table 3.5. The bulk carbon, hydrogen, nitrogen contents of coked catalyst pellets are in close agreement. Differences of 0.3, 0.09, and 0.01 wt % for carbon, hydrogen and nitrogen are observed.

Table 3.5 Repeatability of bulk elemental analyses for catalytic coking experiments

Experiment	Heavy oil(g)	Solvent (g)	Catalyst (g)	C (wt %)	H (wt %)	N (wt %)
Athabasca bitumen	4.5215		0.1513	11.7	1.27	0.28
	4.5602		0.1506	12.1	1.22	0.31
average				11.9	1.25	0.30
nominal error				± 0.2	± 0.02	± 0.01
ABVB	4.4994		0.1508	12.6	0.98	0.35
	4.5006		0.1514	13.1	1.17	0.31
average				12.9	1.07	0.33
nominal error				± 0.3	± 0.09	± 0.01
	1.7958	2.7142	0.1516	11.6	0.96	0.34
ABVB + 1-MN	1.8038	2.7009	0.1546	11.4	1.13	0.31
	1.8031	2.7042	0.1532	11.8	1.11	0.33
Average				11.6	1.07	0.32
nominal error				± 0.2	± 0.06	± 0.01

3.3.2.2 Cross section profiles examined by electron microprobe

Carbon and iridium-coated cross sections of coked catalyst pellets were examined using a JEOL 8900 electron microprobe (Electron Microprobe Laboratory, University of Alberta) at 20 kv and 30 nA with a probe diameter of 5 microns. Prior to analysis, a pellet was sectioned radially at the midpoint and each half was mounted in an epoxy resin. The facing internal surfaces were polished with 15 micron diamond first, then 9 micron diamond, and fine polished with 0.3 micron aluminum oxide on a paper-based pad. The surfaces were then micro polished with 0.03-μm aluminum oxide abrasive and cleaned ultrasonically for 5-10 seconds using dish soap + water. The surfaces were then dried. Some contamination with alumina is anticipated. One of the facing surfaces was then coated with a thin layer of carbon (usual carbon film thickness is in the range of 20 ~ 50 nm) while the other was coated with iridium (film thickness is ~ 10 nm). Local composition measurements were obtained at 6.5 μm intervals from the centre line to the rim of the pellets. Though nominally a surface analysis technique, the depth of penetration is up to a depth of the order of one micron.[8] The impact of smearing due to the polishing process on local composition measurements is expected to be minimal as the penetration depth of the probe beam (5 ~ 7 microns) is far below the coating film and the abrasive used (30 nm) for the last step polishing is larger than the average catalyst pore size (~ 10 nm). The smearing exposed to the top of the surface represents only a very small fractin of the whole volume measured. Thus, the impact from polish can be negligible. The accuracy of quantitative analysis is better than ± 2 % (relative)[8] with detection limits in the range of 10 to 100 ppm.[8] For the present measurements the standard deviation of carbon, molybdenum, and nickel composition are below 3 %, 3 %,

and 2 % of the measured values, respectively. The vanadium content is close to the detection limit in most cases and measurements possess significant error but most of the standard deviations fall below 40 %. The two coatings were used because carbon coating samples overestimate while iridium coating samples underestimate results. These two sets of data are compared after proper correction (deduct carbon content contributed by carbon coating and normalize elemental contents on the cross section of the pellets) and are consistent with one another, thus are reported jointly.

3.3.2.3 Nitrogen isothermal sorption on catalyst pellets

Surface area, pore volume, and pore size distributions for catalyst pellets were determined with an Omnisorb 360 at the Department of Chemical and Materials Engineering, University of Alberta. Nitrogen adsorption measurements combined with the BET equation[9] were used to calculate surface areas, and pore size distributions and pore volume were determined from nitrogen desorption data and the Kelvin equation.[9] The associated standard deviation for repeated measurements of standard reference materials are 3 %, 4 %, and 4 % for surface area, pore volume, and pore size distribution, respectively. Systematic differences between actual and measured areas exceeding ± 10 % can arise with this technique.[9]

References

(1) Zou, X. Y.; Dukhedin-Lalla, L.; Zhang, X. H.; Shaw, J. M., Selective Rejection of Inorganic Fine Solids, Heavy Metals, and Sulfur from Heavy Oils/Bitumen Using Alkane Solvents. *Industrial & Engineering Chemistry Research* **2004,** 43, (22), 7103-7112.

(2) Cheng, X. Sorption of Athabasca Vacuum Residue on Acidic, Neutral, and Basic Surfaces. Master thesis, University of Alberta, Edmonton, 2008.

(3) Kanda, W.; Siu, I.; Adjaye, J.; Nelson, A. E.; Gray, M. R., Inhibition and Deactivation of Hydrodenitrogenation (HDN) Catalysts by Narrow-Boiling Fractions of Athabasca Coker Gas Oil. *Energy & Fuels* **2004,** 18, (2), 539-546.

(4) Unterzaucher, J., Direct Microdetermination of Oxygen in Organic Substances. *Analytical Chemistry* **1952,** 24, (9), 1523-1523.

(5) Unterzaucher, J., The Direct Micro-Determination of Oxygen in Organic Substances. *Analyst* **1952,** 77, (920), 584-587.

(6) Gray, M. R.; McCaffrey, W. C., Role of Chain Reactions and Olefin Formation in Cracking, Hydroconversion, and Coking of Petroleum and Bitumen Fractions. *Energy & Fuels* **2002,** 16, (3), 756-766.

(7) Acevedo, S.; Escobar, G.; Ranaudo, M. A.; Pinate, J.; Amorin, A.; Diaz, M.; Silva, P., Observations about the Structure and Dispersion of Petroleum Asphaltenes Aggregates Obtained from Dialysis Fractionation and Characterization. *Energy & Fuels* **1997,** 11, (4), 774-778.

(8) Reed, S. J. B., *Electron Microprobe Analysis*. 2nd ed.; New York, NY, USA: Cambridge University Press: 1997.

(9) Gregg, S. J., Sing, K. S. W., *Adsorption, Surface Area and Porosity*. 2nd ed.; London; New York: Academic Press: 1982.

4. Composition and Size Distribution of Coherent Nanostructures in Athabasca Bitumen and Maya Crude Oil

4.1 Introduction

An exhaustive review of the research and debates surrounding the nature, shape, size, composition and associative properties and stability of nanostructures present in hydrocarbon resources is beyond the scope of this work. Readers are referred to recent volumes edited by Mullins et al.[1] and by Speight[2] for perspectives on these topics. Briefly, coherent nanostructures present in reservoir fluids and crude oils are commonly assumed to comprise asphaltenes alone or asphaltenes combined with other constituents. A consensus has not been reached on the form, nature, or stability of these nanostructures. Moreover, asphaltenes are defined operationally by the methods of separation. The weight fraction of asphaltenes in a sample is defined by a two-stage filtration process, where samples are first diluted in an alkane solvent. The permeate from the first filtration is discarded while the retentate is mixed with toluene, or another solvent, and filtered a second time. The asphaltene content of the sample is defined as the solvent-free mass recovered from the second permeate divided by the mass of the initial sample. Numerous measurement techniques are employed globally. The effects of temperature, contact time, solvent, solvent-to-feed ratio,[3] and washing[4] on asphaltene separation results have been studied systematically. The filters employed cover a broad range of pore sizes[5-10] from as small as 220 nm to as large as 20-25 μm.

Recently Savvidis et al.[11] studied the impact of filter pore size on asphaltene content measurements. Three petroleum feeds from different sources and filters with a wide

range of pore sizes from 25 nm to 10 μm were used. Asphaltenes were separated following the Association Française de Normalisation (AFNOR) procedure. Their results show clearly that the amount of asphaltenes recovered increases sharply as pore size is decreased. Sheu[12] suggests that asphaltene particles can be as small as 5 nm to 6 nm. Small asphaltene nanoparticles appear to remain dispersed even in paraffinic oils.[13] Gawrys and Kilpatrick[14] also suggest that asphaltenes are polydispersed based on SANS measurements.

Many new techniques have been developed to measure the threshold concentration value above which asphaltene molecules aggregate in solvents. Recent research by high-Q ultrasonic spectroscopy[15] shows that aggregation of asphaltenes can occur in toluene at concentrations as low as ~ 100 mg/L. The similarity of derived parameters such as the compressibility of nanoaggregates of asphaltenes and of micelles of nonionic surfactants lends support for their conclusion that asphaltenes are nonionic surfactants that form nanoaggregates and exhibit a critical nanoaggregation concentration (CNAC)—a term suggested by the authors to avoid debates of appropriateness of micelle concept to describe the behavior of asphaltenes in dilute solvents. Freed et al.[16], using NMR diffusion measurements to obtain information about mean molecular size and their distribution, find a sharp change in diffusion coefficients at asphaltene concentration of ~ 200 mg/L in toluene. The authors attribute this change to the aggregation of asphaltenes. Sheu et al.[17] developed a new approach using AC conductivity measurements to detect asphaltene self-association and phase separation. They show that at low frequency (~ 4 kHz), a discontinuity was observed at an asphaltene concentration of ~ 120 mg/L in toluene for normalized conductivity and attribute this to asphaltene self-association.

Yudin and Anisimov[18], using dynamic light scattering technique combined with viscosity measurement, identify two regimes for asphaltene aggregation in liquid hydrocarbons. At low concentration, they suggest that asphaltene aggregation is dominated by diffusion-limited aggregation mechanism; at high concentration, they suggest that asphaltene aggregation is dominated by reaction-limited aggregation mechanism.

Research investigations related to asphaltenes, such as CMC value, stability, precipitate on-set point, and the works cited specifically above, involve the addition of liquid hydrocarbons, either to extract asphaltenes from their original source or as solvents/dispersants/precipitants. One important issue unresolved in the literature, is whether the nanostructures identified by chemical separation resemble those arising in the original hydrocarbon resource from which they are obtained.

The contribution of asphaltenes to high viscosity, metal content and tendency of coke formation has been known for many years. Great efforts have been made to remove asphaltenes to yield products that are easier to transport and refine. Older commercial technologies,[19, 20] remove asphaltenes in the presence of solvents by precipitation. However, the quality of de-asphalted oil decreases as the yield increases. Newer super critical fluid extraction technology[21] can remove 80 % of total Ni and V in bitumen. The quality and the yield of products depend on the selected solvent and solvent recovery is a must for such techniques.

With the rapid development of membranes, separation processes based on membrane technology become an alternative option for partitioning hydrocarbon resources. Typically, polymeric membranes are employed and solvents are added to reduce viscosity. Examples include solvent recovery following extraction,[22-24] phase

separation,[25, 26] and metal removal.[27-29] However, polymeric membranes cannot be used at high temperature and are not chemically stable in the presence of heavy oil. By contrast, the thermal and chemical stability of ceramic membranes make it possible to apply nanofiltration processes at higher temperatures where the hydrocarbon viscosity is lower and solvent dilution and solvent recovery are unnecessary. Arod et al.[30] describe a nanofiltration process for vacuum residue using a ceramic membrane with an average pore radius of 10 nm at 330 °C. Asphaltene content was reduced from 6.3 wt % to 4.1 wt % and V content was decreased from 128 ppm to 90 ppm concurrently. Hydrocarbon resources are subject to thermolysis reactions at such temperatures. However, their success suggests that direct nanofiltration is feasible. An apparatus was devised for nanofiltration and it is described in Chapter 3 (3.1) along with operation procedures.

4.2 Results and discussion

4.2.1 Impact of nanofiltration on permeate and retentate composition

4.2.1.1 Impact of nanofiltration on SARA content in permeates

Compositions of permeates obtained from Athabasca bitumen and Maya crude oil samples are summarized in Tables 4.1 and 4.2. Bitumen did not pass through the 5 nm membrane. SARA analyses show that the asphaltene content in permeates decreases with membrane pore size, while saturate, aromatic and resin contents increase. For Athabasca bitumen, asphaltene content dropped from 18.6 wt % in the feed to 12.6, 13.0, 13.4, 10.4, and 4.5 wt % for 200, 100, 50, 20, and 10 nm permeates, respectively; while for Maya

crude oil, asphaltene content dropped from 15.7 wt % to 9.4, 8.1, 6.2, and 1.5 wt. % for 50, 20, 10, and 5 nm permeates, respectively. Maya crude appears to pass through the 100 and 200 nm filters. On an asphaltene-free basis (data in Tables 4.1 and 4.2 in parentheses and with an asterisk), saturate, aromatic, and resin contents of permeates obtained from both Athabasca bitumen and Maya crude are unchanged by nanofiltration. Composition variations fall within the range of analysis errors. These data show that the nanostructures present in these feeds, at 473 K, comprise asphaltenes + undifferentiated feed, and that asphaltenes possess a broad size distribution. The cumulative and density distributions for these nanostructures are shown in Figures 4.1 and 4.2, respectively, as a function of the nominal mean pore size of the nanofilters.

Table 4.1 Composition of Athabasca bitumen and filtered samples

	ABP10[1]	ABP10[2]	ABP20	Oxygen-free ABP-20	ABP50	ABP100	ABP200	Oxygen-free AB	AB	Heated AB(20)	ABR200	ABR100	ABR50	Oxygen-free ABR-20	ABR20	ABR10[1]	ABR10[2]
Elemental Analysis, wt %																	
C	84.3	84.2	84.3	84.4	83.8	84.1	84.2	83.6	83.2	83.6	81.1	81.2	80.7	80.1	81.0	80.6	81.2
H	10.0	10.5	10.0	10.7	10.6	9.9	9.6	10.1	9.7	9.2	8.8	8.2	9.2	8.5	8.6	8.4	9.1
N	0.4	0.3	0.4	0.3	0.4	0.4	0.4	0.4	0.4	0.4	0.7	0.6	0.6	0.7	0.6	0.6	0.7
S	4.9	5.0	5.0	5.1	5.2	5.3	5.2	5.4	5.3	5.4	6.1	6.1	6.2	6.1	6.1	6.2	6.7
O	1.6	0.5	1.7	0.9	0.9	1.5	0.7	0.9	1.7	1.6	2.2	2.2	1.4	-	1.9	1.5	1.3
SARA Analysis, wt %																	
saturates	20.2 (21)*	18.9 (20)*	18.4 (21)*	17.5 (20)*	17.1 (20)*	16.0 (18)*	16.1 (18)*	15.1 (19)*	16.1 (20)*	16.6 (20)*	9.4 (20)*	9.4 (20)*	9.5 (20)*	8.7 (19)*	7.9 (18)*	14.3 (21)*	8.9 (21)*
aromatics	54.8 (57)*	56.7 (60)*	53.0 (59)*	53.2 (60)*	53.4 (62)*	51.8 (60)*	50.0 (57)*	45.2 (58)*	48.5 (60)*	46.9 (58)*	26.0 (52)*	24.0 (50)*	27.9 (58)*	25.9 (58)*	21.8 (50)*	44.4 (65)*	25.4 (59)*
resins	20.4 (21)*	19.1 (20)*	18.2 (20)*	18.2 (20)*	15.9 (18)*	19.2 (22)*	21.3 (24)*	17.4 (22)*	16.8 (21)*	17.8 (22)*	14.6 (29)*	14.4 (30)*	10.8 (22)*	10.2 (23)*	13.6 (31)*	10.0 (15)*	8.7 (20)*
asph.C(5)	4.5 (24%)^	5.3 (29%)^	10.4 (56%)^	11.1 (59%)^	13.6 (73%)^	13.0 (70%)^	12.6 (68%)^	22.3	18.6	18.7	50.0	52.2	51.9	55.2	56.7	31.3	57.2
Metal Analysis, mg/kg																	
Al	2.8	1.6	4.6	2.3	32.8	24.5	3.0	356	492	311	752	2693	2002	1528	920	2278	1217
Ba	<0.1	<0.1	<0.1	<0.1	0.27	0.4	0.2	4.6	6.4	4.4	18.6	27.1	21.9	24.5	18.1	19.9	18.5
K	<1.0	1.2	<1.0	0.9	1.1	29.7	6.9	43.1	77	59	181	441	314	263	196	345	240
Ca	43	25	67	53	72	98	61	118	163	121	324	397	1068	348	285	312	324
Cr	1.0	0.4	1.0	0.9	1.4	2.1	1.1	3.0	2.8	2.6	9.2	10.7	8.3	9.0	7.7	7.8	7.0
Fe	16	48	27	56	37	66	40	292	762	319	1196	1560	1623	1576	964	1085	1592
Mg	4.3	4.1	8.8	8.6	11.6	21.7	9.8	42	65	43	115	211	178	149	114	162	140
Mn	2.8	2.4	4.6	4.9	6.6	7.6	5.7	13.3	30	15	57	63	57	58	39	41	61
Mo	0.1	<0.1	1.5	0.9	8.9	6.2	4.2	12.9	12	12	46	51	37	50	45	44	37
Na	76	18	93	40	9.5	208	50	112	91	82	217	391	240	369	251	226	212
Ni	47 (51%)^	47 (51%)^	64 (69%)^	61 (66%)^	96 (100%)^	105 (100%)^	81.2 (87%)^	103	93	93	228	244	183	221	191	196	187
Si	99	59	92	47	81	149	85.7	279	355	171	442	692	689	395	460	709	456
Ti	0.8	0.5	2.2	1.7	5.8	6.7	3.9	22	24	22	68	120	89	83	55	82	78
V	125 (51%)^	118 (48%)^	169 (68%)^	152 (62%)^	259 (100%)^	282 (100%)^	197 (80%)^	270	247	259	487	540	475	542	472	480	507
Zn	1.0	1.5	0.8	2.2	1.5	1.7	1.1	2.5	4.4	2.2	10.3	12.8	14.3	10.7	7.4	7.8	7.9

Notes of Table 4.1:

ABP10: Athabasca bitumen 10 nm permeate,

ABR10: Athabasca bitumen 10 nm retentate,

ABP20: Athabasca bitumen 20 nm permeate,

ABR20: Athabasca bitumen 20 nm retentate,

ABP50: Athabasca bitumen 50 nm permeate,

ABR50: Athabasca bitumen 50 nm retentate,

ABP100: Athabasca bitumen 100 nm permeate,

ABR100: Athabasca bitumen 100 nm retentate,

ABP200: Athabasca bitumen 200 nm permeate,

ABR200: Athabasca bitumen 200 nm retentate;

Heated AB (20), heated Athabasca bitumen collected from the reservoir after 30 days at 473 K;

Oxygen free ABP20: Athabasca bitumen 20 nm permeate collected from bubbled Athabasca bitumen;

Oxygen free AB: Heated Athabasca bitumen collected from the reservoir after filtration of AB. Nitrogen first bubbled through bitumen for 5 days and then followed the same filtration procedure;

Oxygen free ABR20: Athabasca bitumen 20 nm retentate collected from bubbled Athabasca bitumen, filtration through 10 nm was repeated twice.

Superscript 1 and 2 mean the first and the second one,

*: Data are on an asphaltene-free base, wt %,

^: % of asphaltenes, nickel or vanadium relative to the feed.

Table 4.2 Composition of Maya crude oils and filtered samples

	MP5	MP10	MP20	MP50	MP100	MP200	Maya	Heated Maya (10)	MR200	MR100	MR50	MR20	MR10	MR5
Elemental Analysis, wt %														
C	84.7	84.1	84.8	85.1	84.9	84.9	84.5	85.1	84.9	85.0	84.2	84.2	83.9	84.4
H	12.2	11.3	11.1	11.7	10.4	10.7	11.3	10.9	10.4	9.8	9.0	8.5	8.6	9.6
N	0.1	0.2	0.3	0.2	0.3	0.3	0.3	0.3	0.3	0.4	0.8	0.7	0.7	0.6
S	3.0	3.3	3.3	3.4	3.6	3.5	3.3	3.3	3.3	3.4	5.5	5.6	5.4	5.0
O	1.4	1.4	1.4	1.0	1.1	1.1	1.2	1.2	1.2	0.9	0.2	1.3	1.4	0.9
SARA Analysis, wt %														
saturates	39.6 (40)*	34.4 (37)*	34.1 (37)*	31.7 (35)*	27.9 (34)*	28.3 (35)*	31.6 (38)*	33.5 (40)*	-	-	12.4 (34)*	4.5 (17)*	14.6 (44)*	16.9 (32)*
aromatics	46.7 (47)*	43.7 (47)*	43.1 (47)*	47.1 (52)*	42.5 (52)*	33.2 (41)*	42.5 (51)*	39.4 (47)*	-	-	19.1 (53)*	18.1 (67)*	13.6 (41)*	26.4 (50)*
resins	12.3 (12)*	15.7 (17)*	14.8 (16)*	11.8 (13)*	11.5 (14)*	18.8 (23)*	10.2 (12)*	10.8 (13)*	-	-	4.7 (13)*	4.4 (16)*	4.8 (15)*	10.0 (19)*
asphaltenes (C5)	1.5 (10%)^	6.2 (39%)^	8.1 (52%)^	9.4 (60%)^	18.1 (100%)^	19.7 (100%)^	15.7	16.3	-	-	63.8	73.0	67.0	46.7
Metal Analysis, mg/kg														
Al	1.1	1.0	1.0	10.2	79.6	8.13	1.0	1.0	2.8	3.4	3.8	7.0	3.0	3.5
Ba	<0.1	<0.1	<0.1	0.3	<0.1	<0.1	<0.1	<0.1	<0.1	0.2	<0.1	<0.1	<0.1	<0.1
K	0.44	<1.0	<1.0	0.92	3.5	0.5	1	1	3.5	6.0	1.1	3.0	15	06
Ca	17	30	28	79	24	31	29	13	20	28	35	42	38	24
Cr	0.3	0.6	1.0	0.4	0.5	0.5	0.8	0.6	0.5	0.7	1.7	1.8	1.5	1.0
Fe	0.6	9.0	8.0	2.9	11.4	5.5	4.0	8.0	7.3	16	25	51	14	17
Mg	0.5	0.5	0.5	1.2	0.7	1.5	0.7	0.4	0.7	1.9	3.0	2.0	1.8	2.7
Mn	0.1	0.1	0.2	0.2	1.0	<0.1	<0.1	0.04	<0.1	0.3	0.9	1.6	0.4	0.5
Mo	<0.1	<0.1	0.1	0.7	3.2	3.3	3.0	2.7	3.0	5.1	17	20	16	8.6
Na	6.4	91	69	13.5	27	56	112	10.0	44	54	51	90	65	22
Ni	10.3 (18%)^	21 (38%)^	27 (48%)^	30 (54%)^	62 (100%)^	59 (100%)^	56	54	55	87	65	242	217	146
Si	79	88	83	104	127	109	80	85	106	97	65	82	64	51
Ti	0.3	0.4	0.4	0.4	0.4	0.3	0.4	0.3	0.4	0.4	0.6	0.5	0.4	0.4
V	63 (24%)^	125 (48%)^	151 (57%)^	154 (59%)^	295 (99%)^	296 (99%)^	263	298	289	415	1174	1119	999	756
Zn	0.9	1.4	0.6	1.4	1.0	5.7	1.6	0.5	2.2	3.3	2.5	3.3	2.6	5.2

Notes of Table 4.2:

MP5: Maya crude 5 nm permeate,

MR5: Maya crude 5 nm retentate,

MP10: Maya crude 10 nm permeate,

MR10: Maya crude 10 nm retentate,

MP20: Maya crude 20 nm permeate,

MR20: Maya crude 20 nm retentate,

MP50: Maya crude 50 nm permeate,

MR50: Maya crude 50 nm retentate,

MP100: Maya crude 100 nm permeate,

MR100: Maya crude 100 nm retentate,

MP200: Maya crude 200 nm permeate,

MR200: Maya crude 200 nm retentate;

Heated Maya (10): heated Maya crude collected from the reservoir after 30 days at 473 K;

*: Data are on an asphaltene-free base, wt. %;

^: % of asphaltenes, nickel or vanadium relative to the feed.

4.2.1.2 Impact of nanofiltration on SARA content of retentates

Care must be taken not to over interpret the measured composition of retentate samples, particularly on an asphaltene free basis. This arises because the asphaltene content is high – above 70 wt % in some cases, which is more than double the specified range for the ASTM composition measurement techniques. Further when composition is reported on an asphaltene free basis, experimental uncertainties become amplified, even if one restricts consideration to "reproducibility" rather than "repeatability" measures of uncertainty. For example, at 73 wt % asphaltenes (sample MR 20) the uncertainty in the asphaltene free aromatics content is ~ 20 wt %. Individual data points must be treated as semi-quantitative at best from this perspective. For Maya 100 nm and 200 nm retentates, not enough samples could be collected to do SARA analysis. However, as shown in Figure 4.3, saturate, aromatic and resin contents trend linearly toward zero as asphaltene content increases. There is no apparent preferential retention of saturates, aromatics or resins in the retentate. While it is tempting to suggest that the nanostructures comprise asphaltenes exclusively, in the absence of a detailed mass balance, these data only support the conclusion that the nanostructures present in Maya crude oil and Athabasca bitumen comprise asphaltenes + an unknown mass fraction of undifferentiated feed.

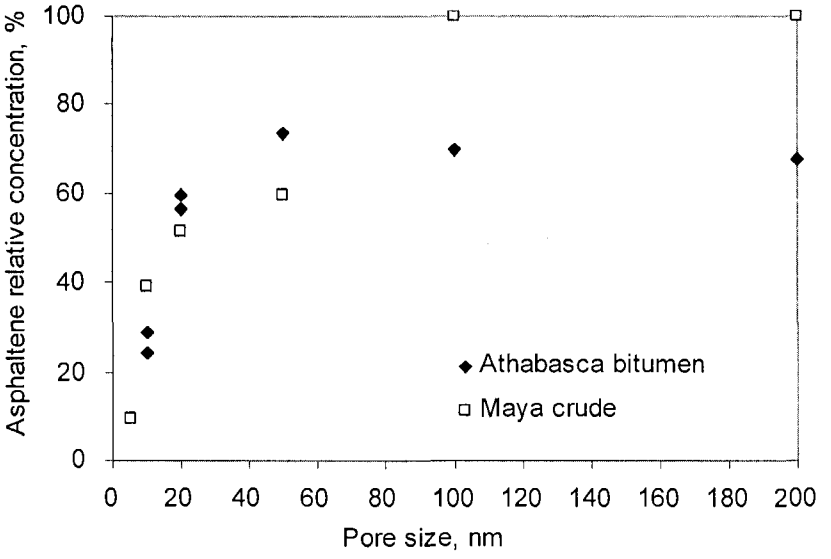

Figure 4.1 Cumulative asphaltene-rich nanostructure size distribution

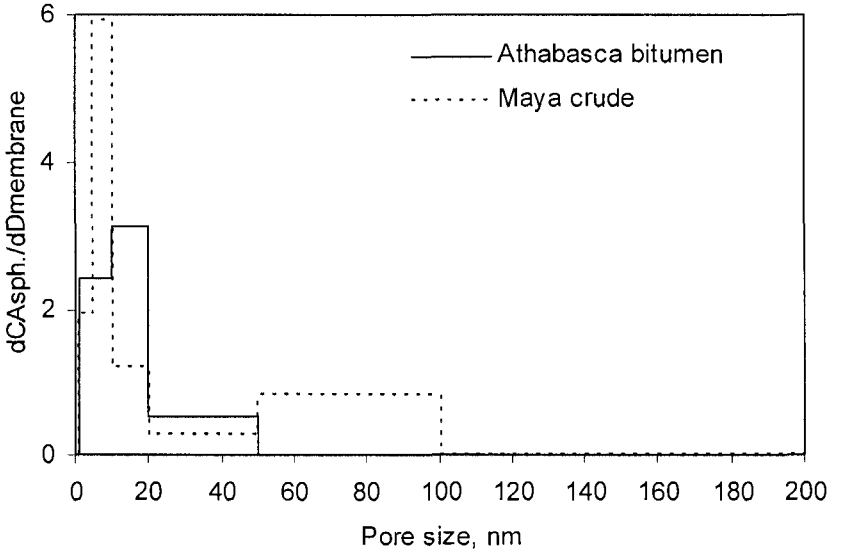

Figure 4.2 Asphaltene-rich nanostructure size distribution

4.2.1.3 Impact of nanofiltration on CHNSO, V and Ni contents of permeates and retentates

The CHNSO, V and Ni mass fractions vary linearly with the asphaltene content of permeates and retentates as shown in Figures 4.4 and 4.5, respectively, for both Athabasca bitumen and Maya crude oil. There are no apparent step changes in composition with asphaltene content suggesting that these elements are distributed among all size ranges of the asphaltene-rich nanostructures. This finding is new.

It is well known that constituents such as Ni and V are found primarily if not exclusively in nanostructures, Figure 4.5, and that sulfur, nitrogen, carbon, hydrogen and oxygen are present in the asphaltene free feeds as well as nanostructures at significant concentrations. The data for Ni and V, in Tables 4.1 and 4.2, suggest that these species are to be found preferentially in the smaller nanostructures present in Athabasca bitumen. This finding is also new.

Estimates for compositions of deasphalted oil and asphaltenes obtained by extrapolation, are provided in Table 4.3. Where available, the values are in agreement with the literature for chemically separated fractions. This suggests that at room temperature the addition of solvent facilitates a physical separation of existing coherent nanostructures that are further aggregated by solvent addition, and is not related to solubility per se. Again this finding is new but it links well with the work of Yudin and Anisomov[1] who show that aggregation can arise in two stages.

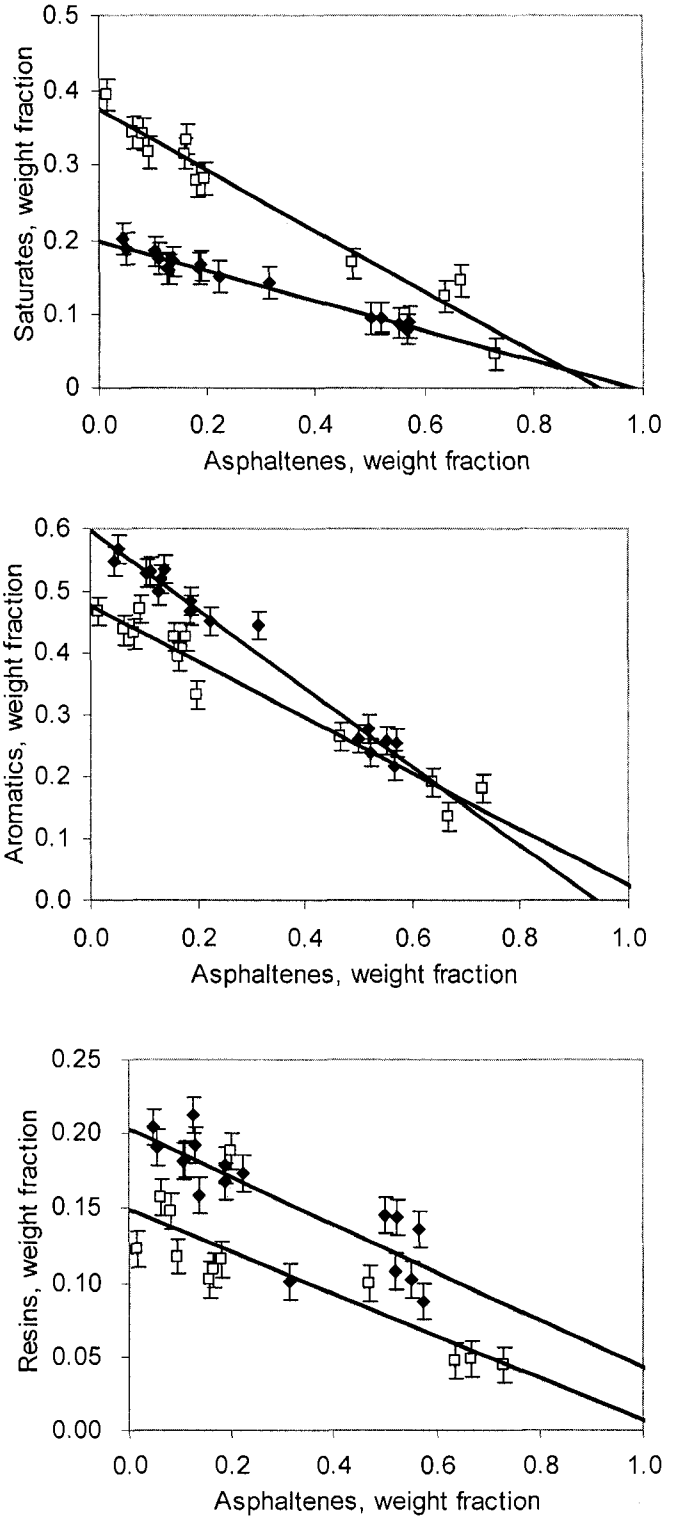

Figure 4.3 Saturate, aromatic and resin contents in permeates, feeds, and retentates.

♦ Athabasca bitumen and □ Maya crude.

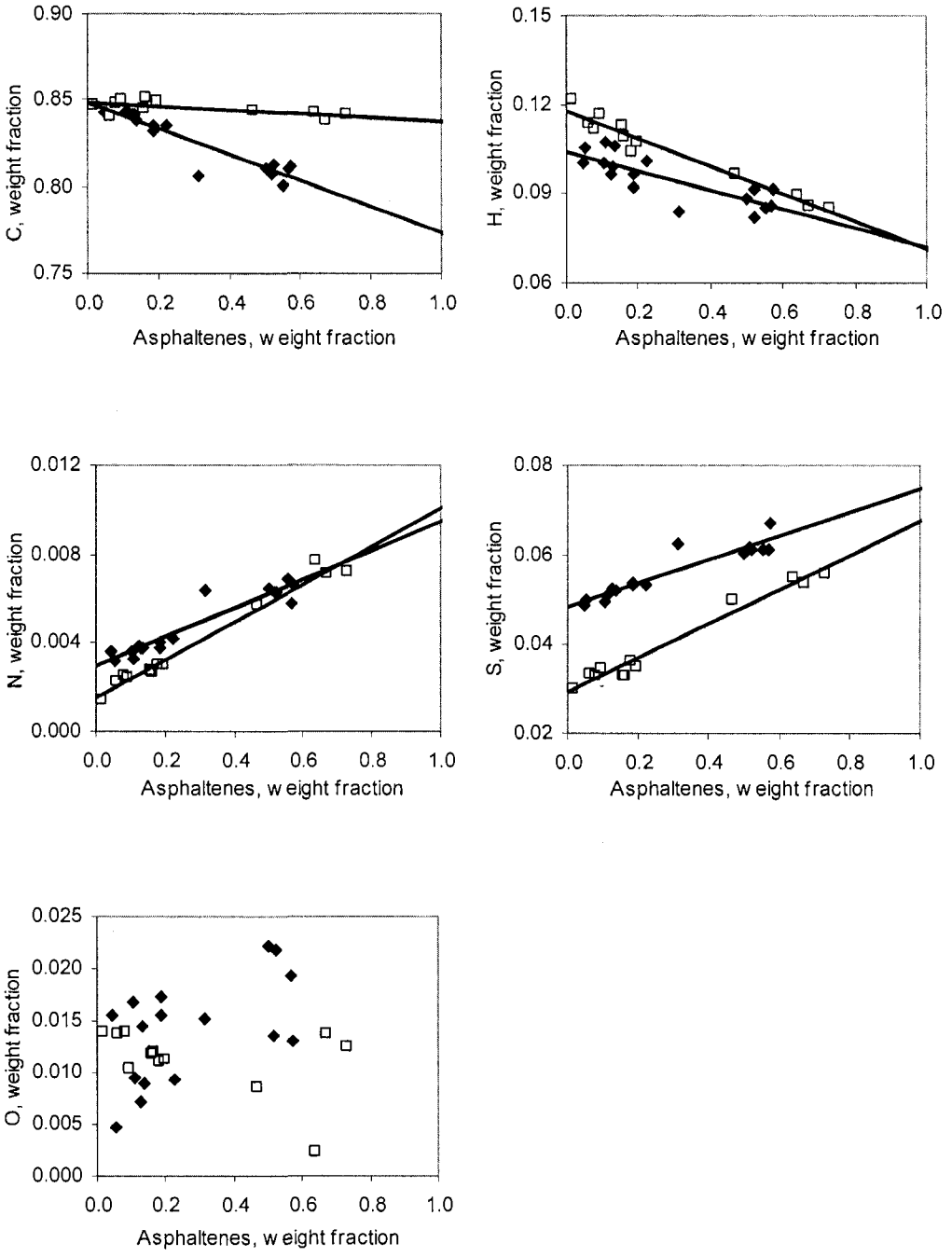

Figure 4.4 CHNSO contents in permeates, feeds, and retentates.

♦ Athabasca bitumen and □ Maya crude.

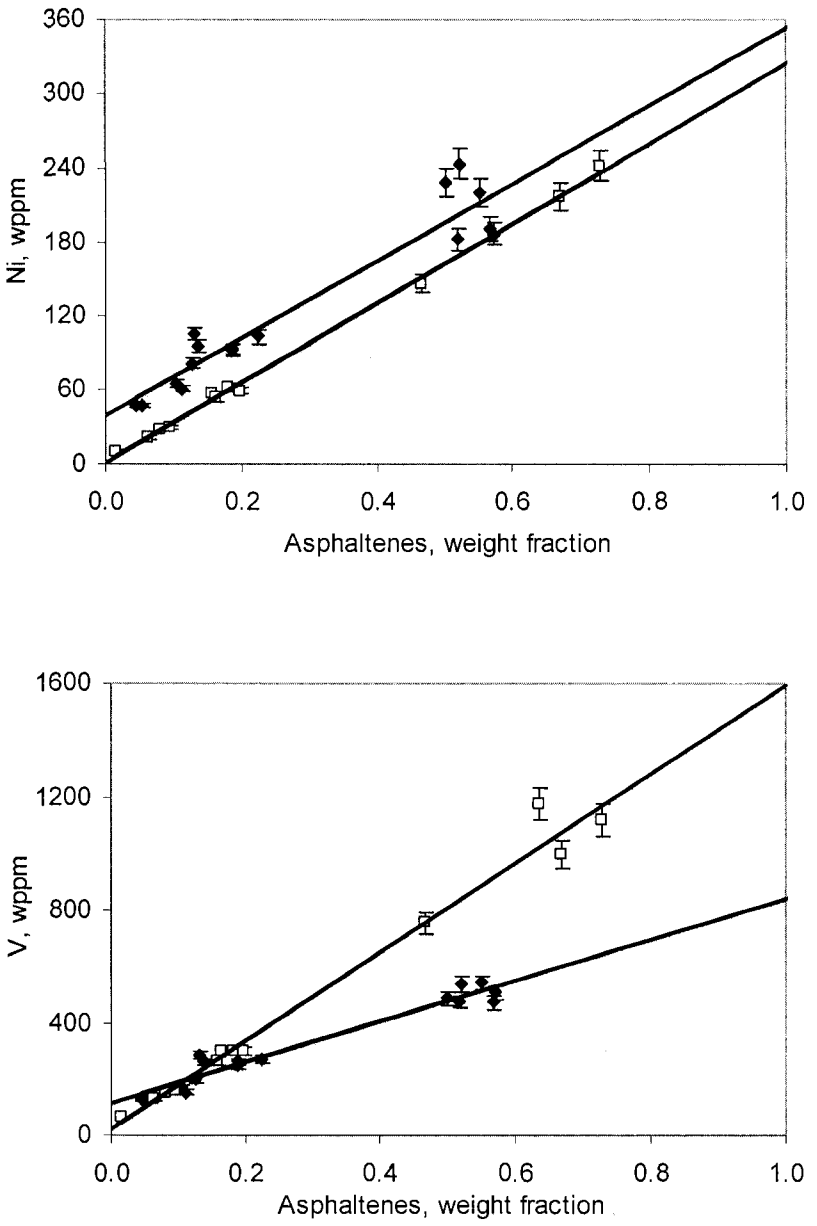

Figure 4.5 Nickel and vanadium contents in permeates, feeds, and retentates.

♦ Athabasca bitumen and □ Maya crude.

Table 4.3 Normalized asphaltene free feed and oil free nanostructure composition

	AB_{Oil}	AB_{Oil}	$Maya_{Oil}$	$Maya_{Oil}$[31]	AB_{NS}	$AB_{Asph.}$[32]	$Maya_{NS}$	$Maya_{Asph.}$[31]
Elemental Analysis, wt %								
C	83.8±1.1	-	84.0±1.5	84.5	81.3±1.7	80.8	84.2±0.8	84.7
H	10.4±1.3	-	11.7±0.5	11.0	7.1±2.3	8.0	7.2±0.8	7.5
N	0.3±0.1	-	0.16±0.06	0.24	0.9±0.2	1.3	1.0±0.2	1.25
S	4.6±0.5	-	2.9±0.4	3.57	8.0±1.0	7.5	6.8±0.5	5.77
O	1.1±0.3	-	1.3±0.2	0.65	2.0±0.3	-	0.7±0.2	0.76
SARA Analysis, wt %								
S	20.0±6.0	-	38.0±8.0	-	~0	-	~0	-
A	60.0±5.0	-	48.0±8.0	-	~0	-	~0	-
R	20.0±5.0	-	14.0±4.0	-	~0	-	~0	-
Metal Analysis, mg/kg								
Ca	~5	-	20±10	-	640±140	-	45±5	-
Ni	38±15	-	~0	-	350±60	-	320±40	-
V	100±50	-	~25	-	850±50	-	1650±250	-

Notes:

AB_{Oil}: Asphaltene-free Athabasca bitumen,

AB_{Asph}: Asphaltenes separated from Athabasca bitumen,

AB_{NS}: Athabasca bitumen enriched in asphaltene nanostructures,

$Maya_{Oil}$: Asphaltene-free Maya crude oil,

$Maya_{Asph}$: Asphaltenes separated from Maya crude oil,

$Maya_{NS}$: Maya enriched in asphaltene nanostructures.

4.2.1.4 Impact of nanofiltration on mineral matter content in permeates and retentates

The mineral matter content for permeates and retentates are also summarized in Tables 4.1 and 4.2. The mineral matter content in bitumen is significantly greater than the mineral matter content in Maya crude oil. Broadly speaking, the mineral matter content of retentates is greater than that of permeates. However, the pattern is different than noted for other constituents. For example, the aluminium, iron and silicon content of bitumen permeate samples, Table 4.1, is largely independent of the filter size employed in the experiment. The behaviour of these constituents is clearly independent of that of asphaltenes – Figure 4.6. The structures containing these species as well as K, Mg, Mn, Mo, Ti, and Ba, in Athabasca bitumen, are clearly large compared to the filter sizes employed and to the structures containing asphaltenes, as these constituents are largely absent from all permeates. For example, the aluminium contents of the 200, 100, 50, 20, and 10 nm bitumen permeates are less than 1, 5, 10, 1, and 1 % of the feed composition, where as by contrast the asphaltene content in the same samples is ~70, ~70, ~70, ~60, and ~25 % of the feed composition. The results for Maya crude oil also show independence. Further, there is no indication that nanostructures present in Maya crude include Al, Fe, Si, K, Mg, Mn, Mo, Ti, and Ba. Calcium is a notable exception with respect to mineral matter behaviour in nanofiltration – Figure 4.7. It, like vanadium and nickel, is closely associated with asphaltene-rich nanostructures.

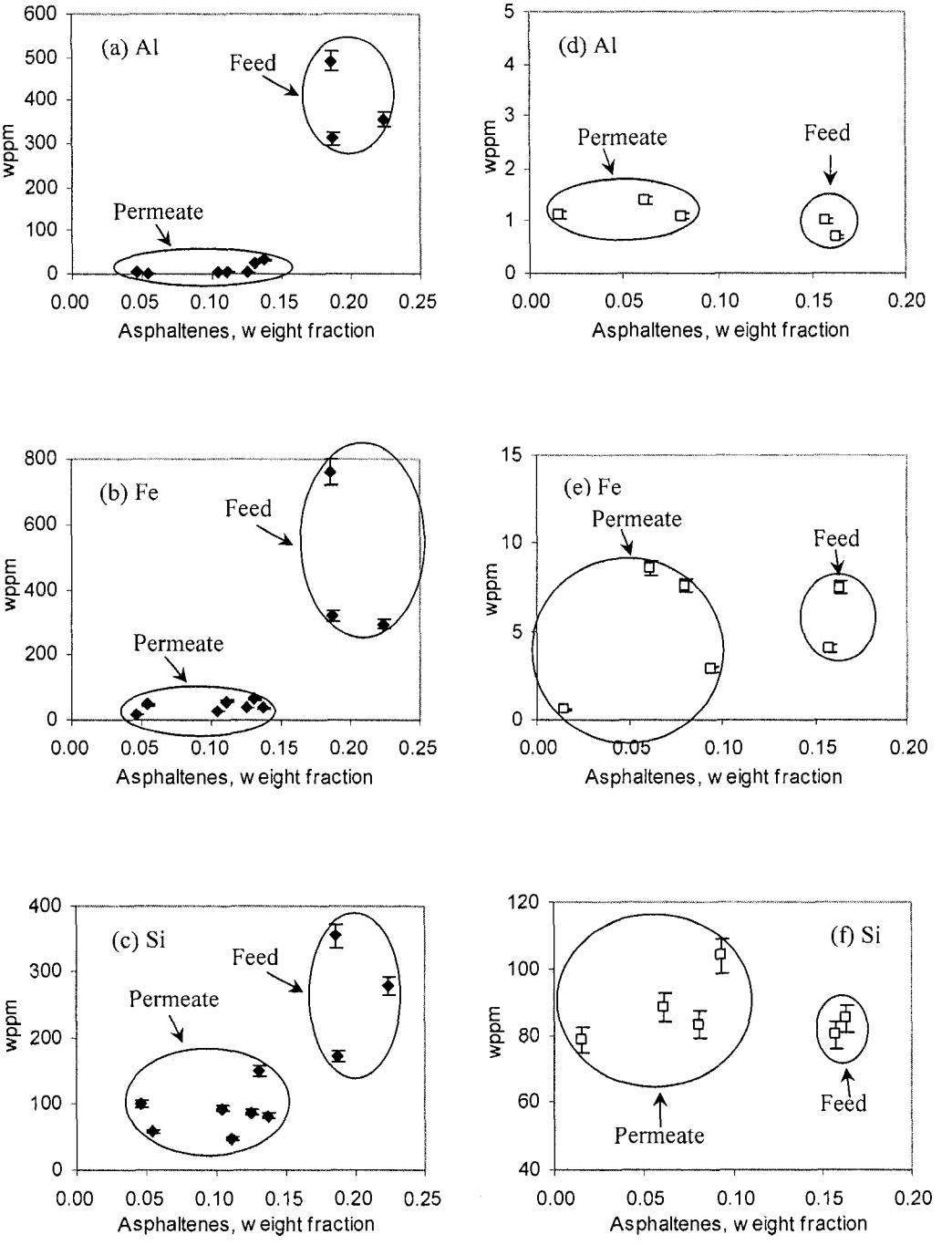

Figure 4.6 Aluminium, iron, and silicon contents in permeates and feeds.

(a –c) Athabasca bitumen and (d –f) Maya crude.

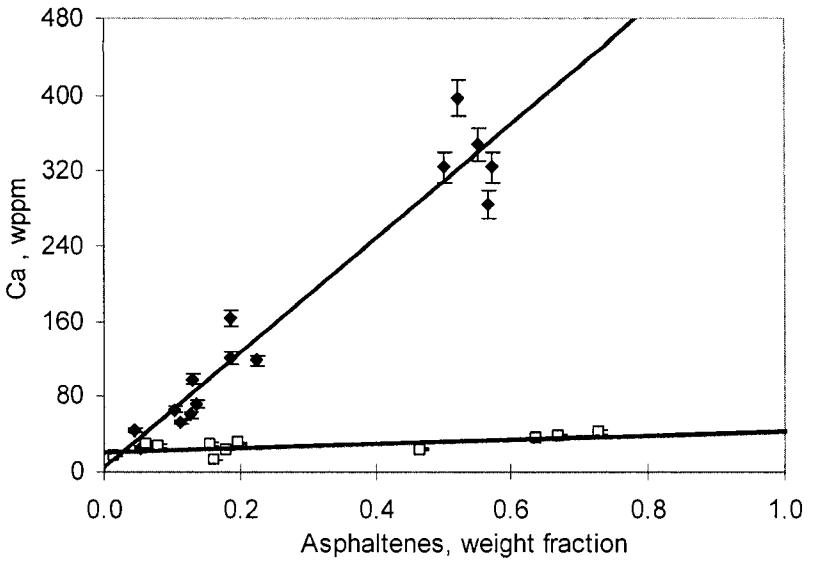

Figure 4.7 Calcium content in permeates, retentates, and feeds.

♦ Athabasca bitumen and □ Maya crude.

4.2.2 Nanoaggregate size distributions

The shape of nanostructures present in these feed stocks is unknown a priori. The cumulative and density distributions for the nanostructures present in Athabasca bitumen and Maya crude are shown in Figures 4.1 and 4.2, respectively, as a function of the nominal mean pore size of nanofilteres, which is used here as a surrogate for the leading dimensions of the structures. For both hydrocarbon resources, more than 50 wt % of the asphaltenes present pass through the 20 nm filter. The Maya asphaltene-rich nanostructure size distribution is dominated by aggregates in the 5 to 10 nm size range. 10 wt % pass through the 5 nm membrane and none of the aggregates appear to be greater than 100 nm. The Athabasca asphaltene-rich nanostructures are larger on average, possessing a peak in the 10 to 20 nm size range. None pass through 5 nm membrane and 30 wt % Athabasca asphaltene-rich nanostructures do not pass through the 200 nm filter.

The size data, as noted above, are coarse but suggest that the size distributions for Maya and Athabasca asphaltene-rich nanostructure are both bimodal and broad.

Experimental work with model asphaltene and solvent mixtures at low asphaltene concentrations suggests that asphaltenes begin to agglomerate, even in toluene, at less than 200 ppm. Further, the aggregates then formed are suggested to have leading dimension of 5 — 6 nm,[12] a value consistent with the smallest aggregates observed in our distributions. A total of 39 wt % of Maya asphaltenes and 28 wt % Athabasca asphaltenes pass through the 10 nm filter. At higher asphaltene concentrations, a second stage of aggregation has been observed.[18] Thus, it should not be surprising that, at concentrations in the range of 15 — 20 wt %, the size distribution is dominated by the aggregates and the size distribution is bimodal in nature.

4.2.3 Implications for asphaltene aggregate and asphaltene aggregation models

There are a number of classic models for asphaltene aggregate structure in native fluids and in solvents. For example, according to the colloidal theory of asphaltene structure in petroleum liquids, asphaltenes form a core in the centre and the core is associated with and stabilized by resins, lighter and neutral polars with their polar head groups orienting toward the surface of the asphaltenes. According to this model, asphaltene aggregates are dispersed in crude oil with a nearly continuous transition from the most polar entities at the centre to the less polar entities at the resin layer and to the least polar entities of the liquid media. In this model, when asphaltenes and resins are both present resin-asphaltene interaction is preferred over asphaltene-asphaltene and resin-resin interaction.[33] Only when resins are depleted, can asphaltenes self associate. The ratios of

resins to asphaltenes in Athabasca bitumen and Maya crude oil are 1:1 and 2:3 respectively. Thus according to this model, significant resin – asphaltene association is expected.

The SARA analyses reported in Tables 4.1 and 4.2 separate asphaltene-rich aggregates by size with smaller ones appearing in the permeates and larger ones appearing in the retentates, without any influence of the media in which asphaltenes are dispersed. If asphaltenes associate significantly and preferentially with another fraction, then the second fraction would have a reduced concentration in the permeate and an increased one in the retentate relative to the others. This effect is not observed. These results do not support the notion that asphaltenes associate preferentially or significantly with resins or other organic constituents at 473 K. These results are however, consistent with a recent independent report from Mullins,[34] which also shows that asphaltene-rich nanostructures are not associated with other organic constituents in reservoir fluids.

Gonzalez et al.[35] argue that asphaltenes and resins should be considered as a continuum or family of complex molecules with a variation in molecular structure and polarity rather than two fractions. Their argument is supported by the similarity of the FTIR spectra for asphaltenes and resins. In this work, two key differences in behaviour between resins and asphaltenes are underscored. Resins do not appear to aggregate on their own nor do they associate with asphaltenes. One would expect both of these effects if the constituents were part of a continuum.

4.2.4 Mineral matter and asphaltene association in Athabasca bitumen processing

The conventional Hot Water Extraction Process separates bitumen as a froth, which is then diluted with naphtha and subjected to two stages of centrifugation. Thus, the bitumen product contains residual water, dissolved salts, and mineral solids. Distillation and super-critical extraction can remove volatile components, but salts and mineral solids remain with the bitumen. Several studies indicate the importance of mineral solids in the bitumen upgrading process. For example, fine and ultra fine clays stabilize oil-water emulsions by adhering to oil water interfaces.[36-38] Other studies[8, 39-41] suggest that mineral matter facilitate coke formation during refining. Kotlyar et al.[38] suggest that the fine solids remaining in bitumen subjected to the conventional hot water extraction process are coated with strongly bound toluene-insoluble organic material that has asphaltene like characteristics. The nanofiltration results reported here were preformed with processed Athabasca bitumen, that is to say post mining, and post froth treatment and separation. Solvent-extracted bitumen may chemisorb up to 1 — 2 wt % organic matters.[42] Carboxylic acids were found chemically bound to inorganic minerals. These results show clearly that calcium is strongly associated with asphaltenes at this stage, Figure 4.7, but also illustrate the robustness of the independence of the behaviours of other mineral matter constituents and asphaltenes, Figure 4.6, at temperatures up to 473 K. The strong association of Ca with asphaltenes may be due to its association to some undifferentiated carboxylic acid groups or to the porphyrins[43] in asphaltenes.

4.3 Conclusions

Nanofiltration of Athabasca bitumen and Maya crude oil was successfully conducted through commercially available ceramic membranes at 473 K, with a moderate differential pressure and without solvent addition. Two distinct nanostructures, one enriched in pentane asphaltenes + (S, N, Ca, V, Ni) and possibly containing other undifferentiated organic constituents, and one enriched in mineral matter and possibly containing undifferentiated SARA constituents, were identified. The composition and size distribution of these distinct nanostructures strengthen the conclusion that asphaltenes are associated preferentially with mineral matter or one or more of the other SARA constituents such as resins, in native feeds. These results also show clearly that asphaltene-rich nanostructures are polydispersed with nominal size distributions extending from less than 5 nm for both Athabasca bitumen and Maya crude, to more than 50 nm for Maya crude but more than 200 nm for Athabasca bitumen, and that asphaltene-rich nanostructure composition is independent of size. In light of these findings, re-evaluation of SAXS/SANS data for asphaltene-rich nanostructures and models for asphaltene-rich nanostructures and their chemistry is warranted.

References

(1) Mullins, O. C., Sheu, E. Y., Hammami, A., and Marshall A. G. (Editors), *Asphaltenes, Heavy Oils, and Petroleomics*. New York: Springer: 2007.

(2) Speight, J. G., *The Chemistry and Technology of Petroleum*. 4th ed.; New York: M. Dekker: 2007.

(3) Speight, J. G.; Long, R. B.; Trowbridge, T. D. Factors Influencing the Separation of Asphaltenes from Heavy Petroleum Feedstocks. *Fuel* **1984,** 63, (5), 616-620.

(4) Alboudwarej, H.; Beck, J.; Svrcek, W. Y.; Yarranton, H. W.; Akbarzadeh, K. Sensitivity of Asphaltene Properties to Separation Techniques. *Energy & Fuels* **2002,** 16, (2), 462-469.

(5) Berna, A. C. S.; Moran, V. C.; Guzman, E. T. R.; Yacaman, M. J. Asphaltene Aggregation from Vacuum Residue and Its Content of Inorganic Particles. *Petroleum Science and Technology* **2006,** 24, (9), 1055-1066.

(6) Nalwaya, V.; Tangtayakom, V.; Piumsomboon, P.; Fogler, S. Studies on Asphaltenes through Analysis of Polar Fractions. *Industrial & Engineering Chemistry Research* **1999,** 38, (3), 964-972.

(7) Wang, J. X.; Buckley, J. S. Asphaltene Stability in Crude Oil and Aromatic Solvents - The Influence of Oil Composition. *Energy & Fuels* **2003,** 17, (6), 1445-1451.

(8) Tanabe, K.; Gray, M. R. Role of Fine Solids in the Coking of Vacuum Residues. *Energy & Fuels* **1997,** 11, (5), 1040-1043.

(9) Yang, X. L.; Hamza, H.; Czarnecki, J. Investigation of Subfractions of Athabasca Asphaltenes and Their Role in Emulsion Stability. *Energy & Fuels* **2004,** 18, (3), 770-777.

(10) Duong, A.; Chattopadhyaya, G.; Kwok, W. Y.; Smith, K. J. An Experimental Study of Heavy Oil Ultrafiltration Using Ceramic Membranes. *Fuel* **1997,** 76, (9), 821-828.

(11) Savvidis, T. G.; Fenistein, D.; Barre, L.; Behar, E. Aggregated Structure of Flocculated Asphaltenes. *Aiche Journal* **2001,** 47, (1), 206-211.

(12) Sheu, E. Y. Small Angle Scattering and Asphaltenes. *Journal of Physics-Condensed Matter* **2006,** 18, (36), S2485-S2498.

(13) Mason, T. G.; Lin, M. Y. Asphaltene Nanoparticle Aggregation in Mixtures of Incompatible Crude Oils. *Physical Review E* **2003,** 67, (5).

(14) Gawrys, K. L.; Kilpatrick, P. K. Asphaltenic Aggregates are Polydisperse Oblate Cylinders. *Journal of Colloid and Interface Science* **2005,** 288, (2), 325-334.

(15) Andreatta, G.; Bostrom, N.; Mullins, O. C. High-Q Ultrasonic Determination of The Critical Nanoaggregate Concentration of Asphaltenes and The Critical Micelle Concentration of Standard Surfactants. *Langmuir* **2005,** 21, (7), 2728-2736.

(16) Freed, D. E.; Lisitza, N. V.; Sen, P. N.; Song, Y.-Q., *Chapter 11. Molecular Composition and Dynamics of Oils from Diffusion Measurements. Asphaltenes, Heavy Oils, and Petroleomics*. Springer: New York, 2007.

(17) Sheu, E.; Long, Y.; Hamza, H., *Chapter 10. Asphaltene Self-Association and Precipitation in Solvent--AC Conductivity Measurements. Asphaltenes, Heavy Oils, and Petroleomics.* . Springer: New York, 2007.

(18) Yudin, I. K.; Anisimov, M. A., *Chapter 17: Dynamic Light Scattering Monitoring of Asphaltene Aggregation in Crude Oils and Hydrocarbon Solutions. Asphaltenes, Heavy Oils, and Petroleomics.* Springer: New York 2007.

(19) Gearhart, J. A. Solvent Treat Resids. *Hydrocarbon Processing* **1980,** 60, (5), 150-151.

(20) Penning, R. T.; Vickers, A. G.; Shah, B. R. Extraction Upgrades Resid. *Hydrocarbon Processing* **1982,** 61, (5), 145-150.

(21) Chung, K. H.; Xu, C. M.; Hu, Y. X.; Wang, R. N. Supercritical Fluid Extraction Reveals Resid Properties. *Oil & Gas Journal* **1997,** 95, (3), 66-69.

(22) Black, L. E.; Miasek, P. G.; Adriaens, G. U.S. Patent No. 4,532,029, 1985.

(23) Black, L. E., and Boucher, H. A. U.S. Patent No. 4,571,444, 1986.

(24) Chen, T. J., and Sweet, J. R. U.S. Patent No. 5,107,058, 1992.

(25) West, T. H.; Thompson, J. A. U.S. Patent No. 4, 432,866, 1984.

(26) Bitter, F. G. A., Haan, J. P., and Rijkens, H. C. Solvent Recovery with Membranes in Lube Oil Dewaxying. *AIChE Symposium Series* **1989,** 85, 98-100.

(27) Osterhuber, E. J. U.S. Patent No. 4, 797,200, 1989.

(28) Bitter, F. G. A.; Clark, R. H.; Den Boestert, J. L. W. C.; Rajani, J. B. U.S. Patent No. 5,133,851, 1992.

(29) Feimer, J. L.; DesJardine, L. T. U.S. Patent No. 5,256,297, 1993.

(30) Arod, J.; Bartoli, B.; Bergez, P.; Biedermann, J.; Martinet, J.-M.; Maurin, J.; Rossaire, J. U.S. Patent No. 4,411,790, 1983.

(31) Douda, J.; Llanos, E.; Alvarez, R.; Franco, C. L.; de la Fuente, J. A. M. Pyrolysis Applied to the Study of a Maya Asphaltene. *Journal of Analytical and Applied Pyrolysis* **2004,** 71, (2), 601-612.

(32) Rahmani, S.; McCaffrey, W.; Gray, M. R. Kinetics of Solvent Interactions with Asphaltenes during Coke Formation. *Energy & Fuels* **2002,** 16, (1), 148-154.

(33) Speight, J. G. Petroleum asphaltenes - Part 1 - Asphaltenes, Resins and the Structure of Petroleum. *Oil & Gas Science and Technology-Revue De L Institut Francais Du Petrole* **2004,** 59, (5), 467-477.

(34) Mullins, O. C.; Betancourt, S. S.; Cribbs, M. E.; Dubost, F. X.; Creek, J. L.; Andrews, A. B.; Venkataramanan, L. The colloidal structure of crude oil and the structure of oil reservoirs. *Energy & Fuels* **2007,** 21, (5), 2785-2794.

(35) Gonzalez, G.; Sousa, M. A.; Lucas, E. F. Asphaltenes Precipitation from Crude Oil and Hydrocarbon Media. *Energy & Fuels* **2006,** 20, (6), 2544-2551.

(36) Yan, N. X.; Masliyah, J. H. Characterization and Demulsification of Solids-Stabilized Oil-in-Water Emulsions .1. Partitioning of Clay Particles and Preparation of Emulsions. *Colloids and Surfaces a-Physicochemical and Engineering Aspects* **1995,** 96, (3), 229-242.

(37) Yan, N. X.; Masliyah, J. H. Characterization and Demulsification of Solids-Stabilized Oil-in-Water Emulsions .2. Demulsification by the Addition of Fresh Oil. *Colloids and Surfaces a-Physicochemical and Engineering Aspects* **1995,** 96, (3), 243-252.

(38) Kotlyar, L. S.; Sparks, B. D.; Woods, J. R.; Raymond, S.; Le Page, Y.; Shelfantook, W. Distribution and Types of Solids Associated with Bitumen. *Petroleum Science and Technology* **1998,** 16, (1-2), 1-19.

(39) Sanaie, N.; Watkinson, A. P.; Bowen, B. D.; Smith, K. J. Effect of Minerals on Coke Precursor Formation. *Fuel* **2001,** 80, (8), 1111-1119.

(40) Rahmani, S.; McCaffrey, W.; Elliott, J. A. W.; Gray, M. R. Liquid-Phase Behavior during the Cracking of Asphaltenes. *Industrial & Engineering Chemistry Research* **2003,** 42, (17), 4101-4108.

(41) Rahimi, P.; Gentzis, T.; Fairbridge, C. Interaction of Clay Additives with Mesophase Formed during Thermal Treatment of Solid-Free Athabasca Bitumen Fraction. *Energy & Fuels* **1999,** 13, (4), 817-825.

(42) Cyr, T. D.; Strausz, O. P. Bound Carboxylic Acids in the Alberta Oil Sands. *Organic Geochemistry* **1984,** 7, (2), 127-140.

(43) Uemori, Y.; Osada, A.; Munakata, H.; Imai, H. Calcium-ion induced color changes of a porphyrin solution. *Inorganica Chimica Acta* **2006,** 359, (14), 4594-4600.

5. Impact of Asphaltene-Rich Aggregate Size on Coke Deposition on a Commercial Hydroprocessing Catalyst

5.1 Introduction

Asphaltene aggregate size distribution in native oils and in model mixtures has been investigated for some time. Pioneering work[1-3] using small angle X-ray scattering showed that asphaltenes in crude oil comprise small aggregates with radii of gyration between 2 and 4 nm as well as large aggregates with leading dimensions in the hundreds of nanometers. Small aggregates have also been observed in asphaltene plus solvent or deasphalted oil mixtures.[4] A review by Sheu[5] concludes that asphaltene molecules are of the order of 0.5 — 0.6 nm in radius and that elementary asphaltene aggregates possess radii of approximately 3.0 nm. At higher concentrations these elementary aggregates appear to cluster. Recent studies[6-9] report threshold concentrations for asphaltene aggregation of 100 to 200 mg/L in toluene where as prior research places the threshold at 2 to 18 g/L. Andreatta et al.[6] suggest that the older literature reports concentration values for the formation of larger secondary aggregates and not the smaller primary aggregates identified more recently. In Chapter 4, it shows that Athabasca bitumen and Maya crude, both of which have high asphaltene concentrations (18 and 16 wt %), possess asphaltene aggregate size distributions ranging from less than 5 nm to more than 100 nm in diameter. Significant aggregation and broad asphaltene size distributions are therefore expected for heavy feed stocks in general where the concentrations of both heavy metals, another source for catalyst foulants, and asphaltenes are high.

Asphaltene diffusion through a porous medium with a narrow pore size distribution[10] reveals an order of magnitude difference in the diffusion rates between some asphaltene subfractions and bulk fluid. A mathematical model[11] describing the transport of rigid nanospheres through membranes yielded diffusivities of the same order of magnitude as the experimental results for asphaltene diffusion.[10, 12] Adsorptive uptake experiments[13] conducted at 308 K with coal and petroleum asphaltenes in a $NiMo/Al_2O_3$ hydrotreating catalyst with tetrohydrofuran as a solvent also show variability. Numerous models[14-18] have been proposed to estimate the effective diffusivity of asphaltenes in commercial catalysts under hydroprocessing conditions. These studies all suggest that hindered diffusion is significant under hydroprocessing conditions.

Typical commercial hydroprocessing catalysts possess pore sizes in the range of 3 nm to over 100 nm.[19] Clearly, asphaltene rich aggregate sizes and catalyst pore sizes overlap. Hindered diffusion for asphaltene aggregates in hydroprocessing catalyst pellets is expected due to this size overlap. Coking outcomes, both deposition modes and amounts deposited, are likely to be sensitive to the details of asphaltene aggregate size distribution or coke precursor molar mass in a feed, and the pore size distribution of catalyst pellets employed. Divergent results reported in the literature[17, 20-26] should be viewed as illustrative of this sensitivity.

Typically, coke deposition data within catalyst pellets are interpreted using uniform surface deposition[23] and pore mouth plugging[22] models. Bulk phase coke deposition[23] involving the formation of mesophase may also arise. Aspects of this latter deposition mode are discussed elsewhere.[27] During uniform surface deposition, the normalized pore-size distribution (number-based) shifts to smaller values without shape change.

Mathematical relationships linking pore surface area and pore volume loss resulting from uniform deposition are readily defined if pore geometry is known or assumed. For example, for a given deposition thickness b, the relationship between the normalized pore size distribution functions pre- (f) and post- (f') reaction is:

$$f'(r-b) = f(r) \tag{5-1}$$

if the pores are assumed to be a distribution of cylinders, the pore surface area, A, and the pore volume, V, of the fresh catalyst are defined as:

$$A = \int 2\pi \cdot rL \cdot f(r)dr \tag{5-2}$$

$$V = \int \pi \cdot r^2 L \cdot f(r)dr \tag{5-3}$$

where $f(r)$ is the fraction of pores of unit length L and radius r, and is independent of the actual pore lengths at a given radius. As the coke layer is deposited, the pore surface area, A', and pore volume, V', become:

$$A' = \int 2\pi \cdot (r-b)L \cdot f(r)dr \tag{5-4}$$

$$V' = \int \pi \cdot (r-b)^2 L \cdot f(r)dr \tag{5-5}$$

and the fractional reductions in pore surface area and pore volume arising from coke deposition are:

$$\frac{\Delta A}{A} = \frac{\int b \cdot fdr}{\int r \cdot fdr} = \frac{b \cdot \int fdr}{\int r \cdot fdr} = \frac{b}{\int r \cdot fdr} \tag{5-6}$$

$$\frac{\Delta V}{V} = \frac{\int [r^2 - (r-b)^2] \cdot fdr}{\int r^2 \cdot fdr} = \frac{\int (2br - b^2) \cdot fdr}{\int r^2 \cdot fdr} = \frac{2b \cdot \int r \cdot fdr - b^2}{\int r^2 \cdot fdr} \tag{5-7}$$

Thus, the ratio of pore area loss to pore volume loss is:

$$\frac{\frac{\Delta A}{A}}{\frac{\Delta V}{V}} = \frac{b}{\int r \cdot f dr} \cdot \frac{\int r^2 \cdot f dr}{2b \cdot \int r \cdot f dr - b^2} = \frac{\int r^2 \cdot f dr}{\int r \cdot f dr} \cdot \frac{1}{2\int r \cdot f dr - b} = \frac{\bar{r}^2 + \sigma^2}{\bar{r}(2\bar{r} - b)} = \frac{1 + \frac{\sigma^2}{\bar{r}^2}}{2 - \frac{b}{\bar{r}}} \quad (5\text{-}8)$$

where σ^2 is the variance and $\bar{r}$ is the mean pore radius of the fresh catalyst. The coke layer thickness, b, must be smaller than the minimum radius of pores in the fresh catalyst. The value of the normalized surface area loss to pore volume loss must fall between 0.5 and 1 for this mechanism to be a dominant one. As the means and variances of pore size distributions and the surface areas and pore volumes pre- and post- reaction can be measured, deposit thickness can be evaluated from experimental data. Exogenous validation of this value using surface analysis techniques (e.g. focused-ion-beam, FIB) is also feasible.

Other potential deposition models, such as the proportional filling model, where the deposit thickness is proportional to the pore radius, yield a similar result:

$$\frac{\frac{\Delta A}{A}}{\frac{\Delta V}{V}} = \frac{1}{2 - \frac{b}{r}} \quad (5\text{-}9)$$

where b/r is a constant. A similar range of pore surface area loss to pore volume loss values arises. Thus, uniform and proportional deposition models are not readily discriminated.

Pore mouth plugging is more readily identified. For example, if plugs isolate small pores, then the ratio of the normalized surface area loss to normalized pore volume loss exceeds unity. This arises because surface area is concentrated in small pores whereas pore volume is concentrated in large pores. If plugging isolates pores that are

representative of the entire pore size distribution, then the ratio of the surface area to pore volume does not change with deposition. Further, plugging can also be detected from changes in the shape of the sorption isotherms.[28]

The objective of this chapter is to evaluate the impact of asphaltene aggregate size on coke deposition mode and the amount of coke deposited in a representative commercial catalyst. To this end, deposition experiments were conducted with nano-filtered Athabasca bitumen and Maya crude permeates, Athabasca bitumen and Maya crude, and Athabasca bitumen and Maya crude retentates. Preparation of filtered samples of Athabasca bitumen and Maya crude, the procedure of coking experiments and the characterization of coked catalyst are described in Chapter 3 (3.1—3.3). Efforts were made to address the roles of potential artifacts and confounding variables in the data sets. For example, asphaltene concentration and mean asphaltene-rich nanoaggregate size are linked. The mass ratio of hydrogen to feed was fixed at two levels, but the ratio of hydrogen to asphaltenes decreases with increasing asphaltene content. Trace dissolved oxygen also influences coke deposition. The potential impact of thermal history of feed samples on the results obtained was also addressed. The inclusion of such control experiments complicated the experimental program and aspects of the interpretation of the resulting data but broaden the application of the results obtained.

5.2 Results and discussion

Nanofiltration nominally separates asphaltene-rich aggregates by size. Smaller aggregates are found in permeates; larger aggregates are found in retentates. However, separation by filtration is imperfect. Due to the build up of a filter cake on the retentate

side of the filter, for example, some aggregates smaller than the nominal pore size remain in retentates. Asphaltene-rich aggregates in permeates tend to be smaller than the nominal pore size of the filter medium. Asphaltene aggregate size, size distribution, and mass fraction also become joint variables. This artifact may well be present elsewhere in the literature where feeds, solvents, or maltenes are seeded with asphaltenes at various concentrations and asphaltene aggregate size is an uncontrolled variable. Further, while the mass ratio of hydrogen to feed is fixed and the solubility of hydrogen in the feeds on an asphaltene free basis is expected to be similar,[29] the variation of hydrogen solubility and availability for reaction with asphaltene content is not evaluated or controlled. The ratio of hydrogen to asphaltenes decreases as the mass fraction of asphaltenes increases. Thus, coke yields at fixed reaction time for added hydrogen and hydrogen free cases should approach one another as the mass fraction of asphaltenes increases. Such effects must be considered during data interpretation.

Other potential confounding variables do not appear to be present. Chapter 4 shows that Asphaltene composition was found to be nanoaggregate size invariant, and the other SARA fractions, for example, were not differentially partitioned by nano filtration. The detailed composition data sets for feeds, permeates and retentates are shown in Table 4.1 for Athabasca bitumen and in Table 4.2 for Maya crude. The composition data for Athabasca bitumen vacuum residue are summarized in Table 5.1. While the size distribution of the asphaltene aggregates present in Athabasca vacuum residue was not measured, one can presume that the nominal size range is comparable to that arising in Athabasca bitumen.

Table 5.1 Composition of Athabasca bitumen vacuum residue

	ABVB[30]
Elemental Analysis, wt %	
C	81.7
H	9.5
N	0.7
S	6.9
O	-
SARA Analysis, wt %	
saturates	6.8
aromatics	42.0
resins	19.2
asph. (C5)	32.2
Metal Analysis, ppm	
Mo	17
Ni	137
V	344

5.2.1 Coke deposition

In general, the roles played by asphaltene concentration, hydrogen, and trace oxygen conform to the expectations present in the coke deposition and coke kinetics literatures. Key points are illustrated in this section.

5.2.1.1 Joint impact of asphaltene content and asphaltene-rich nanoaggregate size

Coking experiments were performed with permeates and retentates associated with Athabasca bitumen and Maya crude oil as well as with the two feeds and Athabasca vacuum residue. Figure 5.1 shows the carbon content of the coked catalyst as a function of asphaltene concentration for all samples. The carbon content increases with asphaltene weight fraction. Further, the data conform with anticipated trends for deposition at a fixed reaction time, temperature, hydrogen mass fraction, and pressure.[31, 32] In general,

coefficients appearing in coke content relationships depend on feed properties, reaction conditions and reactor types. Here, all of the data are well represented by:

$$C_C = 7.4886 C_A^{0.1664} \tag{5-10}$$

where C_C is the carbon weight percent in the catalyst following reaction, C_A is the asphaltene weight percent in the feed. From the coke deposition data and from Equation 10, the amount of coke deposited is insensitive to asphaltene-free feed composition and weakly dependent on asphaltene concentration. For example, the carbon content of the catalyst following reaction with Maya related samples only doubles between an asphaltene content of 1.5 wt % (MP5) and 63 wt % (MR50). The initial size of the asphaltene aggregates decreases as concentration decreases, in general, and for these experiments in particular; one is tempted to assume that asphaltene diffusion into the catalyst pellets is facilitated at low concentrations. This matter is addressed further below.

5.2.1.2 Impact of hydrogen on coke deposition

Coking experiments were performed with and without added hydrogen. The carbon contents of the coked catalyst pellets for these cases are compared in Figure 5.2. As expected, more coke is deposited in the absence of hydrogen,[33] and the coke contents for the two cases converge as the asphaltene mass fraction is increased. For example, for the Athabasca bitumen case, the difference between the carbon wt % for the with and for the without added hydrogen cases decreases as the asphaltene wt % increases – from a 3 wt % difference at 5 wt % asphaltenes to 1 wt % at 19 wt % asphaltenes. For Maya crude the impact is less pronounced.

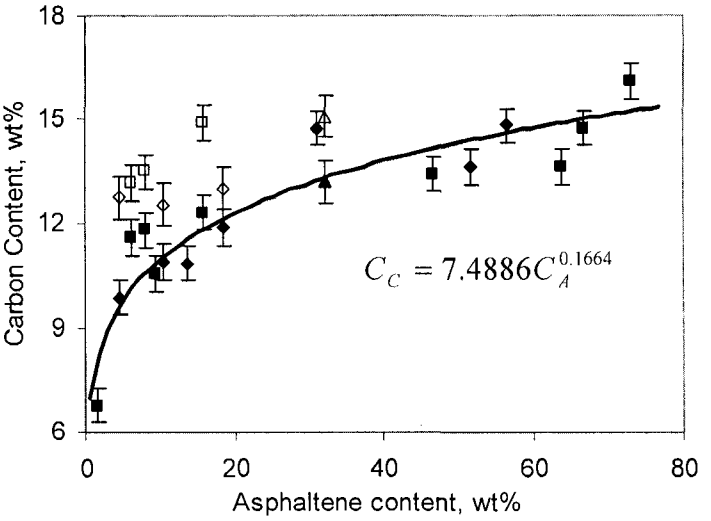

Figure 5.1 Bulk carbon contents of coked catalyst pellets for permeates and retentates associated with Athabasca bitumen and Maya crude oil, T=653K, t=2h, feed(wt)/catalyst(wt)=30, hydrogen(wt)/feed(wt)=0.005.

♦ Athabasca bitumen; ◊ Athabasca bitumen (no added hydrogen); ■ Maya crude; □ Maya crude (no added hydrogen); ▲ABVB; Δ ABVB (no added hydrogen); —Equation 5-10.

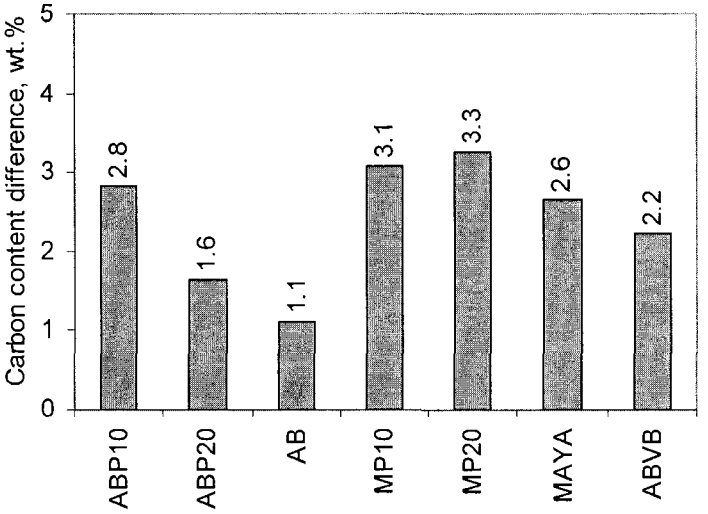

Figure 5.2 Bulk carbon content differences in coked catalyst pellets for added hydrogen /no added hydrogen analogues.

5.2.1.3 Impact of trace oxygen on coke deposition

If trace oxygen is present in a feed, heating per se to 200 °C for prolonged periods does not affect coke deposition during subsequent catalytic processing. The differences between results obtained for feed samples used directly in coking experiments and those heated for 30 days at 200°C are well within experimental error. However, "Oxygen-free" bitumen samples prepared by bubbling nitrogen through bitumen for 5 days at 50 °C (refer to Chapter 4 and Chapter 3, 3.1.2) generate systematically lower coke contents in catalyst pellets as shown in Figure 5.3. For example, coke contents in catalyst pellets for "oxygen-free" ABP20 permeate, "oxygen-free" bitumen and "oxygen-free" ABR20 retentate are 0.7 — 1.4 wt % lower than analogues containing trace oxygen. This conforms qualitatively with prior work.[34, 35] Whether the impact of trace oxygen occurs during initial heating or at reaction temperature needs more investigation.

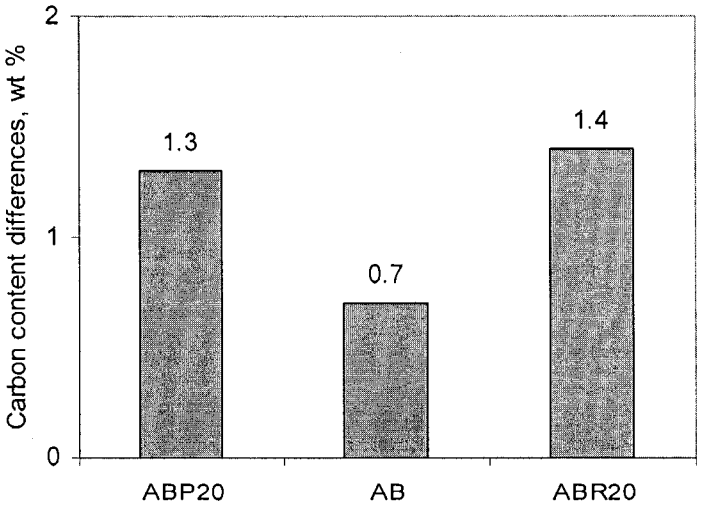

Figure 5.3 Bulk carbon content differences for heat-treated as-received and oxygen-free Athabasca bitumen samples.

5.2.2 Characterization of catalyst pellets

5.2.2.1 Surface area, pore volume and pore size distribution

Surface area, pore volume and pore size distribution statistics for sulfided and coked catalyst pellets are shown in Tables 5.2 and 5.3 for the Athabasca bitumen and Maya crude related experiments, respectively. Pore size distributions are shown in Figure 5.4a,b, and adsorption/desorption hysteresis loops are shown in Figure 5.5a,b. In general, the surface area and pore volume losses for pellets exposed to permeates and retentates are similar. Surface area losses are in the range of 0 — 11 %, for feeds associated with both Athabasca bitumen and Maya crude, while pore volume losses are in the range of 20 — 40 %.

Pore mouth plugging is not a dominant deposition mode because none of the identifying criteria are met. Pore surface area loss is less than pore volume loss for all samples – Tables 5.2 and 5.3. The surface area to pore volume ratio is a function of the extent of deposition – Figure 5.6. The adsorption/desorption isotherms, Figure 5.5, do not change shape but shift to lower pressures relative to sulfided catalyst pellets. This is consistent with pore narrowing and is inconsistent with pore mouth plugging.[28] The results also appear to be inconsistent with uniform or proportional deposition as dominant modes, where according to Equations 5-8 and 5-9, the ratio of surface area loss to pore volume loss should be in the range 0.5 to 1.

Surface area loss is minimal. Most measurements fall within the margin of error, while pore volume loss is significant. The loss ratio falls below 0.5 for all cases. From the pore size distributions, Figure 5.4a,b, pores in the ~ 20 Å size range are being created during coking. These have a negligible impact on pore volume but increase surface area. In prior

work, we have attributed these pores to the formation of a porous coke layer during coking experiments.[27] It is not clear whether the elimination of this effect is large enough to increase the ratio of the fractional pore area loss to fractional pore volume loss above 0.5 for the pellets alone.

For the case of Maya crude, Ancheyta and co-workers[36-39] observed significant changes in the shape of the adsorption/desorption isotherms following reaction for a variety of non-commercial catalysts and a variety of operating conditions. They attributed their observations to the development of restrictions in the pore structure. As anticipated in the introduction, coking outcomes, both deposition modes and amounts deposited, are expected to be sensitive to the details of the pore size distribution within catalyst pellets because of the overlap in the asphaltene aggregate and pore size distributions. The commercial catalyst we employ has a narrow pore size distribution about 18 — 90 Å, while catalyst employed by Ancheyta and co-workers has much broader pore size distributions, extending from ~ 25 Å to more than 200 Å. A larger mass fraction of asphaltenes can therefore penetrate their pellets. So the large surface area and pore volume losses they observe (50 — 80 % of the respective values for fresh catalyst pellets) and any differences in deposition mode are readily anticipated.

Table 5.2 Bulk analytical data for catalyst coked using bitumen derived samples[1]

	SC	ABP10	ABP20	OFBP20	ABP20[2]	ABP50	AB	AB[2]	AB-H	ABR50	OFBR20	ABR20	ABR10
asph. in feed, wt %	-	4.54	10.4	11.1	10.4	13.6	18.6	18.6	18.7	51.9	55.2	56.7	31.3
carbon in catalyst, wt %	-	9.9	10.9	9.6	12.5	10.9	11.9	13.0	12.0	13.6	13.4	14.8	14.7
SA (m^2/g)	179	181	172	174	160	180	186	172	186	161	181	165	160
SAL (%)	-	-1±6	4±6	3±6	11±5	-1±6	-4±6	4±6	-4±6	10±5	-1±6	8±5	11±5
PV (mL/g)	0.55	0.44	0.42	0.44	0.39	0.42	0.41	0.38	0.37	0.35	0.38	0.36	0.36
PVL (%)	-	20±6	24±6	20±6	29±6	24±6	25±6	31±6	33±6	36±5	31 ±5	35±5	35±5
SA/PV($x10^{-6}m^{-1}$)	325	411	410	395	410	429	454	453	503	460	476	458	444
SAL/PVL	-	0.1±0.3	0.2±0.3	0.1±0.3	0.4±0.3	0.0±0.3	-0.2±0.3	0.1±0.3	-0.1±0.2	0.3±0.2	0.0±0.2	0.2±0.2	0.3±0.2
Pore volume distribution in radii													
>300 Å	0	0	0	0	0	0	0	0	0	0	0	0	0
100 Å -300 Å	6.6	7.9	7.7	7.9	7.8	7.0	7.6	7.1	7.9	7.9	7.4	7.6	7.7
40 Å -100 Å	61	49	43	44	40	43	39	38	37	37	38	36	38
20 Å -40 Å	32	41	47	46	49	48	50	51	50	51	50	52	50
10 Å -20 Å	0	1.7	2.7	2.2	2.7	2.1	3.5	3.9	4.5	4.0	4.0	4.3	3.7

[1] SC, sulfided catalyst; SA, surface area; PV, pore volume; SAL, surface area loss; PVL, pore volume loss;

[2] Coking experiments were conducted without hydrogen.

Table 5.3 Bulk analytical data for catalyst coked using Maya crude oil derived samples[1]

	SC	MP5	MP10	MP20	MP50	Maya	MR50	MR20	MR10	MR5
asph. in feed, wt %	-	1.5	6.2	8.1	9.4	15.7	63.8	73.0	67.0	46.7
carbon in catalyst, wt %	-	6.8	10.1	10.2	10.6	12.3	13.6	14.8	16.1	13.4
SA (m^2/g)	179	173	167	180	184	175	162	163	173	173
SAL (%)	-	3.4±6	6.7±6	-0.6±6	-2.8±6	2.2±6	9.5±6	8.9±6	3.4±6	3.4±6
PV (mL/g)	0.55	0.46	0.44	0.42	0.40	0.39	0.33	0.34	0.34	0.36
PVL (%)	-	16±6	20±6	24±6	27±6	29±6	40±5	38±5	38±5	35±5
SA/PV ($x10^{-6}m^{-1}$)	325	376	380	429	460	449	491	479	509	481
SAL/PVL	-	0.2±0.4	0.3±0.4	0.0±0.3	-0.1±0.3	0.1±0.3	0.2±0.2	0.2±0.2	0.1±0.2	0.1±0.2
Pore volume distribution in radii										
>300 Å	0	0	0	0	0	0	0	0	0	0
100 Å -300 Å	6.6	6.7	7.2	8.0	6.6	8.2	6.7	7.3	7.7	6.7
40 Å -100 Å	61	50	44	47	42	42	38	39	41	43
20 Å -40 Å	32	42	47	44	48	47	49	51	46	47
10 Å -20 Å	0	1.1	1.8	1.1	3.4	2.8	5.9	3.3	5.4	3.4

[1] SC, sulfided catalyst; SA, surface area; PV, pore volume; SAL, surface area loss; PVL, pore volume loss.

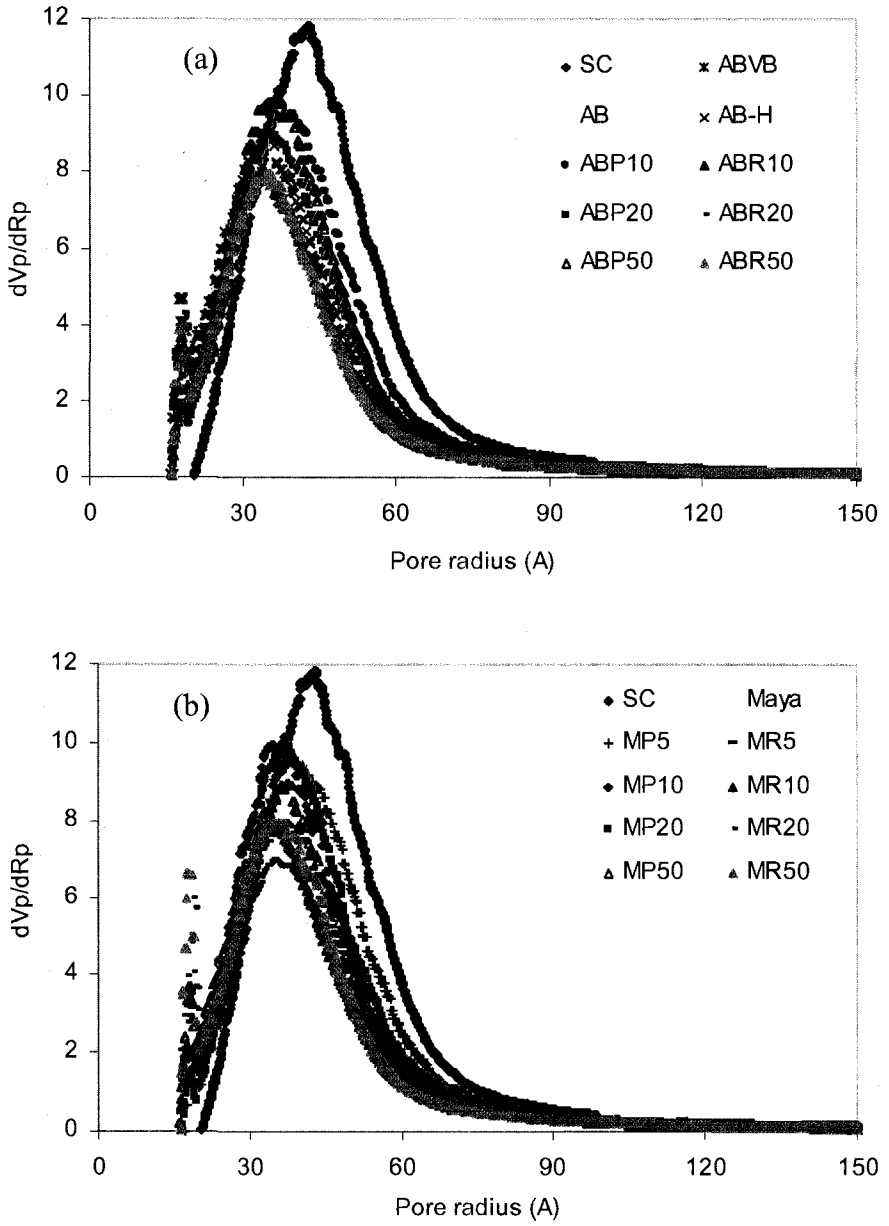

Figure 5.4 Pore size distributions for sulfided and coked catalyst pellets.

(a) Athabasca bitumen related samples and (b) Maya crude related samples.

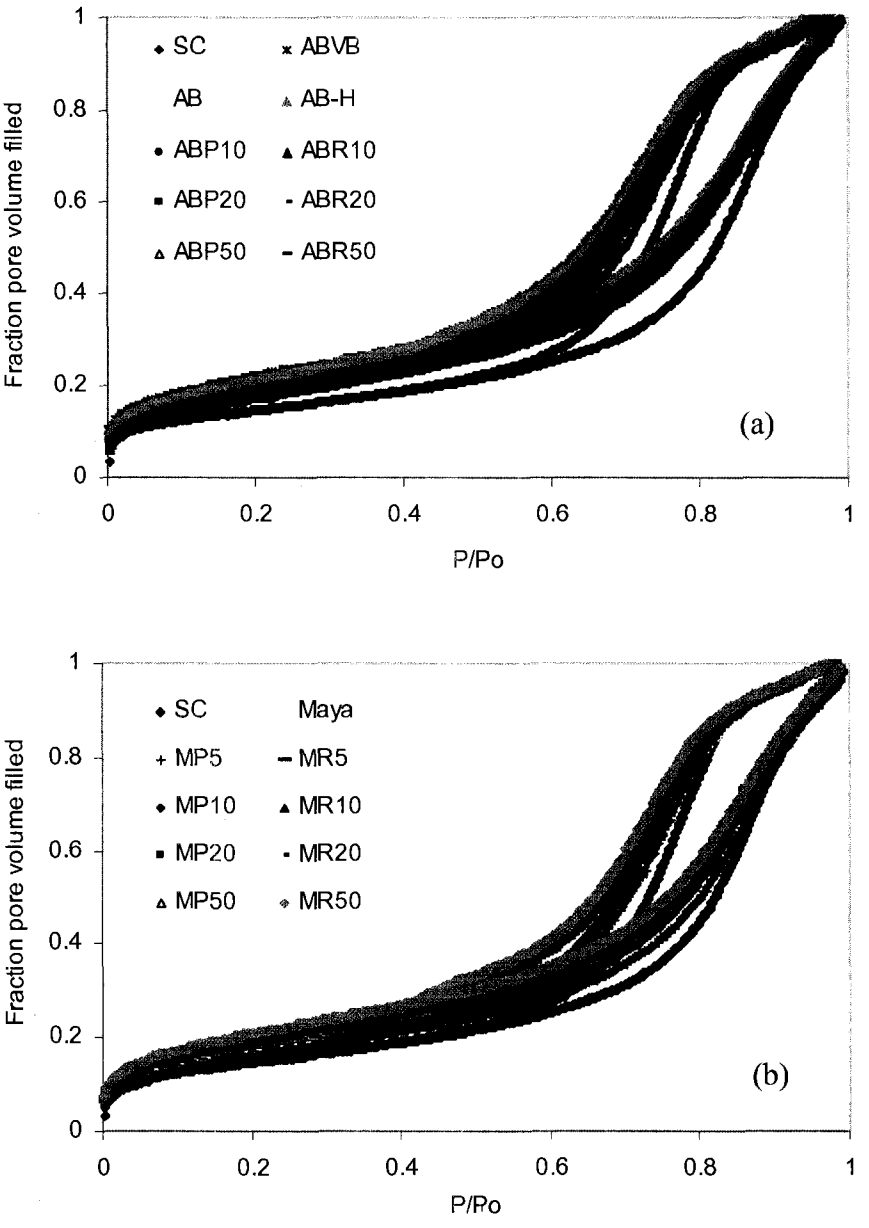

Figure 5.5 Adsorption/desorption isotherms for catalyst pellet samples.

(a) Athabasca bitumen related samples and (b) Maya crude related samples.

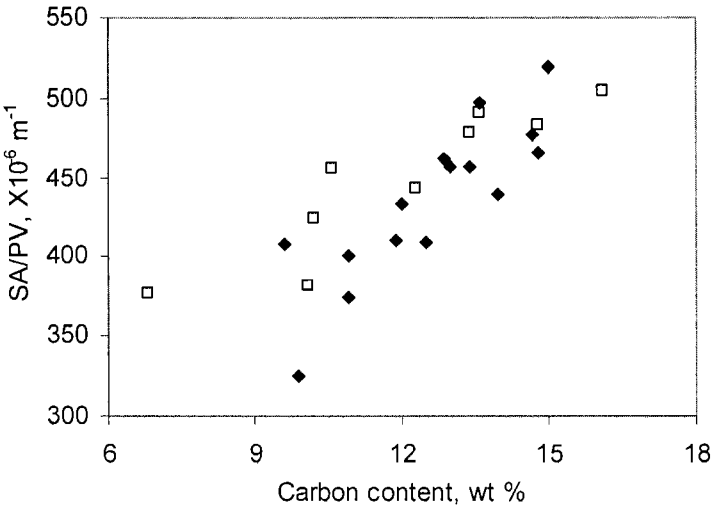

Figure 5.6 Surface area to pore volume ratios for coked catalyst pellets with respect to bulk carbon content: ♦ Athabasca bitumen and □ Maya crude oil.

5.2.2.2 Effect of hydrogen and dissolved oxygen on coke deposition mode

As discussed above, hydrogen and dissolved oxygen in feeds both influence the coke content of catalyst pellets. Figure 5.7 shows the pore size distributions and adsorption/desorption isotherms for coked catalyst pellets arising from with and without added hydrogen analogues, while Figure 5.8 shows the pore size distributions and isotherms for coked catalyst pellets exposed to "oxygen-free" and untreated bitumen. The pore size distributions and the isotherms for all cases evaluated are similar. Neither hydrogen nor oxygen appears to influence the coke deposition mode even though they affect the amount of coke deposited.

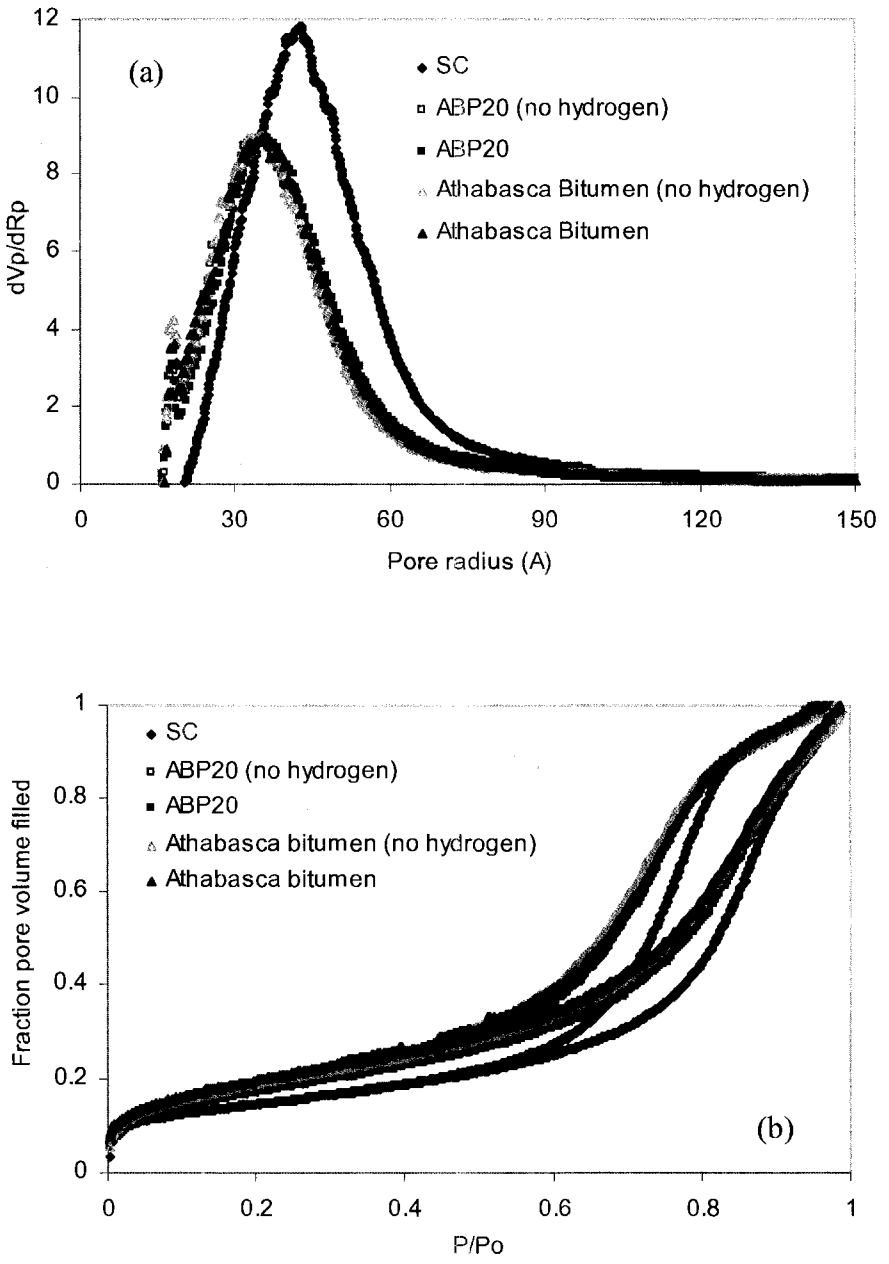

Figure 5.7 (a) Pore size distributions and (b) adsorption/desorption isotherms of coked catalyst pellets for Athabasca bitumen related samples with and without added hydrogen.

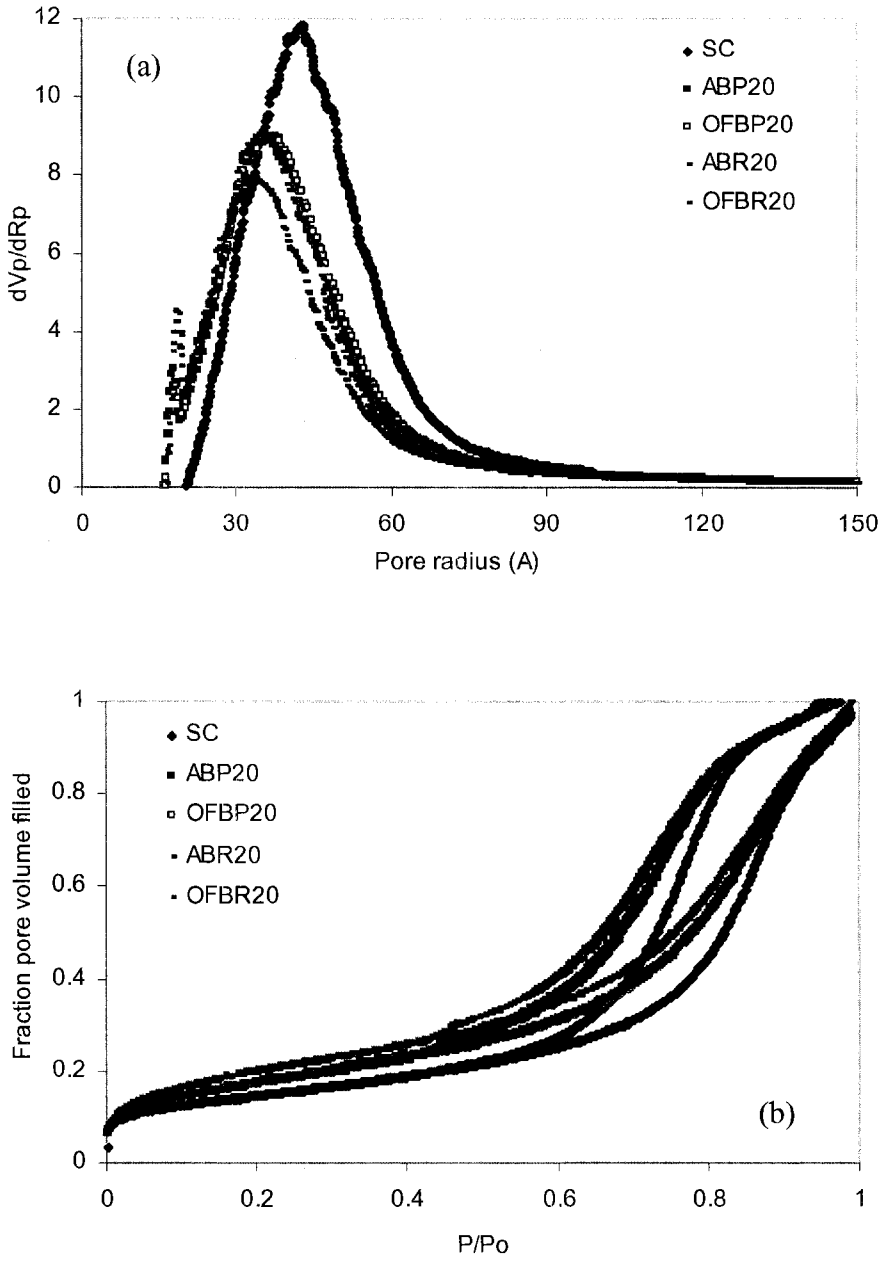

Figure 5.8 (a) Pore size distributions and (b) adsorption/desorption isotherms of coked catalyst pellets for untreated and "oxygen-free" Athabasca bitumen samples.

5.2.2.3 Analysis of catalyst pellet cross sections

Local C, Ni, Mo, and V composition profiles are shown in Figures 5.9 to 5.12 for catalyst pellets exposed to Athabasca bitumen and Maya crude related samples, respectively. Figures 5.9 to 5.12 a-d comprise carbon coated cases; Figures 5.9 to 5.12 e-h comprise iridium coated cases. Both coating types are employed routinely for such analyses. As the two sets of analyses are consistent with one another, they are reported jointly.

In Figures 5.9 to 5.12 a and e, the carbon content is higher at the external edges of the pellets and lower and more uniform in the interior. While iridium coated samples understate carbon content and the carbon coated samples overstate carbon content (if the impact of the 7.5 ± 0.5 wt % carbon coating is ignored), it is clear that the carbon content of the catalyst interiors is less than the corresponding bulk carbon contents in Tables 5.2 and 5.3. As reported in prior work,[27] the pellets here also appear to be coated with a carbon-rich deposit. Ni and Mo, both present in the catalyst at high concentration and in the feed at low concentration, exhibit an opposite trend with position – Figures 5.9 to 5.12 b and f for Ni, and Figures 5.9 to 5.12 c and g for Mo. This inverse trend is consistent with high carbon concentrations at or near the outer surface of catalyst pellets that suppress the concentrations of elements present initially.

Vanadium is only a constituent in the feeds. From the "measured" vanadium content of the sulfided catalyst pellets, the local threshold for detection appears variable and is in the range about 0.003 — 0.01 wt %. As the vanadium contents in the catalyst pellets are of the same order or one order of magnitude higher, the wt % vanadium data are noisy. For the most part, analyses performed with both iridium and carbon coated samples show that

vanadium is distributed uniformly throughout the pellets within measurement error as shown in Figures 5.9 to 5.12 d and h. Exceptions include samples ABP50 (Figure 5.9) and MR5 (Figure 5.10) where both the carbon and iridium coated sample analyses indicate local concentration maxima between the centre of the pellets and external surface. There is weaker support for similar extrema in the concentration profiles for samples MP10 and MR10 (only analyses for carbon coated samples are available) – Figure 5.10. Apparently, contradictory vanadium concentration profiles for the ABP20 (oxygen free) sample (Figure 5.11) obtained from the carbon coated and iridium coated cases suggest caution with respect to the interpretation of vanadium concentration profile data.

These observations differ from reports[40-42] showing vanadium deposition occurs preferentially at the outer edges of coked catalyst pellets (where vanadium deposition is thought to be diffusion limited) and a report by Janssens et al.,[43] who found a maximum in the vanadium concentration at the centre of catalyst pellets during hydrodemetallization (HDM) of vanadyl-tetraphenylporphyrin (VO-TPP) and linked this to a sequential reaction mechanism. The profiles for vanadium deposition observed here suggest that vanadium deposition is not diffusion limited. One possible explanation is that the vanadium found in the deposits is contributed by smaller asphaltene aggregates or present in the maltenes, both of which diffuse readily through catalyst pores. For example, the vanadium content of the feed ABP10 with 4.5 wt % asphaltenes, Table 4.1, is half the value in AB with 18.7 wt % asphaltenes. MP5 with only 1.5 wt % asphaltenes, Table 4.2, has a quarter of the vanadium content of Maya crude which contains 16 wt % asphaltenes.

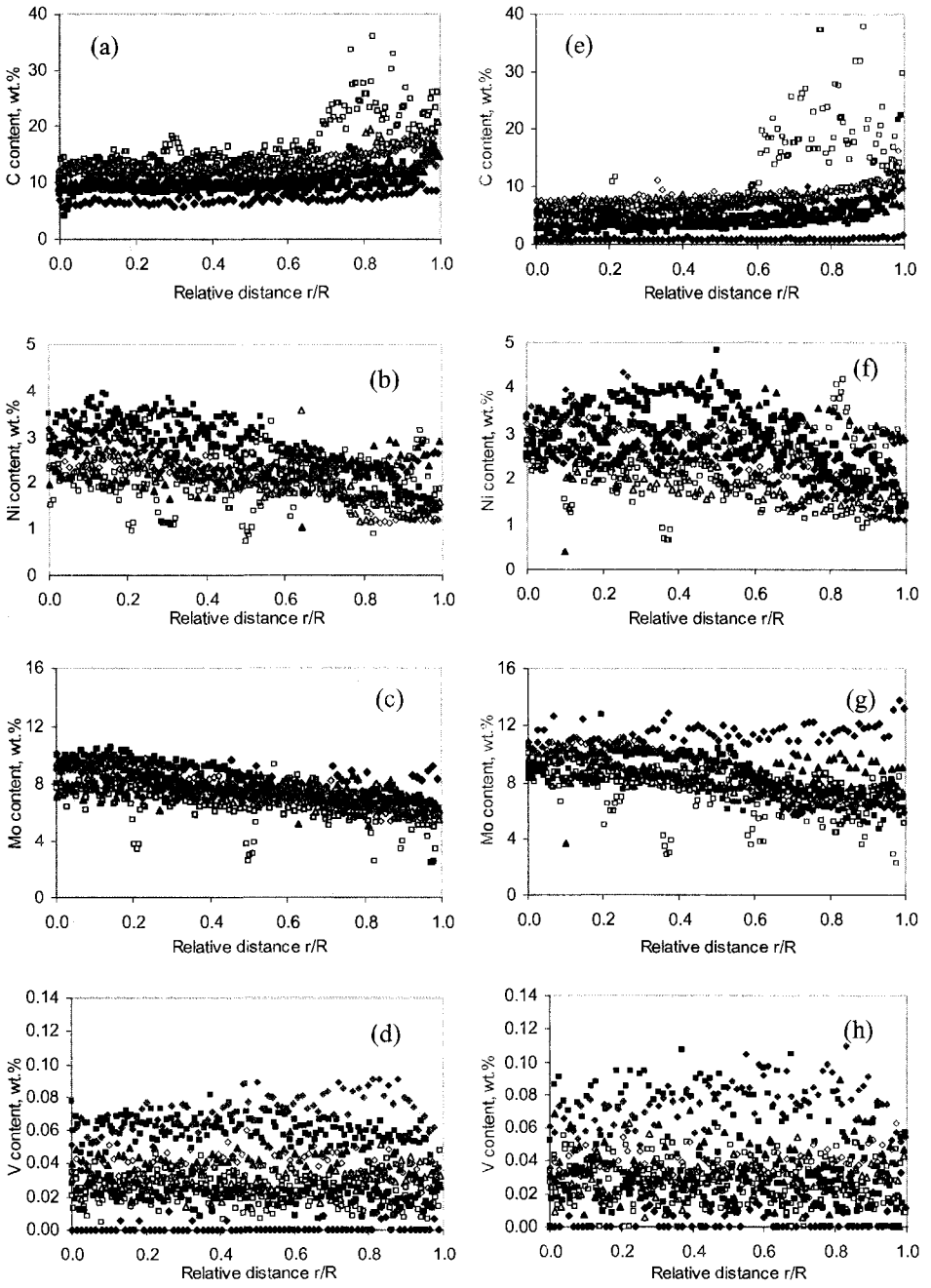

Figure 5.9 Radial element distributions for coked catalyst pellet cross sections (Athabasca bitumen related samples): (a — d) carbon coated, (e — h), Ir coated. ♦: Fresh catalyst; ■: Athabasca bitumen; □: Athabasca bitumen (heated); ▲: AB permeate (10 nm); △: AB retentate (10 nm); ■: AB permeate (20 nm); □: AB retentate (20 nm); ♦: AB permeate (50 nm); ◇: AB retenteate (50 nm)

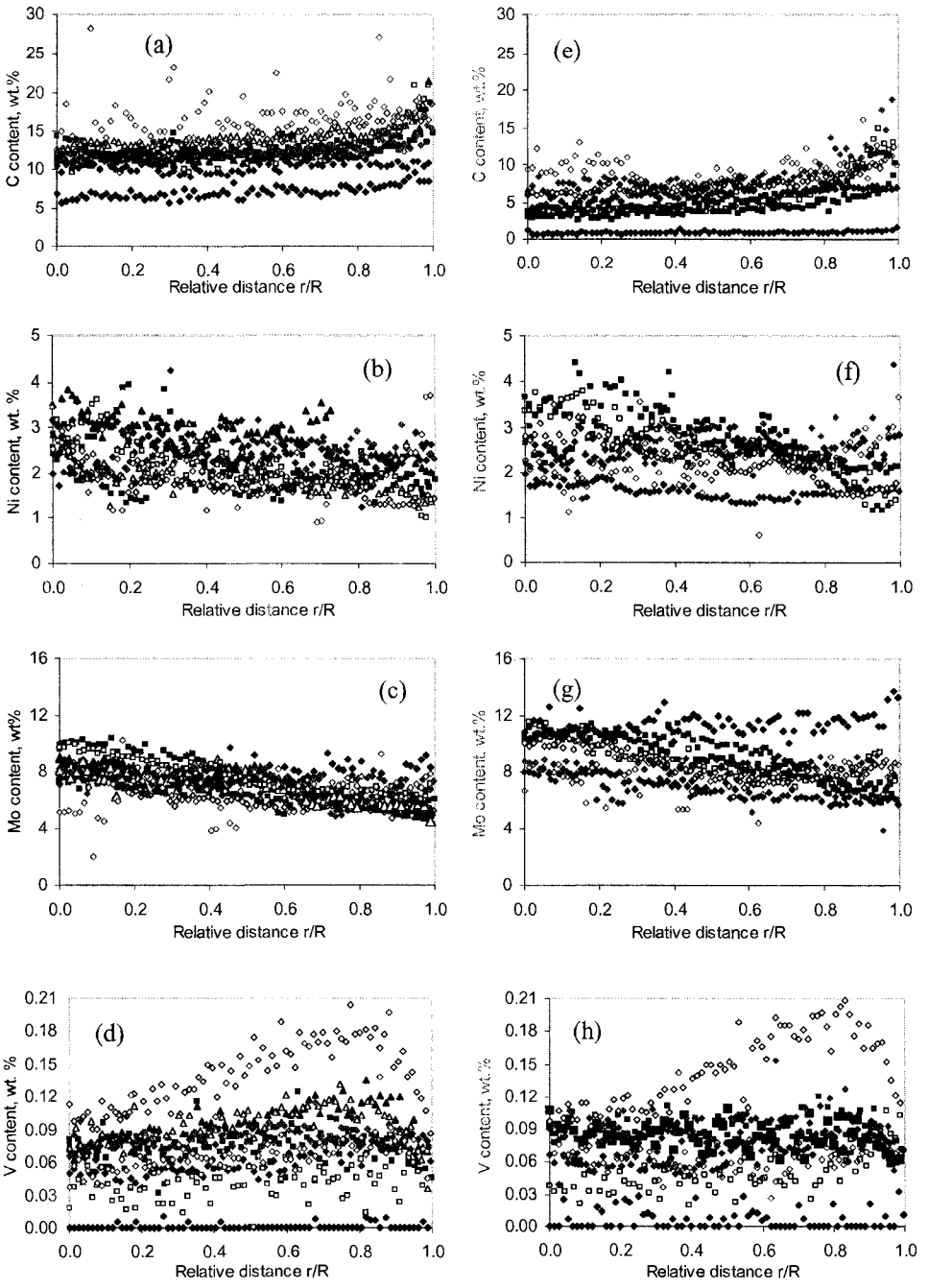

Figure 5.10 Radial element distributions for coked catalyst pellet cross sections (Maya crude related samples), (a — d), carbon coated; (e — h), Ir coated.

♦: Fresh catalyst; ■ : Maya crude; ♦: Maya permeate (5 nm); ◊ : Maya retentate (5 nm); ▲: Maya permeate (10 nm); △ : Maya retentate (10 nm); ■: Maya permeate (20 nm); □: Maya retentate (20 nm); ♦ : Maya permeate (50 nm); ◊: Maya retentate (50 nm).

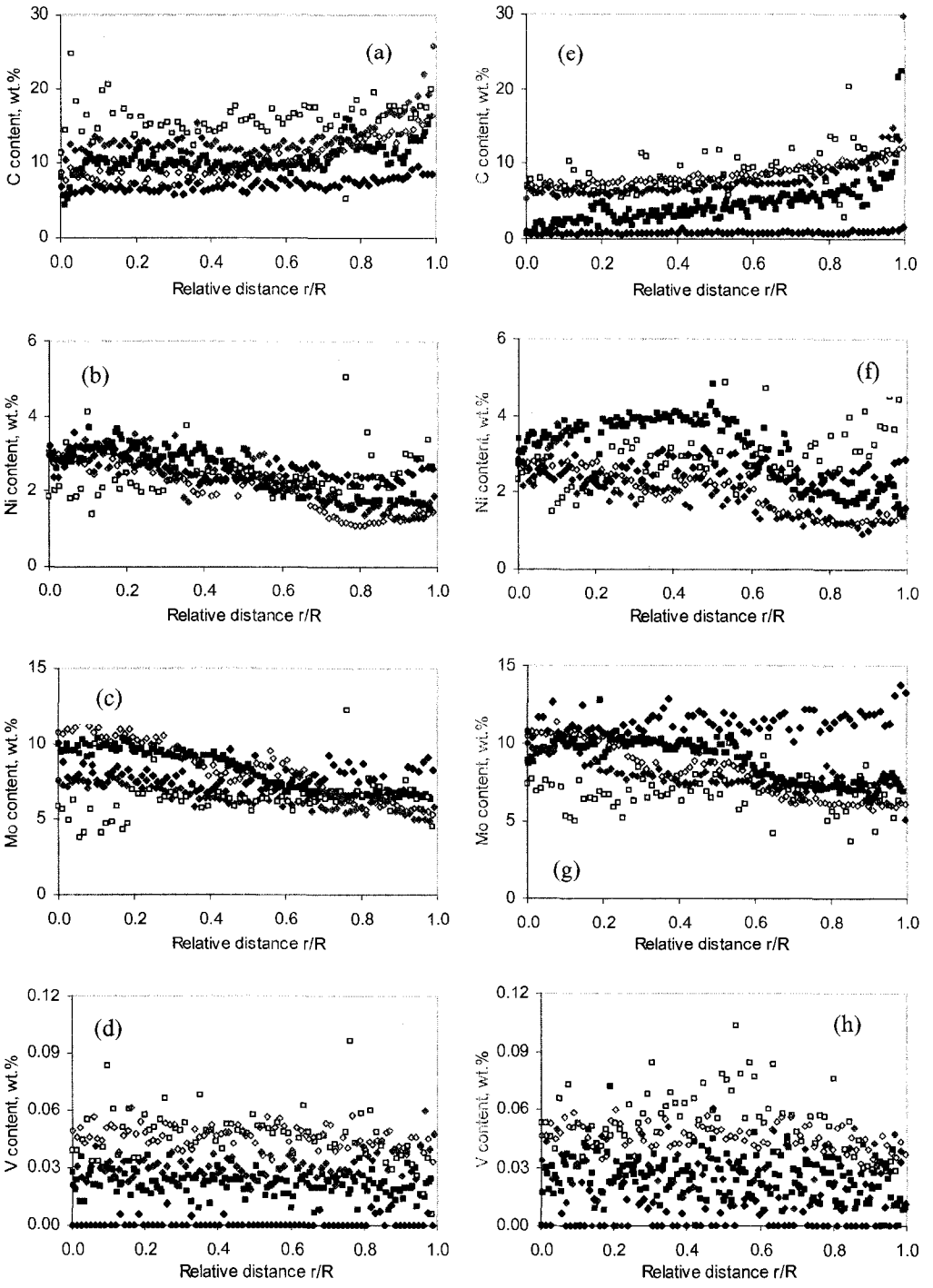

Figure 5.11 Radial element distributions for coked catalyst pellet cross sections (bitumen and "oxygen free" bitumen samples): (a — d), carbon coated; (e — h), Ir coated.

♦: Fresh catalyst; ■ : AB permeate (20 nm); □ : AB permeate (20 nm, "oxygen-free"), ♦: AB retentate (20 nm); ◊ : AB retentate (20 nm, "oxygen-free").

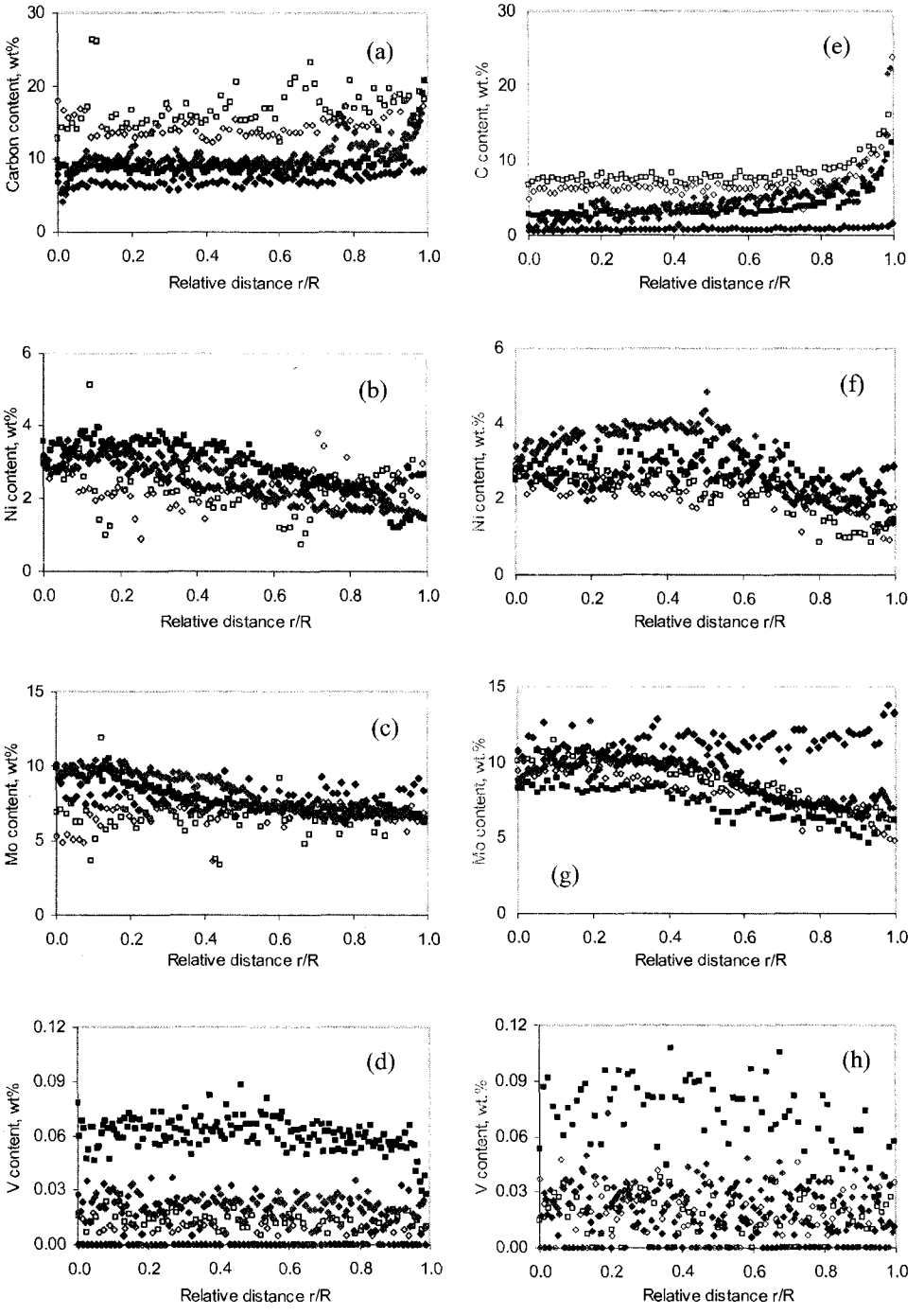

Figure 5.12 Radial element distributions for coked catalyst pellet cross sections (hydrogen vs no added hydrogen bitumen samples): (a — d), carbon coated; (e — h), Ir coated. ♦: Fresh catalyst; ■ : Athabasca bitumen; □ : Athabasca bitumen (no hydrogen); ♦: AB permeate (20 nm); ◊: AB permeate (20 nm, no hydrogen).

The unweighted average vanadium concentration within catalyst pellets is more robust than individual or local measurements, and the average selectivity for vanadium in a coke deposit vis-à-vis a feed, is sensitive to operating conditions and feed compositions as noted in Figure 5.13. Vandium selectivity is defined as the mass ratio of vanadium to carbon in the deposit to the mass ratio of vanadium to carbon in the feed. All deposits are enriched in vanadium relative to their respective feeds and two asymptotes are apparent. One corresponds to the asphaltene-rich nano-aggregates at low maltene wt % where a minimum measured selectivity of ~ 2 is obtained; the other corresponds to high maltene content where measured selectivities exceed 30 for Athabasca bitumen permeate and 120 for Maya permeate samples. These selectivity data suggest that asphaltene-rich nano aggregates are minor contributors to vanadium enrichment in the coke deposits within catalyst pellets. One may argue that the apparent selectivity to maltene vanadium results from saturation effects. For example, asphaltene-rich aggregates contain a lot of vanadium and could saturate the surface sites leading to low selectivity. However, maltenes have little vanadium and would not experience this reduction. This can be excluded from the observation here. The uniform vanadium distributions after 2 h strongly suggest vanadium in deposits comes from smaller asphaltene aggregates and maltenes. Saturation effect may affect only after longer times.

If one assumes that the vanadium selectivities of asphaltene and maltene fractions are independent of their respective mass fractions, then Equation 5-11 gives:

$$S = S_m^0 \times X_{V-m} + S_{Asph.}^0 \times (1 - X_{V-m}) \tag{5-11}$$

where S is the vanadium selectivity in a deposit, S_m^0 is the vanadium selectivity for maltenes, $S_{Asph.}^0$ is the vanadium selectivity for asphaltenes, X_{V-m} is the mass of

vanadium present in the maltenes divided by the total mass of vanadium in a sample. The regressed vanadium selectivities are ~ 280 for Maya maltenes and ~ 35 for Athabasca bitumen maltenes and ~ 1-2 for both Maya and Athabasca bitumen asphaltenes. Vanadium deposition from nanoaggregates is primarily a non-selective physical deposition process whereas the vanadium in maltenes has specific interactions with catalyst surfaces. Maltenes have facile access to the entire pore network irrespective of their mass fraction in the feeds, as do smaller nanoaggregates. From a fluid mechanics perspective, this suggests that, for the cases evaluated here, the feeds (maltenes plus a fraction of nanoaggregates) flow into the pellets and interact with interior surfaces independently but in proportion to their composition in the feed.

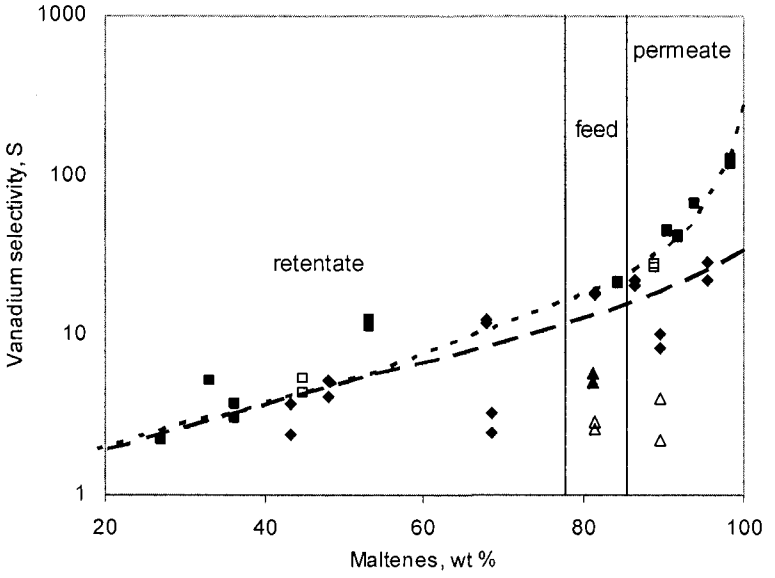

Figure 5.13 Vanadium selectivity in coke deposits vs feeds.

♦ Athabasca bitumen; ■ Maya crude; ▲heated Athabasca bitumen; Δ Athabasca bitumen with no added hydrogen; □ "oxygen-free" Athabasca bitumen; - - - Equation 5-11 fitted to Athabasca bitumen data; ..... Equation 5-11 fitted to Maya crude data.

Again, the link with the divergent results in the literature is clear. Vanadium in large nanoaggregates, relative to the catalyst pore size distribution, is subject to diffusion limitation. Vanadium present in molecules interacts with active sites within the catalyst pellets, and the resulting distribution reflects the distribution of active sites in the pore structure, as well as the details of the reaction mechanisms involved. Over-interpretation of "noisy" concentration profile data may also account for extant interpretations.

With this background in mind, the roles played by hydrogen, trace oxygen, and feed heat treatment in coke deposition, exemplified for AB, ABP20, and ABR20, are readily elucidated. For example, without added hydrogen, the selectivity for vanadium approaches the lower non-selective asymptote, i.e. deposition via a physical process. Clearly, vanadium deposition from maltenes arises from chemical reaction. By contrast, trace oxygen has no measurable impact on vanadium selectivity within catalyst pellets, even though it does affect the amount of coke deposited – possibly on external surfaces. The Athabasca bitumen sample heated for 30 days at 200 °C has a lower selectivity than the fresh analogue. Again the impact appears to be on the maltene fraction. One anticipates that maltenes react with oxygen to produce less reactive or larger species.

5.2.2.4 Impact of prolonged feed heating feeds containing oxygen on coke distribution within catalyst pellets

Prolonged heating at 200 °C of feeds containing oxygen increases the coke content of catalyst pellets vis-à-vis oxygen free analogs. However, the coked catalyst pore structures, and their elemental distribution profiles are similar, as shown in Figures 5.8 and 5.11 for Athabasca bitumen, as are the conclusions one draws from them. Thus, it is

clear that prolonged heating of feeds such as bitumen, which contain trace oxygen, increases the amount of coke deposited but not the mode of deposition.

5.2.2.5 Impact of hydrogen on coke deposition within catalyst pellets

Adding 0.5 wt % hydrogen to the reactant mixture reduces the coke content of catalyst pellets vis-à-vis the no added hydrogen analogs by 10—20 % (1—3 wt %) as shown in Figure 5.2. However, the pore structures and their elemental distribution profiles remain similar, as shown in Figures 5.7 and 5.12, respectively, for Athabasca bitumen. The conclusions one draws are also similar. Hydrogen reduces the amount of coke deposited but does not appear to affect the mode of deposition. It is important to note though that given the high asphaltene contents of the feeds, the high catalyst concentration and the low hydrogen concentration, the reaction environment being probed remains close to the "no added hydrogen" limit.

5.2.3 Effect of asphaltene-rich nanoaggregate size on coke distribution in catalyst pellets

The cumulative size distributions for pores in sulfided catalyst pellets and the nominal size of asphaltene-rich nanoaggregates in Athabasca bitumen and Maya crude oil defined on the basis of nanofiltration are shown in Figure 5.14. The mean pore diameter in sulfided catalyst pellets is ~ 9 nm. The minimum and maximum pore diameters are ~ 4 nm and ~ 20 nm. Maya asphaltene-rich nanoaggregate size ranges from less than 5 nm to 100 nm while those in Athabasca bitumen range from less than 10 nm to more than 200

nm. Approximately 50 wt % of asphaltenes in both feeds pass through a 20 nm filter at 473 K. 10 wt % of nanoaggregates in Maya crude pass through a 5 nm filter and 25 wt % of those in Athabasca bitumen pass through a 10 nm filter at the same conditions.

Clearly, a significant fraction of the asphaltene-rich nanoaggregates in both feedstocks can penetrate the pore structure. However, only asphaltene-rich nanoaggregates in the Maya 5 nm permeate (MP5) have potentially facile access to the entire pore network.

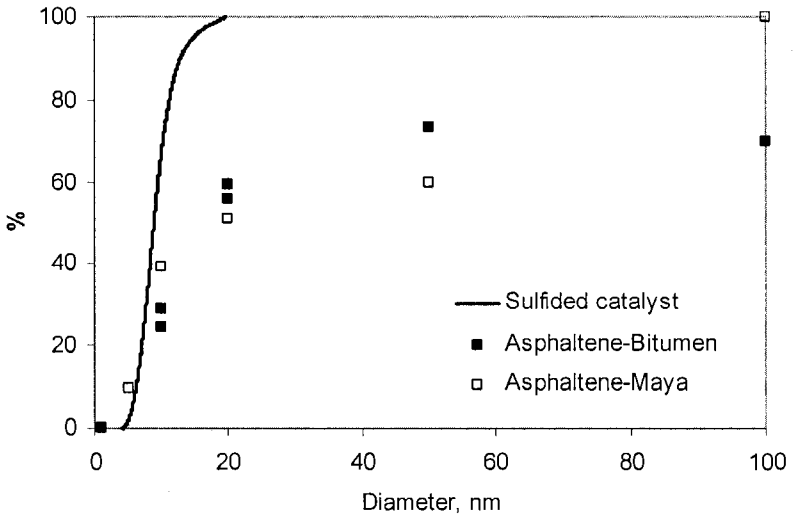

Figure 5.14 Athabasca bitumen and Maya crude asphaltene-rich nanoaggregate and sulfided catalyst pore size distributions.

5.2.4 Implications for coke formation reaction paths

Reaction models for coke formation from asphaltenes include both series[33, 44] and parallel[23, 45] reaction paths. For parallel reaction, where asphaltenes yield coke and other reaction products directly, either a uniform coke distribution (low diffusion resistance) or a preferential deposition (high diffusion resistance) with higher concentrations near the

pellet exterior arises. For series reaction, where asphaltenes produce intermediates that then form coke, higher deposit concentrations are expected in the interior of the pellets and lower ones near the exterior for low diffusion resistance cases. For high diffusion resistance cases, a preferential deposition with higher concentrations near the pellet exterior arises.

The ratio of carbon content at the centre of pellets to the bulk carbon content was evaluated for each coking experiment using both the carbon coated and iridium coated pellet cross sections. The values for carbon-coated samples were corrected for the impact of the coating. No correction was required for the iridium-coated samples as the iridium layer is thin and its mass fraction is small. The results are presented as a function of the asphaltene content in feeds in Figure 5.15.

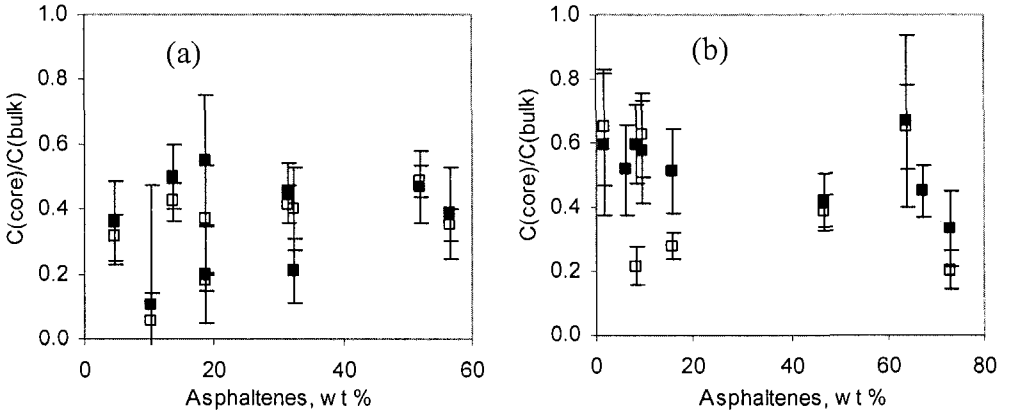

Figure 5.15 The ratio of carbon at pellet cores to the bulk carbon content vs asphaltene content in feeds.

(a) Athabasca bitumen derived samples, (b) Maya crude derived samples. ■: carbon coated, □: iridium coated.

All of the values are less than unity and those obtained from carbon and iridium coated samples agree with one another within experimental error in most cases. There are no trends with asphaltene mass fraction for either the Athabasca bitumen or Maya crude related samples. However, the ratios are generally higher for Maya crude related cases than for the Athabasca bitumen related cases. This is consistent with the smaller maximum size of the Maya asphaltenes. Diffusion resistance is significant for all cases. Thus, the common reaction paths employed in modeling are not discriminated.

5.3 Conclusions

The impact of asphaltene-rich nanoaggregate size on coke deposition in commercial hydroprocessing catalyst pellets was investigated using nanofiltered Athabasca bitumen and Maya crude oil samples as feeds. While asphaltene mass fraction and asphaltene-rich nanoaggregate size are joint variables, aggregate size distributions are broad and overlap with the catalyst pore size distribution for all cases. The amount of coke deposited was found to be a weak function of asphaltene concentration in feeds and maltene composition. Secondary variables such as hydrogen mass fraction and trace oxygen in feeds proved to be of equal importance. Coke deposition within pores is shown to be diffusion limited for all cases evaluated with the smaller Maya asphaltene-rich nanoaggregates less affected by this limitation than the larger Athabasca bitumen asphaltene-rich nanoaggregates. Coke deposits formed within the pellets are shown to restrict but not block pores. By contrast, vanadium deposition within catalyst pellets is shown to arise primarily from the maltene fraction and is shown not to be diffusion limited.

References

(1) Dwiggins, C. W., A Small Angle X-Ray Scattering Study of Colloidal Nature of Petroleum. *Journal of Physical Chemistry* **1965,** 69, (10), 3500-3506.

(2) Dwiggins, C. W., The Study of Colloidal Nature of Petroleum with an Automated Bonse-Hart X-Ray Small Angle Scattering Unit. *Journal of Applied Crystallography* **1978,** 11, (5), 615-619.

(3) Dwiggins, C. W., Absorption Correction and Normalization of X-Ray Small-Angle Scattering Data for Materials Producing Intense Scattering at Extremely Low Angles. *Journal of Applied Crystallography* **1979,** 12, (4), 401-402.

(4) Kim, H. G.; Long, R. B., Characterization of Heavy Residuum by a Small-Angle X-Ray-Scattering Technique. *Industrial & Engineering Chemistry Fundamentals* **1979,** 18, (1), 60-63.

(5) Sheu, J. I.; Sheu, E. Y., Characterization of DNA degradation using direct current conductivity and dynamic dielectric relaxation techniques. *Aaps Pharmscitech* **2006,** 7, (2).

(6) Andreatta, G.; Bostrom, N.; Mullins, O. C., High-Q Ultrasonic Determination of the Critical Nanoaggregate Concentration of Asphaltenes and the Critical Micelle Concentration of Standard Surfactants. *Langmuir* **2005,** 21, (7), 2728-2736.

(7) Sheu, E.; Long, Y.; Hamza, H., *Chapter 10. Asphaltene Self-Association and Precipitation in Solvent--AC Conductivity Measurements. Asphaltenes, Heavy Oils, and Petroleomics.* . Springer: New York, 2007.

(8) Freed, D. E.; Lisitza, N. V.; Sen, P. N.; Song, Y.-Q., *Chapter 11. Molecular Composition and Dynamics of Oils from Diffusion Measurements. Asphaltenes, Heavy Oils, and Petroleomics*. Springer: New York, 2007.

(9) Evdokimov, I. N.; Eliseev, N. Y.; Akhmetov, B. R., Asphaltene Dispersions in Dilute Oil Solutions. *Fuel* **2006,** 85, (10-11), 1465-1472.

(10) Baltus, R. E.; Anderson, J. L., Hindered Diffusion of Asphaltenes through Microporous Membranes. *Chemical Engineering Science* **1983,** 38, (12), 1959-1969.

(11) Ravi-Kumar, V. S.; Tsotsis, T. T.; Sahimi, M., Studies of Transport of Asphaltenes through Membranes Using Hindered Diffusion Theories for Spheres and Spheroids. *Industrial&Engineering Chemistry Research* **1997,** 36, (8), 3154-3162.

(12) Sane, R. C.; Tsotsis, T. T.; Webster, I. A.; Ravikumar, V. S., Studies of Asphaltene Diffusion and Structure and Their Implications for Resid Upgrading. *Chemical Engineering Science* **1992,** 47, (9-11), 2683-2688.

(13) Yang, X. F.; Guin, J. A., Diffusion-Controlled Adsorptive Uptake of Coal and Petroleum Asphaltenes in a $NiMo/Al_2O_3$ Hydrotreating Catalyst. *Chemical Engineering Communications* **1998,** 166, 57-79.

(14) Satterfield.C.N.; Colton, C. K.; Pitcher, W. H., Restricted Diffusion in Liquids within Fine Pores. *AIChE Journal* **1973,** 19, (3), 628-635.

(15) Chantong, A.; Massoth, F. E., Restrictive Diffusion in Aluminas. *AIChE Journal* **1983,** 29, (5), 725-731.

(16) Tsai, C. H.; Massoth, F. E.; Lee, S. Y.; Seader, J. D., Effects of Solvent and Solute Configuration on Restrictive Diffusion in Hydrotreating Catalysts. *Industrial & Engineering Chemistry Research* **1991,** 30, (1), 22-28.

(17) Lee, S. Y.; Seader, J. D.; Tsai, C. H.; Massoth, F. E., Restrictive Diffusion under Catalytic Hydroprocessing Conditions. *Industrial & Engineering Chemistry Research* **1991,** 30, (1), 29-38.

(18) Lee, S. Y.; Seader, J. D.; Tsai, C. H.; Massoth, F. E., Restrictive Liquid-Phase Diffusion and Reaction in Bidispersed Catalysts. *Industrial & Engineering Chemistry Research* **1991,** 30, (8), 1683-1693.

(19) Gray, M. R.; Masliyah, J. H., *Extraction and Upgrading of Oil Sands Bitumen.* University of Alberta: Edmonton, 2004.

(20) Richardson, J. T., Experimental Determination of Catalyst Fouling Parameters - Carbon Profiles. *Industrial & Engineering Chemistry Process Design and Development* **1972,** 11, (1), 8-11.

(21) Johnson, B. G.; Massoth, F. E.; Bartholdy, J., Diffusion and Catalytic Activity Studies on Resid-Deactivated HDS Catalysts. *AIChE Journal* **1986,** 32, (12), 1980-1987.

(22) Muegge, B. D.; Massoth, F. E., Basic Studies of Deactivation of Hydrotreating Catalysts with Anthracene. *Fuel Processing Technology* **1991,** 29, (1-2), 19-30.

(23) Richardson, S. M.; Nagaishi, H.; Gray, M. R., Initial Coke Deposition on a NiMo/gamma-Al_2O_3 Bitumen Hydroprocessing Catalyst. *Industrial & Engineering Chemistry Research* **1996,** 35, (11), 3940-3950.

(24) Diez, F.; Gates, B. C.; Miller, J. T.; Sajkowski, D. J.; Kukes, S. G., Deactivation of a Ni-Mo Gamma-Al_2O_3 Catalyst - Influence of Coke on the Hydroprocessing Activity. *Industrial & Engineering Chemistry Research* **1990,** 29, (10), 1999-2004.

(25) Haldeman, R. G.; Botty, M. C., On the Nature of the Carbon Deposit of Cracking Catalysts. *Journal of Physical Chemistry* **1959,** 63, (4), 489-496.

(26) Ternan, M.; Furimsky, E.; Parsons, B. I., Coke Formation on Hydrodesulphurization Catalysts. *Fuel Processing Technology* **1979,** 2, (1), 45-55.

(27) Zhang, X. H.; Shaw, J. M., Impact of Multiphase Behavior on Coke Deposition in Heavy Oils Hydroprocessing Catalysts. *Energy & Fuels* **2006,** 20, (2), 473-480.

(28) Weissman, J. G.; Edwards, J. C., Characterization and Aging of Hydrotreating Catalysts Exposed to Industrial Processing Conditions. *Applied Catalysis a-General* **1996,** 142, (2), 289-314.

(29) Cai, H. Y.; Shaw, J. M.; Chung, K. H., Hydrogen Solubility Measurements in Heavy Oil and Bitumen Cuts. *Fuel* **2001,** 80, (8), 1055-1063.

(30) Zou, X. Y.; Dukhedin-Lalla, L.; Zhang, X. H.; Shaw, J. M., Selective Rejection of Inorganic Fine Solids, Heavy Metals, and Sulfur from Heavy Oils/Bitumen Using Alkane Solvents. *Industrial & Engineering Chemistry Research* **2004,** 43, (22), 7103-7112.

(31) Furimsky, E.; Massoth, F. E., Deactivation of Hydroprocessing Catalysts. *Catalysis Today* **1999,** 52, (4), 381-495.

(32) Froment, G. F.; Bischoff, K. B., *Chemical Reactor Analysis and Design.* 2nd ed.; New York : Wiley: 1990.

(33) Thakur, D. S.; Thomas, M. G., Catalyst Deactivation in Heavy Petroleum and Synthetic Crude Processing - a Review. *Applied Catalysis* **1985,** 15, (2), 197-225.

(34) Gray, M. R.; McCaffrey, W. C., Role of Chain Reactions and Olefin Formation in Cracking, Hydroconversion, and Coking of Petroleum and Bitumen Fractions. *Energy & Fuels* **2002,** 16, (3), 756-766.

(35) Acevedo, S.; Escobar, G.; Ranaudo, M. A.; Pinate, J.; Amorin, A.; Diaz, M.; Silva, P., Observations about the Structure and Dispersion of Petroleum Asphaltenes

Aggregates Obtained from Dialysis Fractionation and Characterization. *Energy & Fuels* **1997,** 11, (4), 774-778.

(36) Rana, M. S.; Ancheyta, J.; Maity, S. K.; Rayo, P., Characteristics of Maya crude hydrodemetallization and hydrodesulfurization catalysts. *Catalysis Today* **2005,** 104, (1), 86-93.

(37) Rana, M. S.; Ancheyta, J.; Maity, S. K.; Rayo, P., Maya crude hydrodemetallization and hydrodesulfurization catalysts: An effect of TiO2 incorporation in Al2O3. *Catalysis Today* **2005,** 109, (1-4), 61-68.

(38) Rana, M. S.; Ancheyta, J.; Rayo, P., Comparative study for heavy oil hydroprocessing catalysts at micro-flow and bench-scale reactors. *Catalysis Today* **2005,** 109, (1-4), 24-32.

(39) Rana, M. S.; Samano, V.; Ancheyta, J.; Diaz, J. A. I., A review of recent advances on process technologies for upgrading of heavy oils and residua. *Fuel* **2007,** 86, (9), 1216-1231.

(40) Inoguchi, M.; Kagaya, H.; Daigo, K.; Sakurada, S.; Satomi, Y.; Inaba, K.; Tate, K.; Nushiyama, R.; Onishi, S.; Nagal, T., Hydrodesulfurization Catalyst of Residual Fuel. 5. Deposits on the Used Catalyst. *Bulletin of the Japan Petroleum Institute* **1971,** 13, 153-61.

(41) Sato, M.; Takayama, N.; Kurita, S.; Kwan, T., Distribution of Vanadium and Nickel Deposits inside Desulfurization Catalysts. *Nippon Kagaku Zasshi* **1971,** 92, (10), 834-838.

(42) Todo, N.; Kabe, T.; Ogawa, K.; Kurita, M.; Sato, T.; Shimada, K.; Kuriki, Y.; Oshima, T.; Takemats.T; Kotera, Y., X-Ray Microanalytic Studies on MoO_3-CoO-Al_20_3

Hydrodesulfurization Catalysts - Dispersed States of Mo and Co and Distribution of Deposited V and Ni. *Kog Kagaku Zasshi* **1971,** 74, (4), 563-568.

(43) Janssens, J. P.; de Deugd, R. M.; van Langeveld, A. D.; Sie, S. T.; Moulijn, J. A., On the Metal Deposition Process during the Hydrodemetallation of Vanadyl-Tetraphenylporphyrin. In *Catalyst Deactivation*, 1997; Vol. 111, pp 283-294.

(44) Koyama, H.; Nagai, E.; Kumagai, H., Catalyst Deactivation in Commercial Residue Hydrodesulfurization. In *Deactivation and Testing of Hydrocarbon-Processing Catalysts*, 1996; Vol. 634, pp 208-218.

(45) Chang, H. J.; Seapan, M.; Crynes, B. L., Catalyst Decay during Hydrotreatment of a Heavy Coal Oil. *ACS Symposium Series* **1982,** 196, 309-320.

6. Interplay between the Physical Properties of Athabasca Bitumen + Diluent Mixtures and Coke Deposition on a Commercial Hydroprocessing Catalyst

6.1 Introduction

Catalyst deactivation during hydroprocessing of oils arises mainly from coke and metal deposition. For heavy residues, their significant asphaltene and vanadium contents enhance coke deposition. A better understanding of coke deposition under hydroprocessing conditions is crucial if operation efficiency of catalytic residue hydroprocessing processes is to be improved and the yield of distillable products maximized.

Asphaltenes are defined operationally, according to ASTM standards (ASTM D2006, ASTM D2007, and ASTM D4124), as a petroleum fraction that can be filtered from dilute mixtures with n-alkanes using filters with nominal pore sizes in the micron range, but pass through a filter with the same nominal pore size when dispersed in aromatic solvents. The terms, n-alkane insoluble and toluene soluble, are frequently used to describe asphaltenes, but these designations are overly simplistic if not misleading. Pioneering work[1-3] using small angle X-ray scattering showed that asphaltenes comprise small aggregates with radii of gyration between 2 and 4 nm as well as large aggregates with leading dimensions in the hundreds of nanometers in crude oils. Small aggregates have also been observed in asphaltene plus diluent or deasphalted oil mixtures.[4] A review by Sheu[5] concludes that asphaltene molecules are of the order of 0.5 — 0.6 nm in radius and that elementary asphaltene aggregates possess radii of approximately 3.0 nm. At

higher concentrations these elementary aggregates appear to cluster. Recent studies[6-9] report threshold concentrations for asphaltene aggregation of 100 to 200 mg/L in toluene whereas prior research places the threshold at 2 to 18 g/L. Andreatta et al.[6] suggest that the older literature reports concentration values for the formation of larger secondary aggregates and not the smaller primary aggregates identified more recently. In Chapter 4, it shows that Athabasca bitumen and Maya crude, both of which have high asphaltene concentrations (18 and 16 wt % respectively), possess asphaltene-rich aggregate size distributions with leading dimensions ranging from less than 5 nm to more than 100 nm in diameter at 200 °C. Significant aggregation and broad asphaltene size distributions are therefore expected for heavy feed stocks in general where the concentrations of both heavy metals, another source for catalyst fouling, and asphaltenes are high. Further, dilution of such feedstocks in hydrocarbon liquids is anticipated to affect aggregate size distribution. However, as typical commercial hydroprocessing catalysts possess pore sizes in the range of 3 nm to over 100 nm,[10] it is clear that asphaltene-rich aggregate sizes and catalyst pore sizes overlap for a broad range of feed stock + diluent compositions. Hindered diffusion for asphaltene-rich aggregates in hydroprocessing catalyst pellets is expected due to this size overlap.

The phase behavior of heavy oil + diluent mixtures is complex and characterized by large multiphase zones as exemplified recently for Athabasca vacuum residue + n-alkane mixtures.[11] For Athabasca vacuum residue + pentane mixtures comprising ~ 6 wt % asphaltenes, one liquid phase with less than 5 wt % asphaltenes and another with more than 75 wt % asphaltenes are found to be in equilibrium. In a reactor, one would expect catalyst pellets wet by one or the other of these two liquid phases to experience different

coke deposition outcomes. Further, if two liquid phases are present in a reactor, the one with the lower volume fraction (the one with the high asphaltene content in this case) tends to be dispersed in the other. As liquid-liquid mass transfer is slow, reactions within dispersed drops tend to be mass transfer limited if they rely on constituents from the continuous liquid phase, i.e. in this context, condensation reactions are preferred over hydrogenation reactions in dispersed asphaltene-rich drops. Such drops also tend to deposit on external catalyst surfaces and reactor walls. Thus, hydrodynamic effects arising in reactors due to multiphase behavior also affect coke deposition outcomes. The impact of phase behavior on coke deposition outcomes was addressed explicitly for Athabasca residue + decane mixtures,[12] where coke deposition was shown to be greater at low asphaltene concentrations than at higher asphaltene concentrations due to liquid-liquid phase behaviour or because the diluent is found primarily in a dense vapour phase rather than in the liquid phase. Such effects are not accounted for in existing coke deposition models.

In typical parametric investigations, the roles played, for example, by specific diluents in asphaltene conversion to low molar mass products, are frequently masked because asphaltene aggregate size distributions, the phase behaviour of diluent + feed stock mixtures, and molecular or abstractable hydrogen availability by phase comprise unmeasured and therefore uncontrolled variables in experiments. For example, hydrogen solubilities in n-alkanes such as n-dodecane and n-decane are roughly twice the values arising in 1-methylnaphthalene and bitumen fractions at the same temperature and hydrogen partial pressure.[13, 14] Solubility reflects the maximum concentration achievable in a phase and the maximum inventory of a reagent in a phase if the extent of a particular

reaction is limited by reagent transfer from another phase. Hydrogen interfacial mass transfer and labile hydrogen concentration[15] have both been shown to affect coke deposition and Wiehe[16] proposed a coking mechanism that is triggered by liquid-liquid phase separation.

Within catalyst pores, diluent choice affects transport properties and the outcomes of competitive adsorption processes at near ambient conditions (non reactive) and under hydroprocessing conditions.[17, 18] It is well known that diffusion coefficients increase with temperature, and that mutual diffusion coefficients in supercritical fluids[19] and in dense gases are about an order of magnitude larger than in liquids. This is equally true for bitumen or heavy oil + diluent mixtures.[20, 21] Thus, phase state, frequently unreported, is a key variable with respect to the value of transport properties.

When viewed from these perspectives, the diversity of coke deposition models and observed coke deposition outcomes reflected in the literature is not surprising, as direct observation of phase behavior is difficult and samples of all types are analyzed post facto. Coke deposition on catalyst is typically classified into three modes: uniform surface deposition,[22] pore-mouth plugging,[23] and bulk-phase coke formation.[22, 24] These modes are all supported experimentally. The uniform deposition mode assumes that coke deposition accumulates uniformly through the catalyst structure. According to this model, pores narrow and the number-based pore size distribution shifts to smaller radii. Pore-mouth plugging includes uniform coke deposition but also allows for blockages to arise at pore junctions. These two deposition modes are debated because they link to differing expectations related to coke layer thickness, catalyst deactivation and reaction selectivity, as well as to probable locations for coke deposition.[22] The third mode, bulk-phase coke

formation, requires the presence of a dispersed liquid phase, or large asphaltene-rich flocs, or aggregates. Coke arising in this latter manner may accumulate anywhere in a reactor.

Prior work in our group[12] addressed aspects of the impacts of multiphase behaviour and asphaltene-rich nanoaggregate size on coke deposition in commercial hydroprocessing catalyst pellets. In this Chapter, we apply the insights gained to the interpretation of coking outcomes on a commercial NiMo/γ-Al_2O_3 catalyst where Athabasca bitumen and Athabasca vacuum residue are diluted in hydrocarbons with apparently similar and apparently contrasting properties. Again, the focus is on coke deposition mode and related physical phenomena. Detailed description of coking experiment procedure and characterization of coked catalyst are available in Chapter 3 (3.2 and 3.3).

6.2 Results and discussion

6.2.1 Impact of feed dilution on the carbon content in coked catalyst pellets

The carbon content of coked catalyst pellets is presented graphically in Figure 6.1 for all cases evaluated. In Figure 6.1a, the impact of diluting Athabasca vacuum residue in 1-methylnaphthalene, a good physical solvent, versus n-decane, a poor physical solvent, is presented. In Figure 6.1b, the impact of diluting Athabasca bitumen in 1-methylnaphthalene and n-dodecane is presented along with the coking results obtained for nano-filtered Athabasca bitumen (Chapter 5) where large asphaltene-rich nanoaggregates were filtered at 200 °C using 50, 20, and 10 nm filters to reduce the

asphaltene content. The composition of the other constituents was unaffected by filtration on an asphaltene free basis (Chapter 4). Contradictory trends are clearly evident for the two sets of data. Dilution of Athabasca bitumen with 1-methylnaphthalene yields systematically higher carbon contents than dilution with n-dodecane, an unexpected outcome; while dilution of Athabasca vacuum residue, a closely related feed, with 1-methylnaphthalene yields systematically lower carbon contents than dilution with n-decane, an expected outcome.

For these experiments, the mass charged to the reactor, reaction temperature and reactor volume were fixed and global composition controlled but system pressure and the mass fraction of constituents in specific phases were uncontrolled variables. ABVB + n-decane and ABVB + n-decane + hydrogen mixtures exhibit liquid-liquid-vapour phase behavior[12] over the composition interval ~ 20 wt % ABVB to ~ 50 wt % ABVB, which corresponds to ~ 6 wt % asphaltenes to ~ 16 wt % asphaltenes in the mixture, over a broad pressure range at 380 °C. At lower ABVB contents, mixtures exhibit L2V phase behavior where L2 is a dense liquid phase comprising primarily ABVB constituents notably asphaltenes and V is a vapour phase comprising primarily decane and hydrogen. The L2 phase composition and physical properties differ markedly from the bulk composition. This phase behavior arises because the critical temperature of n-decane, $T_C = 345°C$, is significantly lower than the reaction temperature, 380°C. In the liquid-liquid-vapour region, multiphase kinetic and hydrodynamic effects play a role, all of which lead to the expected outcome vis-à-vis 1-methylnaphthalene. The critical temperature of 1-methylnaphthalene, $T_C = 499°C$, is above the reaction temperature and because it is a good physical solvent, multiphase equilibrium does not occur. Carbon

deposition decreases on dilution and because 1-methylnaphthalene is less volatile than n-decane, the dilution effect in the liquid phase is greater than for n-decane even in the low-density decane rich liquid-vapour (L1V) region which arises at low feed stock concentrations. Consequently, carbon deposition on dilution of Athabasca vacuum residue with 1-methylnaphthalene is systematically lower than dilution with n-decane.

One also sees this effect with toluene. A single illustrative coking experiment was conducted with 20 wt % ABVB + 80 wt % toluene under the same reaction conditions. Toluene is also a good physical solvent for ABVB, but having a low critical temperature, $T_C = 319°C$, relative to the reaction condition. The carbon content in coked catalyst pellets was 11.2 wt %, vis-à-vis 10.5 wt % for 20 wt % ABVB + 80 wt % 1-methylnaphthalene. Toluene solubility in ABVB at $380°C$ was not measured but it is significantly more volatile than 1-methylnaphthaltene. Under reaction conditions a smaller fraction of the toluene is present in the liquid phase. The dilution effect is less and more coke is deposited.

By contrast, Athabasca bitumen + n-dodecane mixtures do not appear to exhibit liquid-liquid-vapour phase behavior under the reaction conditions selected, and the critical temperature of n-dodecane, $T_C = 385°C$, like that of 1-methylnaphthalene, is above the reaction temperature. Differences in hydrogen availability in the liquid phase appear to dominate. Hydrogen is a key reagent in hydroprocessing. In batch hydroprocessing experiments, one focuses on hydrogen pressure, or on global composition, but not on composition by phase. The maximum concentration of a gas in a liquid phase is dictated by its solubility. As noted in the introduction, at a fixed hydrogen partial pressure,

hydrogen solubility in n-alkanes such as n-dodecane and n-decane is roughly twice the values arising in 1-methylnaphthalene and bitumen fractions.[13, 14] So, at any given

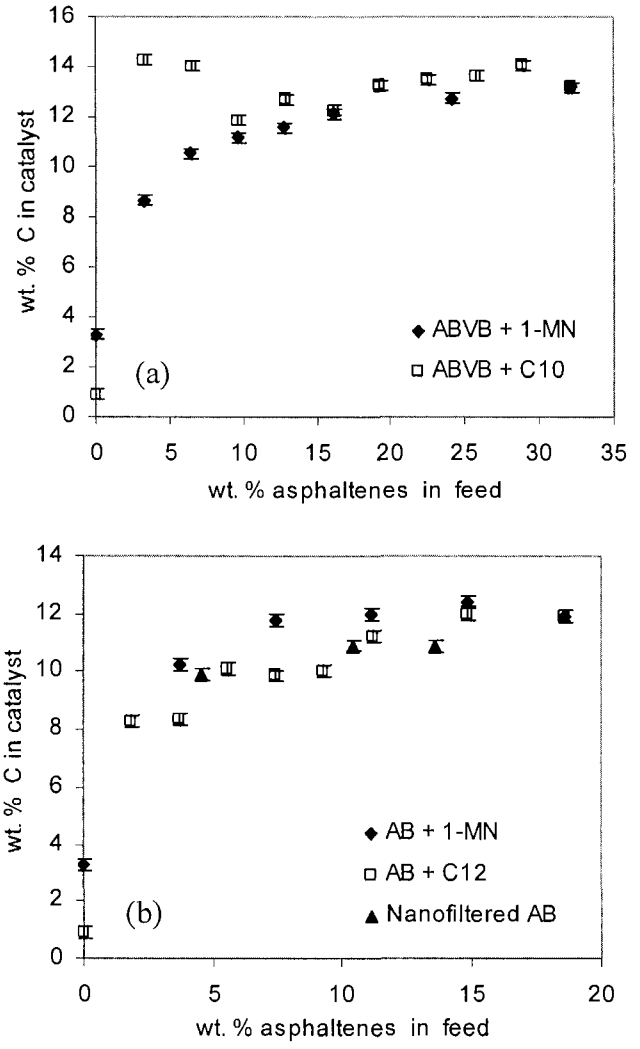

Figure 6.1 Bulk carbon content in coked catalyst pellets, T=673K, t=2h, feed(wt)/catalyst(wt)=30, hydrogen(wt)/feed(wt)=0.005

(a) Athabasca vacuum residue (ABVB) + 1-methylnaphthalene (1-MN), + n-decane (C10) and (b) Athabasca bitumen (AB) + 1-methylnaphthalene (1-MN), + n-dodecane (C12), and nanofiltered Athabasca bitumen.

pressure and temperature, significantly more hydrogen is present in liquid phases with higher mass fractions of n-alkanes. Consequently, carbon deposition on dilution with n-dodecane is systematically less than that arising for dilution with 1-methylnaphthalene. It is also worth noting that coke deposition remains high even when the asphaltene content is reduced to ~ 1 wt %. Dilution is not an effective way to reduce coke deposition irrespective of the nature of the diluents.

6.2.2 Impact of feed dilution on coked catalyst pore volume, pore surface area, and pore size distribution

Coked catalyst pellet samples from each set of experiments were selected for pore surface area, pore volume, and pore size distribution measurements. The samples and key results are listed in Table 6.1 for Athabasca vacuum residue and in Table 6.2 for Athabasca bitumen. Figures 6.2a and 6.2b show pore size distributions for 20, 40, 50, and 75 wt % ABVB in 1-methylnaphthalene and 20, 40, 60, and 80 wt % ABVB in n-decane, while Figures 6.2c and 6.2d show results for 20 and 80 wt % AB in 1-methylnaphthalene and n-dodecane, respectively. As asphaltene concentration increases, the peak in the pore size distribution shifts from ~ 45 Å to ~ 35 Å and to smaller numbers of pores in each size range relative to the sulfidized pellets. The growth of a secondary peak at 18.4 Å is also evident at higher ABVB and AB concentrations. In the prior work[12] and the results in Chapter 5, this secondary peak was contributed to the development of a coke layer on external pellet surfaces, as have others,[25, 26] but it may reflect small pores created in catalyst structures during coke deposition. From all four sets of distributions, Figures 6.2 a-d, above a threshold concentration for the feed stocks, there is little difference between

the pore size distributions for AB and ABVB + diluent mixtures and those of the feed stocks themselves. The similarity of the coked catalyst pellet pore size distributions for ABVB and 20 to 80 wt % ABVB + n-decane mixtures, Figure 6.2b, reinforces the point made above regarding the composition of phases to which catalysts are exposed. For these cases the liquid phase compositions to which the catalyst pellets are exposed appear to differ little despite the large differences in global composition. Once bulk phase behavior is accounted for, there are no apparent differences in the pore size distributions arising from feedstock dilution with poor or good physical solvents. This might well reflect the fact that asphaltene-rich aggregates in heavy feed stocks are large on average compared to the pore size distribution in commercial catalyst pellets. For example, in Athabasca bitumen at 200 °C, approximately half of the asphaltenes are present in aggregates with radii exceeding 100 Å – the nominal upper limit for "chemically active" pore size distributions in catalyst pellets (Chapter 4). Dilution with n-alkanes tends to enlarge average asphaltene-rich aggregate size as they are precipitants, while dilution with aromatics has only a limited impact on the mean aggregate size in the concentration range evaluated here, as noted in the introduction.

Nitrogen sorption/desorption isotherms are shown for the same cases in Figures 6.3 a-d. The hysteresis loops shift to lower pressures without shape change for all cases relative to the sulfided catalyst pellets. The shift is most pronounced for the ABVB + 1-methylnaphthalene and n-decane cases, less for AB + 1-methylnaphthalene cases, and least for AB + n-dodecane cases. However, all of these cases are consistent with pore narrowing as the dominant coke deposition mode (Chapter 5). Pore volume and pore surface area data are reported in Tables 6.1 and 6.2 for feedstock + 1-methylnaphthalene

and n-alkane mixtures, respectively. Catalyst surface areas change little on coking. For all cases, the differences fall within the measurement error. By contrast, pore volume loss is significant, with values ranging from 15 to 36 %. Evaluation of trends within the pore volume data sets is precluded due to the uncertainty of the pore volume data (± 0.02 mL/g). Ratios of pellet surface area loss to pore volume loss on coking are ~ 0. For uniform or proportional surface deposition, ratio values between 0.5 and 1 are expected (Chapter 5). These observations are consistent with coke deposition arising through the preferential partial filling of large pores as the dominant coke deposition mode. Neither uniform nor proportional pore filling nor pore mouth plugging appears to be significant deposition modes. Given the large size of the asphaltene-rich nanoaggregates, these observations also suggest that diffusion within pellets, irrespective of the extent or the nature of dilution, clearly plays an important role in coke deposition.

Table 6.1 Bulk analytical data for Athabasca vacuum residue (ABVB) diluted in 1-methylnaphthalene (1-MN) and n-decane (C10)

	SC	ABVB	75%ABVB +25%1-MN	50%ABVB +50%1-MN	40%ABVB +60%1-MN	20%ABVB +80% 1-MN	80%ABVB +20%C10	60%ABVB +40%C10	40%ABVB +60%C10	20%ABVB +80%C10
asph. content in feed, wt %	-	32.2	24.1	16.1	12.8	6.4	25.8	19.3	12.9	6.5
carbon content, wt %	-	12.9	12.8	12.1	11.6	10.5	13.6	13.3	12.7	14.0
surface area (m^2/g)	179	198	188	188	191	195	179	166	172	176
pore volume (mL/g)	0.55	0.38	0.40	0.41	0.42	0.42	0.37	0.37	0.39	0.35
pore volume loss (%)	-	31	27	26	23	24	33	33	29	36
surface area/pore volume ($x10^{-6}m^{-1}$)	325	521	470	459	455	464	484	449	441	503
>300 Å	0	0	0	0	0	0	0	0	0	0
100 Å -300 Å	6.6	6.9	7.2	6.6	6.7	7.1	7.8	20.9	9.2	7.5
40 Å -100 Å	61	35.7	39	38.8	40.6	44	39	31	26	39
20 Å - 40 Å	32	52.9	51	51.9	50.1	47	48	44	62	48
10 Å - 20 Å	0	4.5	2.5	2.7	2.7	2.6	5.1	4.8	2.8	5.6

Table 6.2 Bulk analytical data for Athabasca bitumen (AB) diluted in 1-methylnaphthalene (1-MN) and n-dodecane (C12)

	SC	AB	80%AB+ 20%1-MN	60%AB+ 40%1-MN	40%AB+ 60%1-MN	20%AB+ 80%1-MN	80%AB+ 20%C12	60%AB+ 40%C12	40%AB+ 60%C12	20%AB+ 80%C12
asph. content in feed, wt %	-	18.6	14.9	11.2	7.4	3.7	14.9	11.2	7.4	3.8
carbon content, wt %	-	11.9	12.4	12.0	11.8	10.2	12.0	11.2	9.9	8.4
surface area (m^2/g)	179	186	179	187	172	188	173	185	188	179
pore volume (mL/g)	0.55	0.41	0.38	0.41	0.41	0.45	0.40	0.41	0.44	0.47
pore volume loss (%)	-	25	31	26	25	18	27	25	20	15
surface area/pore volume ($x10^{-6}m^{-1}$)	325	454	471	456	420	418	433	451	427	381
>300 Å	0	0	0	0	0	0	0	0	0	0
100 Å -300 Å	6.6	8.0	6.6	5.8	6.5	8.2	7.2	6.7	20	6.7
40 Å -100 Å	61	47	42	31.0	42.8	42	44	43	41	50
20 Å - 40 Å	32	44	48	36.6	48.6	47	47	48	38	42
10 Å - 20 Å	0	1.1	3.4	26.6	2.1	2.8	1.8	2.1	1.1	1.1

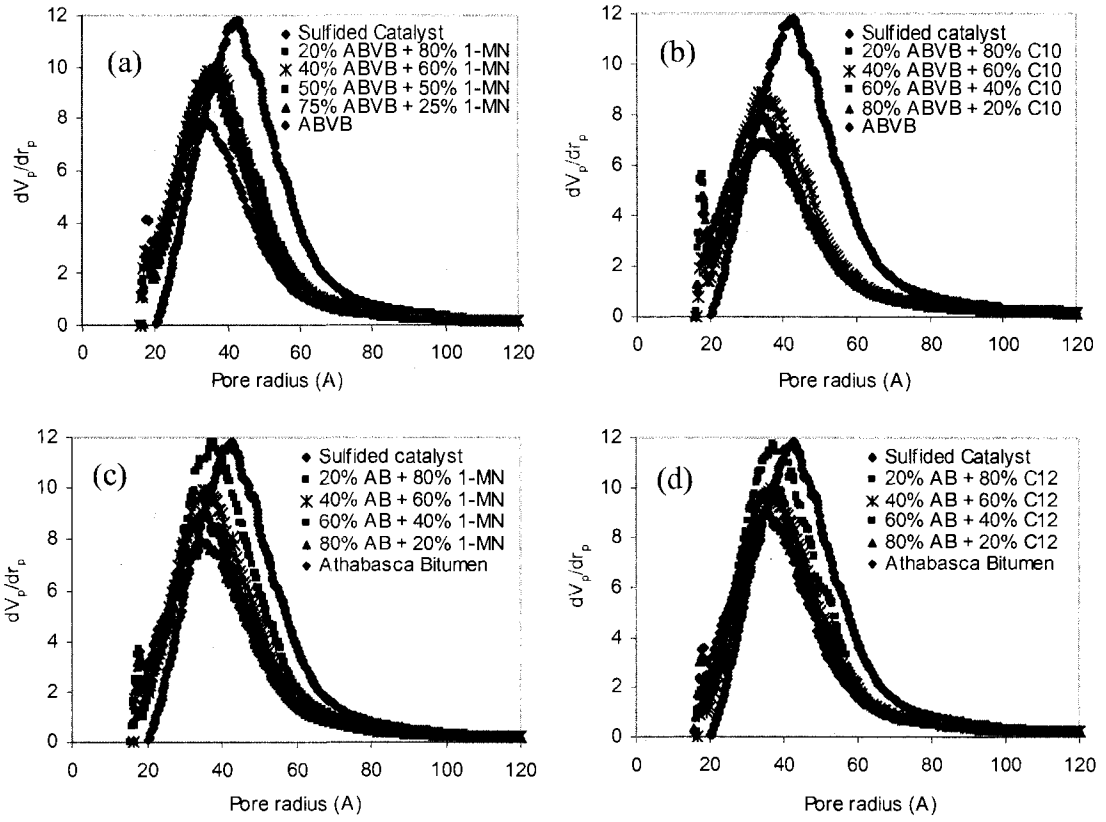

Figure 6.2 Pore size distributions for coked catalyst pellets.

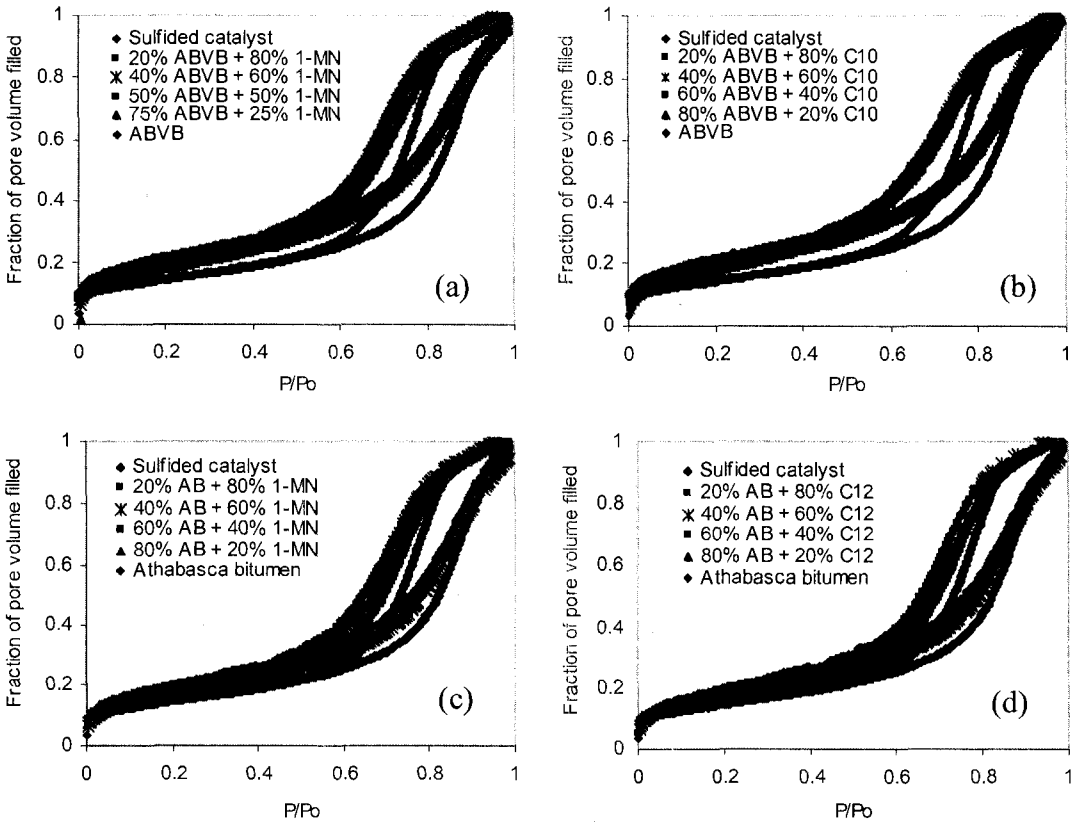

Figure 6.3 Adsorption/desorption isotherms for coked catalyst pellets.

6.2.3 Radial distribution of C, Ni, and Mo within coked catalyst pellets

Radial distributions for the elements carbon, nickel, and molybdenum in coked catalyst pellets are shown in Figures 6.4 and 6.5 for ABVB diluted in 1-methylnaphthaltene and n-decane, respectively, and in Figures 6.6 and 6.7 for AB diluted in 1-methylnaphthalene and n-dodecane, respectively. As noted in the experimental section, both carbon and iridium surface coatings are employed routinely for such analyses. As the two sets of

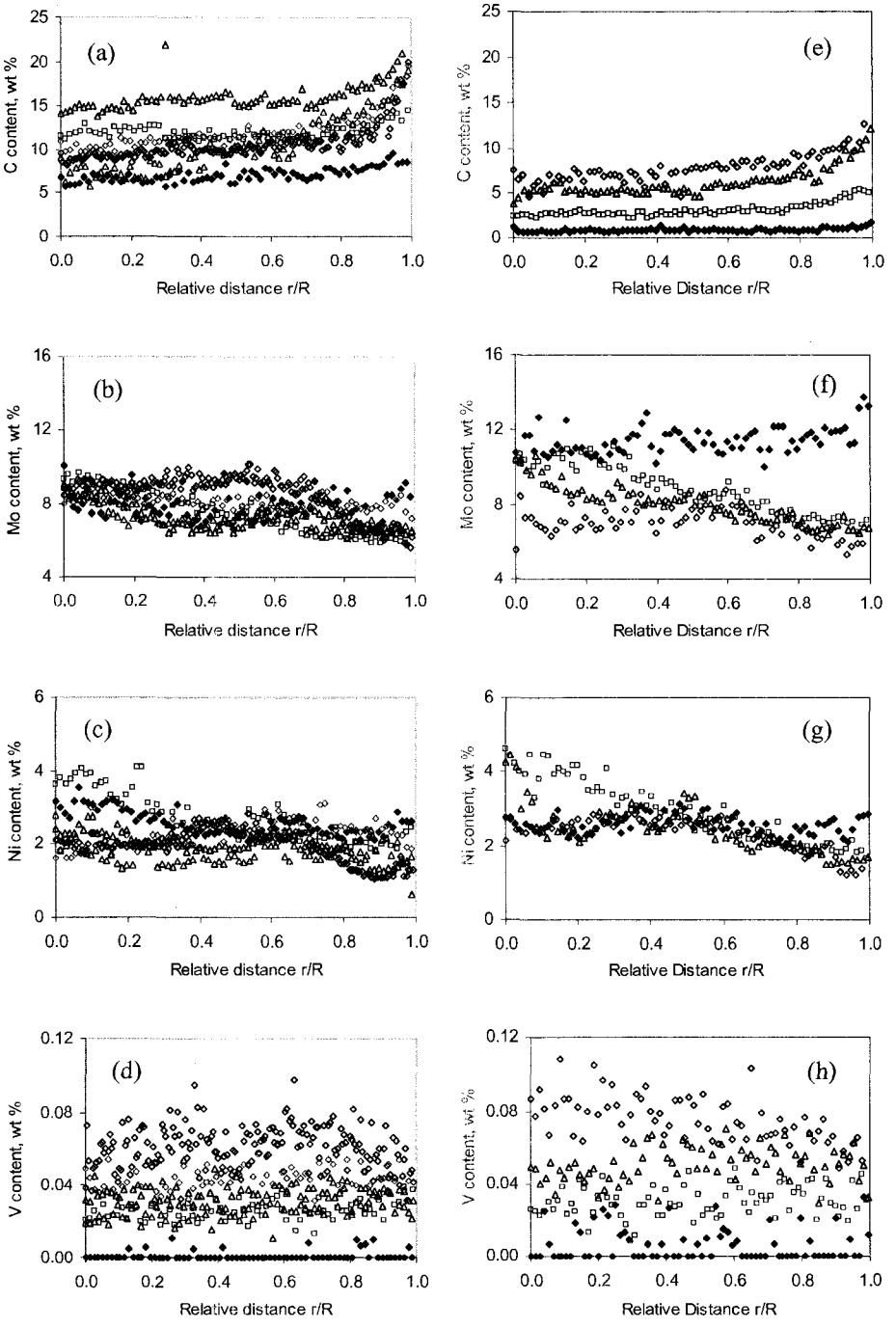

Figure 6.4 Radial element distributions for coked catalyst pellet cross sections (ABVB + 1-MN): (a – d) carbon coated, (e – h) Ir coated.

♦: fresh catalyst; □: 20 % ABVB + 80 % 1-MN; ◊: 40 % ABVB + 60 % 1-MN, △: 50 % ABVB + 50 % 1-MN, △: 75 % ABVB + 25 % 1-MN; ◊: ABVB.

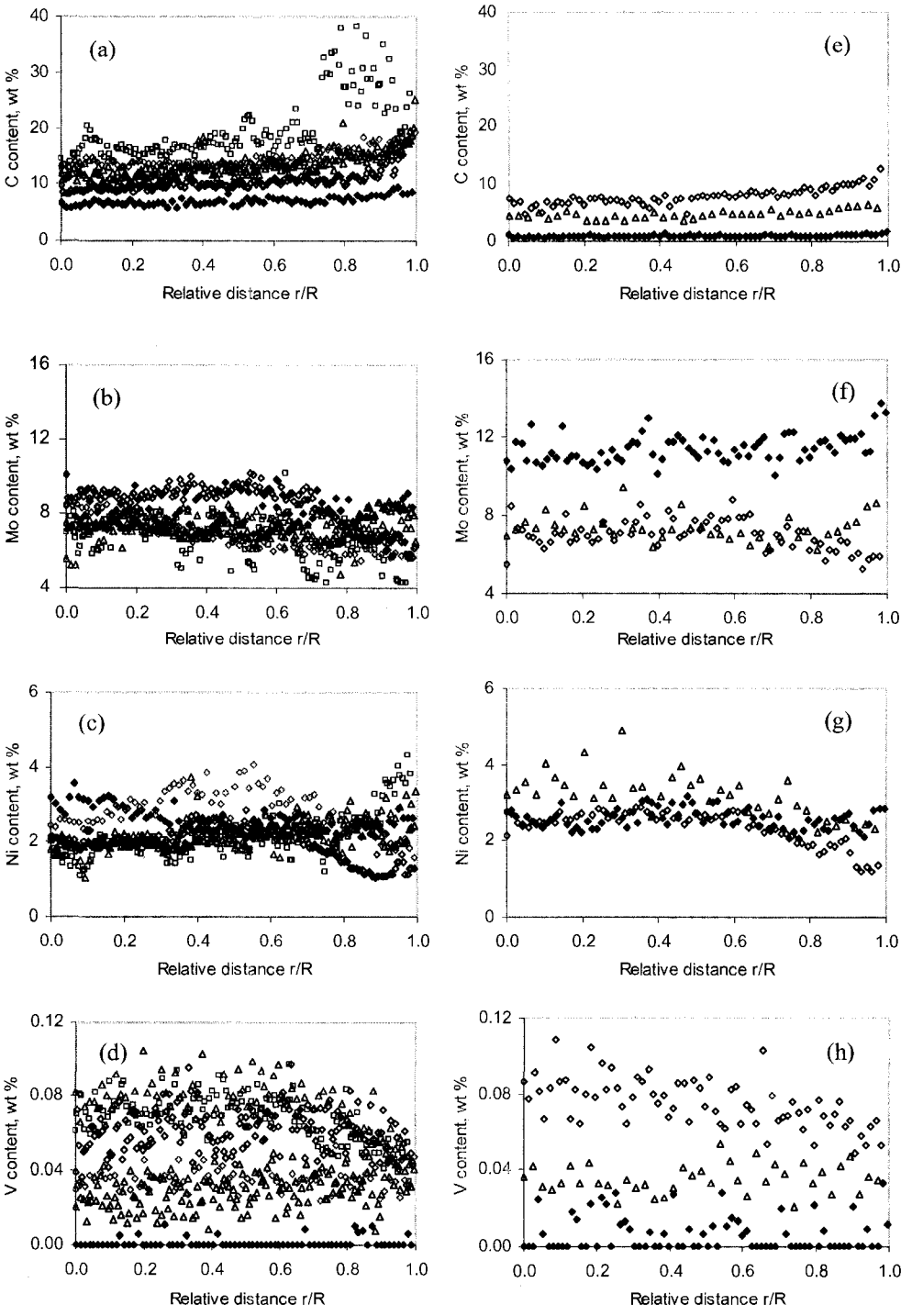

Figure 6.5 Radial element distributions for coked catalyst pellet cross sections (ABVB + C10): (a – d) carbon coated, (e – h) Ir coated.

♦: fresh catalyst; □: 20 % ABVB + 80 % C10; ◊: 40% ABVB + 60% C10, △: 60% ABVB + 60% C10, Δ: 80 % ABVB + 20 % C10; ◊: ABVB.

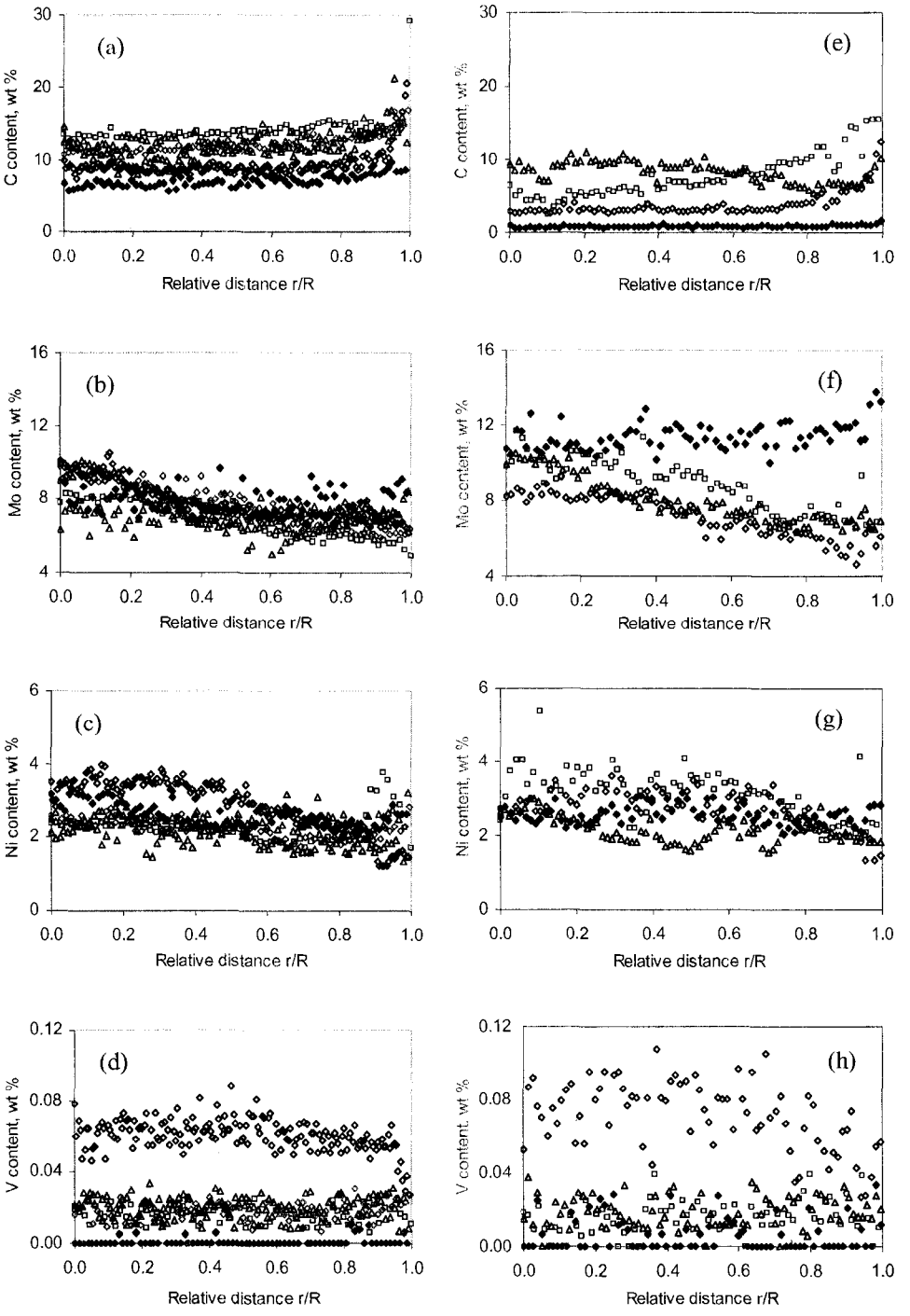

Figure 6.6 Radial element distributions for coked catalyst pellet cross sections (AB + 1-MN): (a – d) carbon coated, (e – h) Ir coated.

♦: fresh catalyst; □: 20 % AB + 80 % 1-MN; ◊: 40% AB + 60% 1-MN, Δ: 60% AB + 40% 1-MN, Δ: 80 % AB + 20 % 1-MN; ◊: AB.

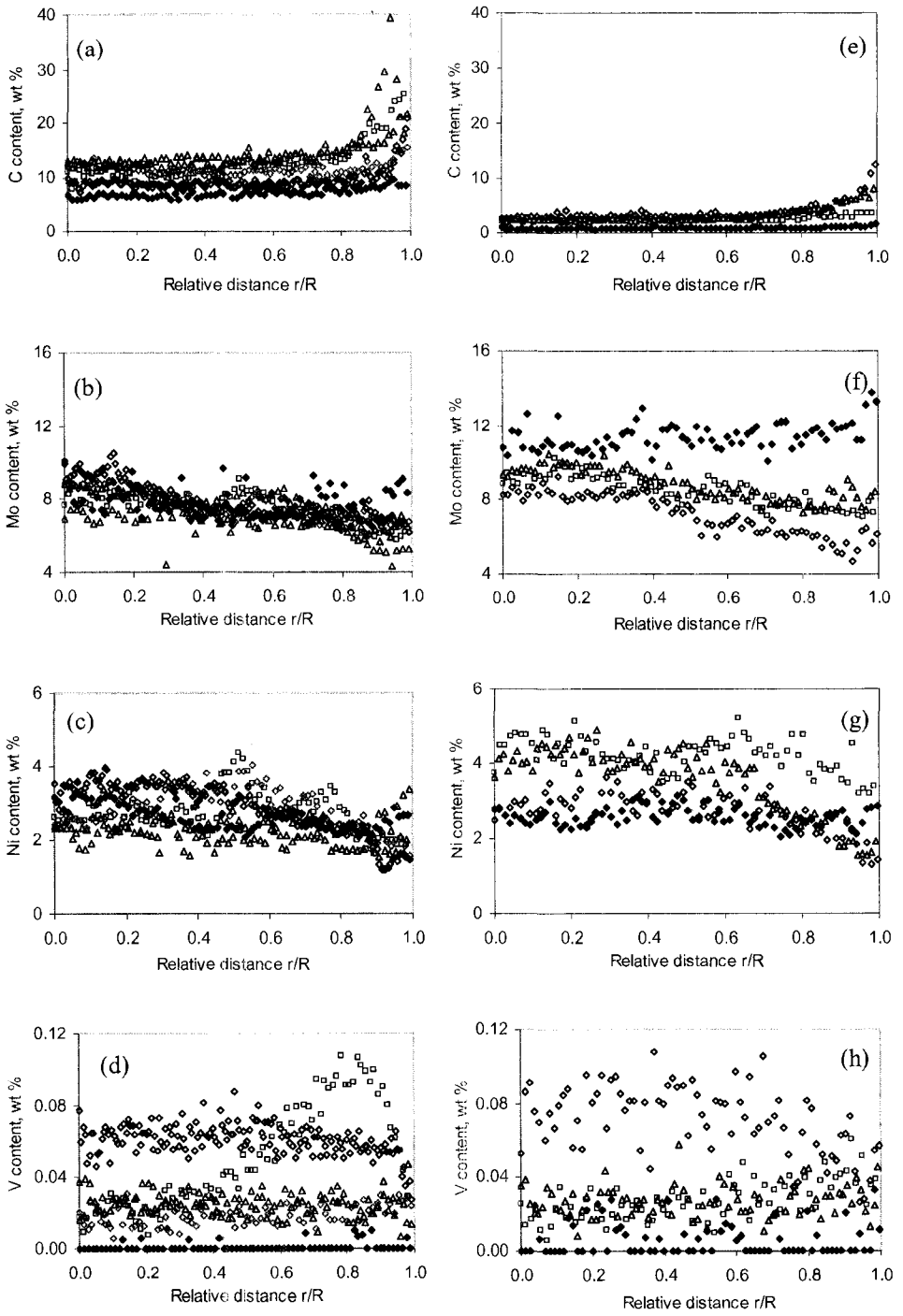

Figure 6.7 Radial element distributions for coked catalyst pellet cross sections (AB + C12): (a – d) carbon coated, (e – h) Ir coated.

♦: fresh catalyst; □: 20 % AB + 80 % C12; ◊ : 40% AB + 60% C12, △: 60% AB + 60% C12, △: 80 % AB + 20 % C12; ◊ : ABVB.

analyses are consistent with one another, they are reported jointly. Figures 6.4-6.7 a-d are for carbon coated samples and Figures 6.4-6.7 e-h are for iridium coated samples. A number of general trends are evident within the accuracy of the data. Carbon concentration profiles are flat at the core of the particles but trend to higher values as external surfaces of the catalyst are approached. Ni and Mo, both present in the sulfidized catalyst, trend to lower values from the core to external surfaces for coked pellets – a trend consistent with preferential carbon deposition near external surfaces. By contrast, vanadium content is largely independent of radial position. Similar trends were observed in Chapter 5.

The carbon deposition profiles within catalyst pellets suggest that coke deposition is diffusion limited. This is more readily visualized in Figures 6.8a and 6.8b where the ratio of carbon content at particle cores to the bulk carbon content of the coked pellets is presented for the mixtures containing ABVB and AB, respectively. Diluent is a parameter. The values for carbon coated samples were corrected for the impact of the coating by subtracting 6.3 wt % from the total (equivalent to the coating thickness on as received catalyst pellets). This correction is approximate. For the experiments reported here, coating thickness appears to vary. No correction was required for the iridium-coated samples as the iridium layer is thin and its mass fraction is small. Despite the collective uncertainties of such measures, the ratio is consistently less than unity. Asphaltene penetration within pellets is diffusion limited. Further, there are no apparent trends with dilution or solvent properties, suggesting that this effect is pervasive. Consequently, it is not possible to discriminate among the common reaction paths for coke deposition from asphaltenes as both series[27, 28] and parallel[22,

[29] reaction paths exhibit preferential deposition near catalyst pellet exteriors when diffusion effects are significant.

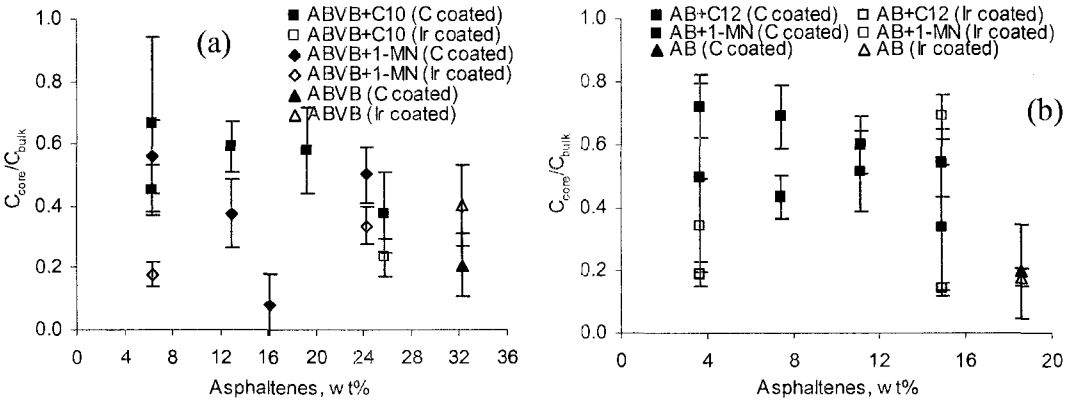

Figure 6.8 Impact of dilution on the ratio of carbon at pellet cores to the bulk carbon content of coked catalyst pellets.

6.2.4 Vanadium deposition in catalyst pellets

Vanadium deposition profiles are also shown in Figures 6.4d to 6.7d and Figures 6.4h to 6.7h. These profiles are flat. Vanadium does not exhibit a diffusion limitation for the cases evaluated, suggesting that vanadium deposition is largely independent of the coke deposition process. The maltene fractions of heavy feed stocks, such as Athabasca bitumen and Athabasca vacuum residue, contain vanadium. The vanadium content of AB maltenes is ~ 100 ppm and the vanadium content of AB asphaltenes is ~ 850 ppm (Chapter 4, Table4.3). In Chapter 5, a simple model for vanadium deposition within catalyst pellets was proposed based on independent deposition from the maltene and asphaltene fractions. Vanadium selectivity, defined as the mass ratio

of vanadium to carbon in the deposit to the mass ratio of vanadium to carbon in the feed, S, is expressed as a linear function of S_m^0, the vanadium selectivity for deposition from the maltene fraction, and $S_{Asph.}^0$, the vanadium selectivity for deposition from asphaltenes, weighted by X_{V-m}, the mass of vanadium present in the maltenes divided by the total mass of vanadium in a sample:

$$S = S_m^0 \times X_{V-m} + S_{Asph.}^0 \times (1 - X_{V-m}) \qquad (6\text{-}1)$$

This model was fit to vanadium deposition data in Chapter 5. For Athabasca bitumen, the parameter, $S_{Asph.}^0$ is ~ 1, whereas, S_m^0 ~ 35. For Maya crude, the best fit values for $S_{Asph.}^0$ and S_m^0 are ~ 1 and ~ 280, respectively. Both cases suggest that vanadium deposition from asphaltene-rich nanoaggregates is non selective while deposition from maltenes is highly selective. We concluded that maltenes, which do not aggregate, have facile access to the entire pore network irrespective of their mass fraction in the feeds, as do smaller asphaltene-rich nanoaggregates. From a fluid mechanics perspective, the feeds (maltenes plus a fraction of nanoaggregates) flow into the pellets and interact with interior surfaces independently but in proportion to their composition in the feed.

In this Chapter, ABVB and AB were diluted with n-alkanes and 1-methylnaphthalene. The global ratio of asphaltenes to maltenes in Athabasca bitumen is unaffected by dilution and selectivity is expected to be independent of diluent mass fraction according to Equation 6-1. However, the asphaltene to maltene ratio in the liquid is expected to vary by phase if two liquid phases are present. Consequently, care must be exercised in the interpretation of vanadium deposition selectivity data, which are based on global composition and not individual phase compositions.

Further, as all three diluents are more volatile than Athabasca bitumen or vacuum residue maltenes, the diluent mass fraction in the liquid phase, based on global composition, overstates diluent mass fraction if there is only one liquid phase, and may over or underestimate the diluent mass fraction if two liquid phases are present. Thus, vanadium deposition selectivity can be either over estimated (one liquid phase) or either over or underestimated (two liquid phases) vis-à-vis Athabasca vacuum residue or Athabasca bitumen - our baselines for vanadium deposition selectivity. Vanadium deposition selectivity data shown in Figure 6.9 are based on global compositions. The values for Athabasca bitumen and Athabasca vacuum residue are 18.5 and 12.3, respectively.

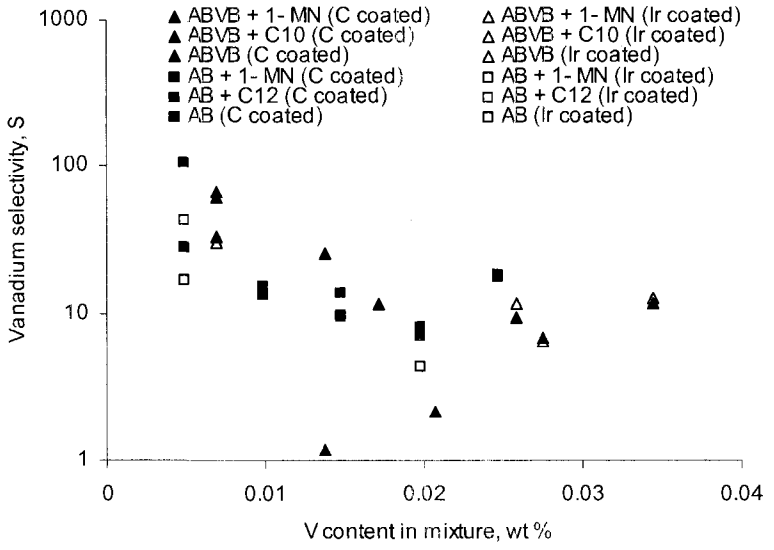

Figure 6.9 Vanadium deposition selectively based on global composition.

The impact of phase behavior on liquid composition can be assessed readily using a combination of Equation of State models, in this case the PRSV equation of state as

implemented in HYSYS version 2004.2, and phase behavior and phase property measurements.[12] The vapour pressure of 1-methylnaphthalene is ~ 12 bar at 380 °C, and the vapour and liquid densities at saturation are ~ 37 and 700 kg/m^3, according to the PRSV EOS. If the 15 mL reactor is charged with 4.5 g of pure 1-methylnaphthalene, less than 10 % of the charge is in the vapour phase. For 1-methylnaphthalene + ABVB or AB mixtures, more than 90 % 1-methylnaphthalene remains in the liquid phase and the mixtures do not exhibit liquid-liquid-vapour phase behavior under these conditions. Thus, selectivities based on global feed compositions closely approximate those based on liquid phase compositions. Vanadium deposition selectivity clearly decreases to a shallow minimum and then increase when either AB or ABVB are diluted with 1-methylnaphthalene. The vapour pressure of n-dodecane is ~ 17 bar at 380 °C and the vapour and liquid densities at saturation, ~ 130 and 330 kg/m^3 respectively, were also obtained using the PRSV EOS. If the 15 mL reactor is charged with 4.5 g of pure n-dodecane, less than 10 % of the charge is in the vapour phase. Again, in the absence of liquid-liquid-vapour phase behavior, the global feed and liquid phase compositions are similar. Dilution of Athabasca bitumen in n-dodecane decreases vanadium deposition selectivity to a shallow minimum and then selectivity increases on further dilution, as is the case for 1-methylnaphthalene.

By contrast, 380 °C is above the critical point of n-decane. It does not condense at this temperature. If the 15 mL reactor is charged with 4.5 g of pure n-decane at 380 °C, the pressure is ~ 44.6 bar (according to the PRSV EOS) for a vapour density of 300 kg/m^3, dictated by the mass balance. Contrary to 1-methynaphthalene + ABVB

or AB mixtures and n-dodecane + AB mixtures, where most the diluent remains in the liquid phase, in ABVB + n-decane mixtures at 380 °C, most of the decane goes to the vapour phase. For example, ABVB (20 wt %) + n-decane (80 wt %) + hydrogen (0.57 wt %) exhibits dense ABVB and asphaltene-rich liquid + vapour (L2V) phase behavior from the dew pressure of ABVB to more than 150 bar.[12] Based on phase behaviour and phase property measurements, in a 15 mL reactor charged with 4.5 g of mixture, the pressure is ~ 100 bar. The liquid volume is ~ 1 mL and the vapour volume is ~ 14 mL. The liquid and vapour densities are ~ 1000 and ~ 250 kg/m^3, respectively. The density and volume values are approximate because the mixture is reacting. As ABVB constituents are primarily found in the liquid phase, the decane content in the liquid does not exceed ~ 20 %. Clearly, the extent of dilution and hence the vanadium deposition selectivity is over stated when based on global composition. Thus, the apparent vanadium selectivity value, 63, based on global composition overstates the actual vanadium deposition selectivity from the liquid phase, ~ 16, a value comparable to that of the Athabasca vacuum residue.

Over all, the effect of dilution on vanadium deposition selectivity, irrespective of whether the solvent is a good or poor physical solvent, are similar. At low extents of dilution, vanadium deposition selectivity is the same as or less than for the parent material. At higher extents of dilution, vanadium deposition selectivity is enhanced. The origins of these two effects are unclear as they may be related to interactions between the diluents and the maltenes or the asphaltenes or both. For example, dilution with n-alkanes is known to increase asphaltene aggregate size (above a threshold concentration) and to increase hydrogen solubility, while reducing liquid

viscosity. Dilution with 1-methylnaphthalene has little impact on asphaltene aggregate size, but does not increase hydrogen solubility or decease liquid viscosity as much as alkane solvents. Further investigation is warranted.

6.3 Conclusions

The interplay between the physical properties of Athabasca bitumen + diluent mixtures at diverse length scales and coke deposition outcomes on a commercial hydroprocessing catalyst are illustrated. At the macroscopic scale, we show that in a batch micro reactor significantly more coke is deposited on a commercial, nanoporous, hydrotreating catalyst ($NiMo/\gamma\text{-}Al_2O_3$) in a dense asphaltene-rich liquid phase or if two liquid phases are present than in a low density diluent-rich liquid phase, at fixed global composition. At the nano-scale we confirm that asphaltene penetration into this catalyst pellet pore structure is diffusion limited irrespective of diluent used. Asphaltenes are aggregated and the leading dimensions of asphaltenes overlap with the pore size distribution. Consequently, coke deposition occurs primarily in larger pores, which become partially filled during deposition. The amount of coke deposited is also linked to effects at the molecular level and is particularly sensitive to hydrogen availability. Hydrogen solubilities in dodecane and decane are roughly twice the corresponding values for 1-methylnaphthalene and bitumen maltenes and coke deposition is shown to be lower in n-dodecane than in 1-methylnaphthalene over a broad range of compositions as a consequence, where other phase behaviour effects do not dominate. Over all, coke deposition, both the amount

and the nature of the deposit, is insensitive to dilution per se. By contrast, vanadium deposition selectivity is affected by dilution. The relationship between vanadium deposition selectivity and dilution merits more detailed investigation.

References

(1) Dwiggins, C. W., A Small Angle X-Ray Scattering Study of Colloidal Nature of Petroleum. *Journal of Physical Chemistry* **1965,** 69, (10), 3500-3506.

(2) Dwiggins, C. W., The Study of Colloidal Nature of Petroleum with an Automated Bonse-Hart X-Ray Small Angle Scattering Unit. *Journal of Applied Crystallography* **1978,** 11, (5), 615-619.

(3) Dwiggins, C. W., Absorption Correction and Normalization of X-Ray Small-Angle Scattering Data for Materials Producing Intense Scattering at Extremely Low Angles. *Journal of Applied Crystallography* **1979,** 12, (4), 401-402.

(4) Kim, H. G.; Long, R. B., Characterization of Heavy Residuum by a Small-Angle X-Ray-Scattering Technique. *Industrial & Engineering Chemistry Fundamentals* **1979,** 18, (1), 60-63.

(5) Sheu, J. I.; Sheu, E. Y., Characterization of DNA degradation using direct current conductivity and dynamic dielectric relaxation techniques. *Aaps Pharmscitech* **2006,** 7, (2).

(6) Andreatta, G.; Bostrom, N.; Mullins, O. C., High-Q Ultrasonic Determination of the Critical Nanoaggregate Concentration of Asphaltenes and the Critical Micelle Concentration of Standard Surfactants. *Langmuir* **2005,** 21, (7), 2728-2736.

(7) Sheu, E.; Long, Y.; Hamza, H., *Chapter 10. Asphaltene Self-Association and Precipitation in Solvent--AC Conductivity Measurements. Asphaltenes, Heavy Oils, and Petroleomics.* . Springer: New York, 2007.

(8) Freed, D. E.; Lisitza, N. V.; Sen, P. N.; Song, Y.-Q., *Chapter 11. Molecular Composition and Dynamics of Oils from Diffusion Measurements. Asphaltenes, Heavy Oils, and Petroleomics*. Springer: New York, 2007.

(9) Evdokimov, I. N.; Eliseev, N. Y.; Akhmetov, B. R., Asphaltene Dispersions in Dilute Oil Solutions. *Fuel* **2006,** 85, (10-11), 1465-1472.

(10) Gray, M. R.; Masliyah, J. H., *Extraction and Upgrading of Oil Sands Bitumen.* University of Alberta: Edmonton, 2004.

(11) Zou, X. Y.; Zhang, X. H.; Shaw, J. M., Phase Behavior of Athabasca Vacuum Bottoms plus n-Alkane Mixtures. *Spe Production & Operations* **2007,** 22, (2), 265-272.

(12) Zhang, X. H.; Shaw, J. M., Impact of Multiphase Behavior on Coke Deposition in Heavy Oils Hydroprocessing Catalysts. *Energy & Fuels* **2006,** 20, (2), 473-480.

(13) Cai, H. Y.; Shaw, J. M.; Chung, K. H., Hydrogen Solubility Measurements in Heavy Oil and Bitumen Cuts. *Fuel* **2001,** 80, (8), 1055-1063.

(14) Shaw, J. M., A Correlation for Hydrogen Solubility in Alicyclic and Aromatic Solvents. *Canadian Journal of Chemical Engineering* **1987,** 65, (2), 293-298.

(15) Rahmani, S.; McCaffrey, W.; Gray, M. R., Kinetics of Solvent Interactions with Asphaltenes during Coke Formation. *Energy & Fuels* **2002,** 16, (1), 148-154.

(16) Wiehe, I. A., A Phase-Separation Kinetic-Model for Coke Formation. *Industrial & Engineering Chemistry Research* **1993,** 32, (11), 2447-2454.

(17) Satterfield, C. N.; Colton, C. K.; Pitcher, W. H., Restricted Diffusion in Liquids within Fine Pores. *AIChE Journal* **1973,** 19, (3), 628-635.

(18) Prasher, B. D.; Ma, Y. H., Liquid Diffusion in Microporous Alumina Pellets. *AIChE Journal* **1977,** 23, (3), 303-311.

(19) Paulaitis, M. E.; Krukonis, V. J.; Kurnick, R. T.; Reid, R. C., Supercritical Fluid Extraction. *Reviews in Chemical Engineering* **1983,** 1, (2), 179-250.

(20) Zhang, X. H.; Fulem, M.; Shaw, J. M., Liquid-Phase Mutual Diffusion Coefficients for Athabasca Bitumen plus Pentane Mixtures. *Journal of Chemical and Engineering Data* **2007,** 52, (3), 691-694.

(21) Zhang, X.; Shaw, J. M., Liquid-Phase Mutual Diffusion Coefficients for Heavy Oil plus Light Hydrocarbon Mixtures. *Petroleum Science and Technology* **2007,** 25, (5-6), 773-790.

(22) Richardson, S. M.; Nagaishi, H.; Gray, M. R., Initial Coke Deposition on a NiMo/gamma-Al_2O_3 Bitumen Hydroprocessing Catalyst. *Industrial & Engineering Chemistry Research* **1996,** 35, (11), 3940-3950.

(23) Muegge, B. D.; Massoth, F. E., Basic Studies of Deactivation of Hydrotreating Catalysts with Anthracene. *Fuel Processing Technology* **1991,** 29, (1-2), 19-30.

(24) Zhang, X. H.; Chodakowski, M.; Shaw, J. M., Impact of Multiphase Behavior on Coke Deposition in a Commercial Hydrotreating Catalyst under Sedimentation Conditions. *Energy & Fuels* **2005,** 19, (4), 1405-1411.

(25) Chu, K. S.; Hanson, F. V.; Massoth, F. E., Effect of Bitumen-Derived Coke on Deactivation of an HDM Catalyst. *Fuel Processing Technology* **1994,** 40, (1), 79-95.

(26) Tsai, C. H.; Deo, M. D.; Hanson, F. V.; Oblad, A. G., Characterization and Potential Utilization of Whiterocks (Utah) Tar Sand Bitumen. II. Pyrolysis Mass Spectrometry and Nuclear Magnetic Resonance Analyses. *Fuel Science & Technology International* **1992,** 10, (9), 1437-1459.

(27) Thakur, D. S.; Thomas, M. G., Catalyst Deactivation in Heavy Petroleum and Synthetic Crude Processing - a Review. *Applied Catalysis* **1985,** 15, (2), 197-225.

(28) Koyama, H.; Nagai, E.; Kumagai, H., Catalyst Deactivation in Commercial Residue Hydrodesulfurization. In *Deactivation and Testing of Hydrocarbon-Processing Catalysts*, 1996; Vol. 634, pp 208-218.

(29) Chang, H. J.; Seapan, M.; Crynes, B. L., Catalyst Decay during Hydrotreatment of a Heavy Coal Oil. *ACS Symposium Series* **1982,** 196, 309-320.

7. General Discussion and Suggestions for Future Work

In this chapter, a general discussion based on results from Chapters 4 — 6 that have potential implications for production, transport, and upgrading process development and operation. General recommendations and recommendations for further study are noted following each topic.

7.1 Asphaltene nanoaggregates

Asphaltenes are operationally defined as a petroleum fraction that can be filtered from dilute mixtures with n-alkanes using filters with nominal pore sizes in the micron range. However, the amount of asphaltenes obtained by standard solvent separation method based on the definition increases when using filters with smaller pore size. This suggests that a significant amount of small asphaltene aggregates are present in n-alkanes. The reported asphaltene aggregate sizes are in the range from several nanometers to hundreds nanometers. This means asphaltene aggregates can be filtered directly from their original resource without n-alkane dilution.

Nanofiltration experiment results show that asphaltene aggregates possess broad size distributions even in feed stocks such as Athabasca bitumen and Maya crude. Compared with Athabasca bitumen, asphaltene aggregates in Maya crude are smaller but they are present in both cases. The impacts of nanoaggregrated asphaltenes in production, transport, and refining environments is frequently underappreciated or miss-attributed because asphaltenes are assumed to be soluble on a molecular basis in feed stocks or in

feed stocks diluted in aromatic media. The nanofiltration results also show clearly that Maya and Athabasca asphaltenes are not associated preferentially with other feed stock constituents at 200 °C. This result refutes a second prevalent notion, namely that asphaltenes and resins associate.

Coking experiment results show that the broad size distributions of Athabasca bitumen and Maya crude asphaltene aggregates significantly overlap with typical catalyst pore size distributions. Diffusion limitation for asphaltene penetration into catalyst pores is pervasive for all filtered samples (Athabasca bitumen and Maya crude, Figure 5.15) and for the feeds mixed with diluents (both Athabasca bitumen and Athabasca bitumen residue, Figure 6.8). Removal of large asphaltene aggregates or dilution is not an effective way to reduce this diffusion limitation. The coke deposition mode is a great concern in this study. The results do not support either pore mouth plugging or uniform surface deposition modes. Coke deposits primarily in large pores which become partially filled during hydroprocessing. It is noted that factors, such as dilution, hydrogen availability, trace oxygen, and asphaltene concentrations, may influence coke deposition amount, but do not show significant influence on coke deposition modes during batch experiments.

These findings have specific implications for production, transport, and refining applications and open new lines of inquiry:

1. Rheology:
    a. The presence of filterable aggregates in these feed stocks affects how rheological data are interpreted and suggests new approaches for how viscosity can be reduced. It is well known that at high solids/dispersed

phase loadings even small reductions in the dispersed phase volume fraction have significant impacts on viscosity.

b. If asphaltenes are nanoaggregated and not associated with other feed stock constituents, an explanation for the high viscosity of these feed stocks at room temperature vis-à-vis higher temperatures must be sought elsewhere.

2. Separation process design

   a. If asphaltenes and other feed stock constituents do not associate preferentially, this notion can be eliminated from the conceptual development of tailored separation processes for feed stock partitioning.

   b. Independent asphaltene aggregation in feed stocks may be exploited in separation process development.

3. Development of improved hydrogenation catalyst design

   a. The asphaltene aggregate size distribution overlaps with the pore size distribution of hydrogenation catalysts. By modifying the pore size distribution, pore volume and surface areas of catalyst, asphaltenes access can be controlled and high conversion of asphaltenes to low molar mass product and high removal of metals can be achieved.

   b. By designing proper shapes and choosing proper particle sizes of catalyst pellets used in different stage/bed/layer, asphaltenes access to the interior part of catalysts can be improved.

7.2 Phase behavior and coke deposition

When only one liquid phase arises during batch coking experiments with the permeates and retentates from Athabasca bitumen and Maya crude or with Athabasca bitumen or Athabasca vacuum residue + diluents, coke deposition amount is only a weak function of asphaltene content and maltene or maltene + diluent composition. The impact of dilution on coke deposition depends on the critical temperature of the diluent used. Diluents having a critical temperature higher than the reaction temperature have a greater impact on reducing coking outcomes than ones having a critical temperature lower than the reaction temperature because the former remain in liquid state and act as diluents, while the latter report primarily to the vapor phase. If two liquid phases arise during batch coking experiments with Athabasca vacuum residue + alkanes, the amount of coke deposited is sensitive to the presence of a dense asphaltene-rich liquid phase, L2. When this dense asphaltene-rich liquid phase is present (L2V, L1L2V), coking outcomes increase greatly.

It is well known that hydrogen suppresses coke deposition. The literature[1-4] focuses on either the influence of partial hydrogen pressure (both continuous and batch experiments) or hydrogen flow rate (continuous flow experiments) on coke deposition. Typically, coke deposition decreases with increasing hydrogen pressure or hydrogen flow rate. The batch experiments performed as part of this thesis, with low hydrogen to feed stock mass ratios, conform to this expectation. However, for a range of feed stock + hydrogen + product or diluent compositions, such mixtures tend to exhibit multiphase behavior over a range of pressures at fixed temperature. Should such a condition arise, coking outcomes are

sensitive to hydrogen availability in the liquid phase(s). At a fixed hydrogen partial pressure, hydrogen solubility in n-alkanes is roughly twice that in aromatics or maltenes.

These findings have some important implications for solvent-added hydrogenation process applications:

1. Process design
    a. As long as multiphase behavior is avoided, through temperature and pressure control, the fluid medium has a limited impact on coking outcomes. Hydrogenation process designers appear to have more flexibility with respect to fluid composition than they might be aware they have.
    b. Though dilution can help to reduce the viscosity and enhance flow of the feed stocks in industrial operations, it has a limited impact on coke formation.
    c. If diluent choices are available, those having higher critical temperatures are preferred, as are those with higher hydrogen solubilities.
2. Multiphase thermodynamics measurements
    a. Feed stock + diluent phase behavior investigations are a prerequisite for solvent selection and are a necessary input for coke deposition model development.
3. Coke deposition kinetics
    a. Coking outcomes depend on the properties of the liquid phase and not on global or feed stock compositions. Phase based information should be

measured for studies and this information should be incorporated into models for coke formation and deposition kinetics.

b. As multiphase behavior can arise under a wide range of conditions and has important implications for the amount if not the nature of coke deposited, phase behavior calculations should be included in coke deposition models.

7.3 Vanadium deposition

Unexpectedly, vanadium deposition was found to be uniform throughout the catalyst pellet and independent of coke deposition for cases evaluated. Maltenes and asphaltenes make independent contributions to vanadium deposition with maltenes being the major vanadium source, despite the high relative concentration in asphaltenes. This implies that vanadium deposition from asphaltene-rich aggregates is primarily a non selective physical deposition while vanadium in maltenes interacts selectively with catalyst surfaces.

Process design implications:

a. The impacts of coke deposition and vanadium poisoning are separate and must be addressed separately even though most of the vanadium is present in asphaltenes. It is not clear if this presents a window of opportunity or an additional complication for catalytic hydrogenation process development.

References

(1) Thakur, D. S.; Thomas, M. G. Catalyst Deactivation in Heavy Petroleum and Synthetic Crude Processing - a Review. *Applied Catalysis* **1985,** 15, (2), 197-225.

(2) Aitken, A. R.; Merrill, W. H.; Pleet, M. P. Hydrogenation of Coker Distillate Derived from Athabasca Bitumen. *Canadian Journal of Chemical Engineering* **1964,** 42, (5), 234-238.

(3) Zeuthen, P.; Cooper, B. H.; Clark, F. T.; Arters, D. Characterization and Deactivation Studies of Spent Resid Catalyst from Ebullating Bed Service. *Industrial & Engineering Chemistry Research* **1995,** 34, (3), 755-762.

(4) Inoguchi, M.; KaneKo, Y.; Satomi, Y.; Inaba, K.; Kagaya, H.; Tate, K.; Mizutori, T.; Nishiyama, R.; Ota, T.; Niume, K. Studies in the Hydrodesulfurization Catalyst of Residual Fuels (Part 6). *Bull. Jpn. Petrol. Inst.* **1972,** 14, 7-17.

8. Conclusions

The asphaltene aggregate size distributions in neat Athabasca bitumen and Maya crude were explored by nanofiltering samples directly. No solvents were employed. Samples were successfully partitioned at 473 K to obtain aggregate size distributions. The impact of asphaltene aggregate size on coke deposition was subsequently investigated under typical hydroprocessing conditions on a commercial catalyst. The interactions of physical properties of bitumen + diluent mixtures, such as multiphase behavior and hydrogen availability, on coke deposition, were also explored.

The key conclusions from this work are:

1. Two nanoaggregate structures were identified in Athabasca bitumen and Maya crude: one is rich in asphaltenes and another is rich in mineral matter,
2. Asphaltene-rich aggregates possess very broad size distributions in Athabasca bitumen and Maya crude. The aggregate sizes range from less than 5 nm to more than 100 nm for Maya crude and to more than 200 nm for Athabasca bitumen,
3. Mineral matter-rich nanoaggregates are larger, and partition independently during filtration,
4. Asphaltene-rich nanoaggregates obtained by nanofiltration, at 473 K, possess similar compositions to those obtained by standard solvent separation methods at room temperature, on a maltene free basis. Their elemental composition does not vary by size,
5. Asphaltenes do not preferentially associate with the resin or aromatic fractions at 473 K,

6. Ni, V, and Ca partition jointly with asphaltenes. While Ni and V are typically associated with asphaltenes, this is the first report associating Ca with asphaltenes,
7. The size distribution of asphaltene-rich aggregates, measured at 473 K, overlaps with the pore size distribution of typical hydrogenation catalyst pellets,
8. Asphaltene penetration into the catalyst pellet pore structures is diffusion limited due to this size overlap and common mechanisms for asphaltene deposition cannot be discriminated on the basis of data obtained,
9. Coke deposits preferentially in large pores which become partially filled during hydroprocessing; coke deposition, both the amount and the nature of the deposit, is insensitive concentration,
10. By contrast, vanadium deposition within catalyst pellets does not appear to be diffusion limited. The bulk of the vanadium deposited comes from the maltene fraction,
11. The amount of coke deposited in catalyst pellets, during batch coking experiments, is sensitive to hydrogen availability; Trace oxygen in feeds plays an equally importance role,
12. The number and compositions of phases present and hydrodynamic effects influence the amount of coke deposited in a batch micro reactor. Apparently, counter intuitive results can arise, at otherwise similar conditions, if phase behavior and phase composition are not known.